Centre for Sensors, Instruments and Systems Development
UNIVERSITAT POLITECNICA DE CATALUNYA
Shaping light to your needs

DOCTORAL THESIS

FOR OBTAINING THE DOCTORAL DEGREE
IN THE FIELD OF OPTICAL ENGINEERING FROM THE

TECHNICAL UNIVERSITY OF CATALONIA
UPC-BARCELONATECH

Generalized ray tracing method for the calculation of the induced peripheral refraction by an ophthalmic lens

Author:

PILAR ROJO BADENAS

Thesis Director:

SANTIAGO ROYO ROYO

Tribunal Members:

MEMBER 1 JOSEP ARASA MARTÍ
MEMBER 2 JOSÉ ALONSO FERNÁNDEZ
MEMBER 3 SALVADOR BARÁ VIÑAS

Presented in Terrassa, Spain, Dissertation Date

Contents

1. Introduction..... 4
2. Background..... 7
2.1. Ophthalmic lens..... 7
2.2. Refractive error and its compensation..... 8
2.3. Ray tracing procedure in an ophthalmic lens. Classical Coddington equations..... 13
2.4. Power vectors..... 16
3. State of the art..... 18
3.1. Generalized ray tracing..... 18
3.2. Peripheral refraction..... 21
3.2.1. Peripheral refraction and myopia..... 21
3.2.2. Measures of peripheral refraction..... 26
3.2.3. Peripheral refraction and ophthalmic lenses..... 30
4. Ray tracing in ophthalmic lenses..... 40
4.1. Geometric properties of the surfaces. Parametrization of spherical, aspherical and toroidal surfaces. 40
4.2. Theoretical approach to finite ray tracing 46
4.3. Theoretical approach to generalized ray tracing..... 47
4.4. Step by step ray tracing procedure in an ophthalmic lens 51
4.4.1. General procedure..... 51
4.4.2. Detailed case for astigmatic lenses..... 56
4.5. Validation of results..... 62
4.6. Implementation of ray tracing code. Results..... 65
4.6.1. Spherical lenses 65
4.6.2. Aspherical lenses..... 67
4.6.3. Astigmatic lenses..... 70
5. Evaluation of peripheral refraction in ophthalmic lenses..... 73
5.1. Modeling a retinal conjugate surface..... 74
5.1.1. Theoretical retinal conjugate surface model..... 76
5.1.2. Experimental retinal conjugate surface model..... 77
5.2. Peripheral refracted surface of an ophthalmic lens..... 82
5.3. Calculation of induced peripheral refraction. 88
5.3.1. Induced peripheral refraction for retinal conjugate surface obtained by experimental values. 89
5.3.2. Induced peripheral refraction in over-correction and under-correction..... 93
6. Conclusions..... 99
7. References..... 104

UNIVERSITAT POLITÈCNICA DE CATALUNYA
BARCELONATECH
Escola de Doctorat

Acta de qualificació de tesi doctoral

Curs acadèmic:

Nom i cognoms
PILAR ROJO BADENAS

Programa de doctorat
ENGINYERIA ÒPTICA

Unitat estructural responsable del programa
DEPARTAMENT D'ÒPTICA I OPTOMETRIA

Resolució del Tribunal

Reunit el Tribunal designat a l'efecte, el doctorand / la doctoranda exposa el tema de la seva tesi doctoral titulada

GENERALIZED RAY TRACING METHOD FOR THE CALCULATION OF THE PERIPHERAL REFRACTION INDUCED BY AN OPHTHALMIC LENS

Acabada la lectura i després de donar resposta a les qüestions formulades pels membres titulars del tribunal, aquest atorga la qualificació:

☐ NO APTE ☐ APROVAT ☐ NOTABLE ☐ EXCEL·LENT

(Nom, cognoms i signatura)	(Nom, cognoms i signatura)
President/a	Secretari/ària

(Nom, cognoms i signatura)	(Nom, cognoms i signatura)	(Nom, cognoms i signatura)
Vocal	Vocal	Vocal

_____, _____ d'/de _____ de _____

El resultat de l'escrutini dels vots emesos pels membres titulars del tribunal, efectuat per l'Escola de Doctorat, a instància de la Comissió de Doctorat de la UPC, atorga la MENCIÓ CUM LAUDE:

☐ SÍ ☐ NO

(Nom, cognoms i signatura)	(Nom, cognoms i signatura)
President de la Comissió Permanent de l'Escola de Doctorat	Secretari de la Comissió Permanent de l'Escola de Doctorat

Barcelona, _____ d'/de _____ de _____

Acknowledgements

When I finished my studies in Optics and Optometry I was twenty years old. I thought that I had studied a very interesting and nice degree but my interest then was focused in obtaining money to start an independent life and build a family. Now, twenty years later, I am not only proud of my family, but also of my continuous interest for vision and optometry, which have led me to continue studying and working in this area. There are many people who I would like to thank and for whom without their help this work would not have been possible. First, I would like to express my special appreciation and thanks to my advisor Professor Dr. Santiago Royo, for introducing me to the field of ophthalmic lenses and Matlab® programming, mentoring me over the years, trusting in my abilities and encouraging me all this time. I would also like to thank Industrias de Optica Prats, specially Jorge Ramírez and Inés Maradiaga whose experience and help have been essential to developing the methodology of this Thesis. A special thanks to my family: words cannot express how grateful I am to my husband, for all the sacrifices, advice and encouragements. Albert, Laura and Lídia please excuse me for the time that this work has taken up.

1. Introduction

Progression and incidence of myopia are issues that have arisen a great amount of interest in the late years. This refractive error, leaving aside the visual impairment it entails, can be associated with various ocular pathologies (retinal detachment, glaucoma, subretinal neovascularization, cataracts…). The progressive increase of the axial length of the eye seems to be the cause of these problems (1). Therefore, different techniques have been developed to try to reduce the progression of myopia, although the success obtained in most cases has not been relevant, except for certain approaches based on pharmacological treatment and orthokeratology (2). Classical optical strategies for the treatment of the progression of myopia have been based on the manipulation of the focus of the eye for foveal vision (3–6) and have had limited success. A better understanding of the process of development of the refractive error is allowing the design of different types of treatments, which recently have included the concept of peripheral refraction, leaving traditional methods for the prevention of the progression of myopia under question.

In the last years, different studies have shown how peripheral retina can play a key role in the process of emmetropization and in the development of a particular refractive error (7–9). Specifically, a hyperopic defocus in the periphery of the eye can probably lead to the progression of myopia due to a progressive increase in the axial length (7,10,11). This fact has led to the revision of the different compensatory elements used in ophthalmic optics, which were initially conceived to compensate the refractive error of the eye, which for many years was considered as just the image on the fovea, without taking into account the effects of the compensation elements on peripheral vision. This is the case in ophthalmic spectacle lenses, where the compensation of the central refractive error in all directions of gaze has been the objective, without considering the refractive error induced outside the fovea. Different studies have shown an increase of this peripheral refractive error towards the hyperopic direction with the use of ophthalmic single-vision lenses(12,13).

Single-vision lenses are used in large quantities by children and teenagers, many of them classic subjects of myopic progression, and susceptible to diseases associated with myopia. Due to the relevance of the topic a generalized approach for the optimization of the ophthalmic lens performance would be highly desirable. At first, we believe that is essential to dispose a reliable method for the calculation of the induced peripheral refraction (IPR) by an ophthalmic lens. This methodology should consider a reliable, accurate and quick ray tracing procedure to

assess ophthalmic lens performance and a reliable reference of measure for the IPR, which we define as a retinal conjugate surface (RCS). We will explain in the state of the art that there isn't a common pattern of peripheral refraction for myopes, even for those having the same central refractive error(14). Then, the introduction of a modeled RCS presents an indispensable tool under our point of view.

Therefore, the main goal of this thesis is the development of a reliable method to quantify the IPR by an ophthalmic lens. The proposed method must allow an accurate evaluation and quantification of the IPR using an ophthalmic lens in a given eye taking into account personalized data of the patient's eye. With this purpose, we will take advantage of the classical ray tracing strategies used in ophthalmic lens design and will apply them, with modifications, to the evaluation of the peripheral refractive error of the eye. One relevant issue is how, for ophthalmic lens design, the optical system of the eye is ignored by replacing it with concepts like the remote sphere and an aperture situated in the center of rotation of the eye. We will adapt these concepts to our purpose, developing the concepts of RCS and nodal point, which will have comparable roles. The basis of the proposed method will be finite ray tracing (FRT) and generalized ray tracing (GRT) procedures, which will be coded within a software application. GRT procedures (also called wavefront tracing procedures) will enable fast evaluation of oblique astigmatism (OA), i.e., the tangential and sagittal powers of the lens in all the field of vision with an accurate evaluation of ophthalmic lens performance. The author wants to stress that the full coding and testing of FRT and GRT procedures has been one a large part of the workload performed along this Thesis, as no preliminary code existed.

To achieve this purpose, this Thesis has been arranged in six Sections plus this introduction. The next section introduces the basic concepts for the proper understanding of the Thesis, in order to make it easier to read to non-experts in ophthalmic lens design. We introduce the concepts of refractive error and its compensation, ophthalmic lenses, classical Coddington equations. We also will introduce the power vectors, which will be recalled when we calculate the IPR surfaces. The state of the art on both ophthalmic lens design and peripheral refraction, including the relationship of the latter with the progression of myopia and with ophthalmic lenses is presented along Section 3, showing the relevance of a method with the characteristics which have been described. Along Section 4, the fundamentals of FRT and GRT are exposed, implemented in a self-developed software code and validated. Using this implementation, different lens geometries of ophthalmic lenses are analyzed in different directions of gaze and visualized by plots of tangential and sagittal power, and also as power vectors. The detailed

ray tracing procedure for an astigmatic lens is presented as an example. Once the implementation of tracing algorithms has been validated in the classical ophthalmic lens design conditions, it will be adapted and applied in Section 5 to evaluate the IPR induced by a given ophthalmic lens, using the nodal point of the eye as reference for the ray tracing procedures and a modeled RCS. We will propose both a theoretical model of RCS for myopic eyes and a model of RCS obtained using experimental values of measured peripheral refraction for myopic and for emmetropic eyes. The calculation of IPR for different lens geometries, in terms of sphere, cilynder and axis surfaces is then presented, and an analysis of the effects on IPR of different geometrical parameters. Finally, the effects of over and under correction conditions on peripheral refraction, both for myopic and emmetropic eyes, are presented and discussed. In Section 6 we will introduce the main conclusions derived from this Thesis and the possibilities of the method developed in further work.

2. Background

2.1. Ophthalmic lens

An ophthalmic lens is an optical element used to alter the vergence of the light beams before they reach the eye. The term comes from the Latin lens, lentis, meaning lentil, and was adopted because of the similarity in the shape. An optical medium is any substance through which light can travel. Most optical media with interest in ophthalmic optics are isotropic, meaning that light travels at the same speed in all directions within this environment. A lens can be defined as an optical medium bounded by two polished surfaces, with at least one of them curved. For ophthalmic lens manufacturing, a very limited number of optical media are used (when compared with technical optics), being natural substances, either glass or plastic(15).

An ophthalmic lens is characterized by geometrical parameters such as the radius of curvature of its first (convex) surface, the radius of curvature of its second (concave) surface, its central thickness, its edge thickness and its diameter. It is also characterized by material parameters such as refractive index or Abbe number, and combinations of geometric and material parameters such as dioptric power or back vertex power (BVP). There are only two surfaces to be considered as a single lens element is involved, which leads to deal with the surface shape rather than with the properties and positions of a variety of lens elements, such in conventional optical system design.

The basic theory of ophthalmic lens design is based on the fundamental laws of geometrical optics and is dominated by refraction effects. An ophthalmic lens is intended to modify properly the vergence of the rays from an object before it reaches the eye, in order to compensate the eye's refractive error, forming the image of the observed object onto the retina. Geometrical and optical parameters of the lens can be changed and adjusted to obtain the desired power of the lens. There are endless possibilities to combine these parameters with each other and still get the same power of the lens, which is usually described as the BVP, namely, the inverse of the distance from the back vertex of the lens to the image focal point. BVP is a very convenient magnitude as it has a physical reference (the second lens surface) to fix the position of the focal point, rather than a virtual principal plane.

However, different combinations of parameters yielding the same performance of the lens on-axis cause very different performance of the lens off-axis (15)(16)(17)(18)(19). If a material

with a certain refractive index is used and the radius of the first surface and diameter of the lens are fixed for a given BVP, the central thickness and the radius of the second surface of the lens are univocally determined. In the same way, if the radius of the second surface is fixed, the central thickness and the radius of the first surface are determined. We can state then that, for lenses with two spherical surfaces, the ophthalmic lens design process has a single degree of freedom to be fixed, which is the curvature of one of the surfaces.

Finally, as a definition, the vertex distance is the distance from the second lens surface to the first surface of the cornea of the eye (Fig. 2.1). This parameter influences the BVP choice to compensate a given refractive error as discussed in Section 2.2 (16–18).

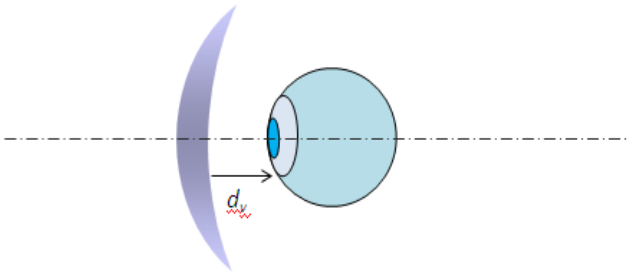

Figure 2.1. Vertex distance (d_v)

2.2. Refractive error and its compensation

An emmetropic eye has the infinity as the conjugate pair of the retina (if not using accommodation, which would happen in near vision), namely the conjugate of the fovea. Therefore, the rays coming from infinity are focused onto the fovea in distance vision conditions. (Fig.2.2)

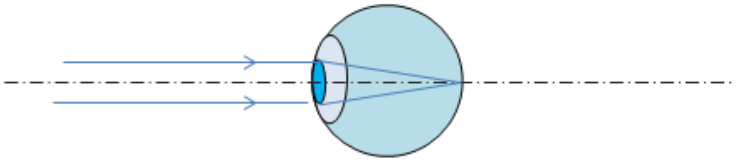

Figure 2.2. Emmetropic eye. Rays coming from infinity focus on the fovea.

When a refractive error exists, the conjugate of the fovea is not infinity anymore, but a point called the remote point (R_p) of the eye. It is a real point in front of the cornea in the case of myopia and a virtual point behind the retina in the case of hyperopia. In both ammetropias, rays coming from infinity aren't focused on the fovea and the eye presents a certain level of defocus on the retina. However, we can always find a point conjugate to the fovea in such ametropic eyes, which we will call the remote point of such eye. The image of the remote point, thus, is always focused onto the fovea. (Fig.2.3).

a) b)

Figure 2.3. Ammetropic eyes. The conjugate of the fovea is the remote point of the eye. a) Myopic eye, with its real remote point in front of the cornea. b) Hyperopic eye, with a virtual remote point behind the retina.

The ophthalmic lens compensation condition is thus defined by the coincidence of the image focal point of the lens with the remote point of the eye in a non-accommodated eye. Thus, the eye-lens system becomes a compound system which conjugates infinity with the retina via the remote point. Next diagrams show this principle for a myopic eye and for a hyperopic eye (Fig.2.4):

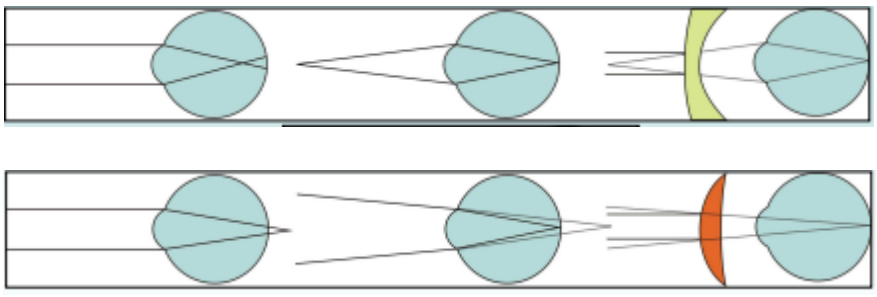

Figure 2.4. Basic principle of refractive error compensation for a myopic eye (top) and a hyperopic eye(bottom).

The role of vertex distance and its relationship with BVP is now clear, as an ophthalmic lens placed at different distances in front of the eye would mean that BVP should change to match the image focal point of the lens with the remote point of the eye (16–19)

Over the on-axis performance of the lens-eye system we have described, the classical theory of ophthalmic lens design proposes that the condition of compensation of the refractive error should be kept over the surface defined by the position of the remote point at all directions of gaze. This collection of three-dimensional remote points forms an imaginary sphere with center at the center of rotation of the eye (CR), named the remote sphere. Similarly, a vertex sphere can be defined, which will be used to define precisely the BVP for each direction of gaze (Fig. 2.5).

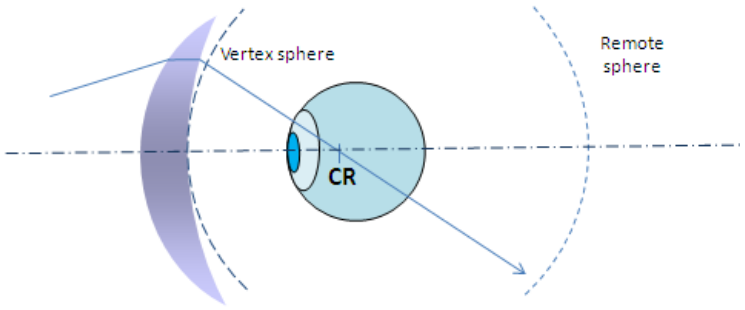

Figure 2.5. Remote sphere and vertex sphere

This simplifies extraordinarily the ophthalmic lens design problem because the details of the optical system of the eye can be ignored and replaced by the remote sphere as final image surface and an aperture at the position of the CR (15,20–22). Although the pupil of the eye moves around the CR for all directions of gaze the performance of the lens is modeled as if the eye had a fixed aperture with the size of the pupil at the CR as shown in Fig. 2.6.

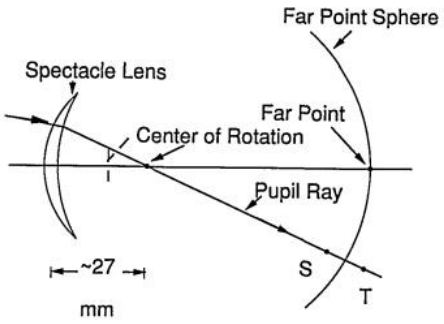

Figure 2.6. Basis for the conventional ophthalmic lens design problem (20). S and T are the tangential and sagittal foci of the beam cited later in the text.

Although the aperture of the eye may be considered small in general, for directions of gaze outside the optical axis the image of an object blurs due to the presence of off-axis aberrations. Typical pupil eye sizes allow disregarding aperture aberrations, such as spherical aberration and coma. Distortion and chromatic aberration are in general not considered, since the visual system learns to adapt to them with use. Thus, small aperture off-axis aberrations are the ones which need be considered, meaning that only astigmatism (termed oblique astigmatism (OA) in ophthalmic optics) has relevant effects in lens performance. For off-axis gazing the image of eccentric object points will generate both a tangential and a sagittal focal line which change with the oblique angle in different ways (see Fig. 2.7) modifying the effective power of the lens in each direction.

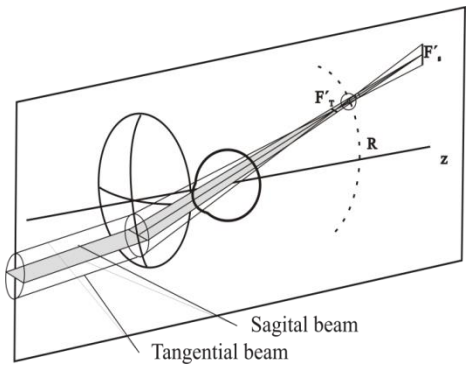

Figure 2.7. Oblique astigmatism in an off-axis object point for the lens-eye system. The different behaviour in the sagittal and tangential planes induces two different foci.

The existence of aberrations makes the ideal condition of compensation of the refractive error on the whole remote sphere impossible to attain in practice with spherical surfaces, due to the

lack of degrees of freedom in the lens-eye system, where only the curvature of one surface may be chosen by the designer.

A number of different classical solutions for ophthalmic lens design exist, which vary in the criteria to manage the focus shift, i.e. the different position of tangential and sagittal foci positions across the field, when changing the curvature of a single surface of the lens. Percival lenses, point-focal lenses and minimal tangential error lenses are some of the solutions used in practice (15,19,22).

Field diagrams are plots used to evaluate the amount of OA introduced by eccentricity in a given lens design. They represent the tangential and sagittal power of the ophthalmic lens in different directions of gaze. An example of the behavior of OA depending of the base curve of the lens is shown in the field diagrams of Fig. 2.8, obtained for a BVP lens of +6.00 D, with centre thickness of 3mm, refractive index 1.5, vertex distance of 12mm and object at infinity. The blue curve represents the tangential power and the red curve the sagittal power. It may be appreciated how with a base curve of +9.00D the tangential and sagittal foci are relatively symmetrical about the BVP, corresponding to a Percival design (Fig. 2.8(a)). When the base curve is +12.00D both tangential and sagittal foci are coincident for all directions of gaze, corresponding to a point-focal lens (Fig. 2.8(b)). Finally, when the base curve is +10.50D, the tangential foci and the BVP of the lens are coincident in practice, which corresponds to a minimum tangential error lens (Fig.2.8(c)). It should be noted that OA has a second effect, which is the deviation of the real power at eccentric incidence from the foveal BVP, inducing what in ophthalmic lens design is called power error: thus, Percival lenses minimize power error in the whole field forgetting the value of OA introduced (which is defined as the difference between both focals), while point focal lenses minimize OA disregarding the value of power error present at oblique incidence. Tangential error lenses are an intermediate solution to those. Plots in Fig. 2.8 have been obtained using the software developed in this thesis.

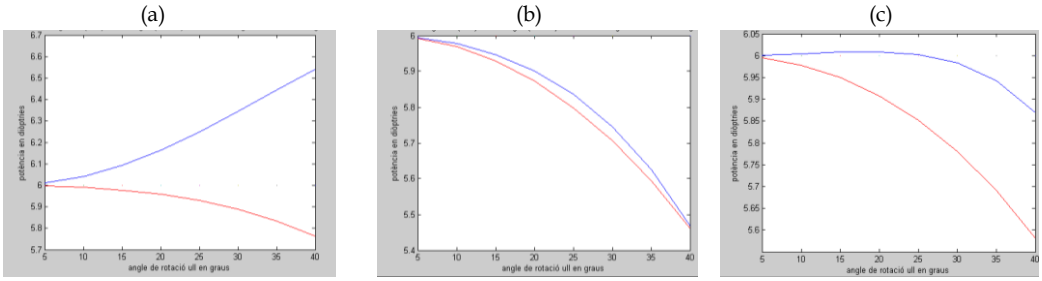

Figure 2.8. Field diagrams for an ophthalmic lens of BVP of +6.00 D. Tangential power is plotted as a blue line and sagittal power as a red line. a) Base curve of +9.00, Percival lens. B) Base curve of +12.00D, point-focal lens. c) Base curve of +10.50D, minimum tangential error lens

The lack of degrees of freedom implies that the designer is limited to reduce various aberrations simultaneously using the single degree of freedom available. When alternatives have been used to obtain better designs and thinner lenses, they have been centered in varying the surface geometry so a higher number of degrees of freedom become available. The use of aspherical and free-form surfaces has been the most used alternative to overcome the lens design problem and enhance the performance of ophthalmic lenses.

2.3. Ray tracing procedure in an ophthalmic lens. Classical and modern ophthalmic lens design.

The ray tracing procedure for obtaining the best design for an ophthalmic lens with a given BVP follows a number of well-defined steps. Normally a range of different curves for the lens surfaces are chosen to be evaluated as possible solutions for the lens, and third-order calculations are used to provide the first choice. Then, given a central thickness for the lens, a diameter and the curvature of one surface, the power of the other surface is determined to achieve the desired BVP. Next, a typical value for the distance from the posterior surface of the lens to the CR of the eye is chosen (typically, 27mm). This value includes the vertex distance which can be variable. Once all these steps are taken, the ray tracing procedure may start (15).

In the general configuration, it is considered that the lens has a refractive index n, a central thickness e and the distance from the second lens surface to the center of rotation of the eye is d_v+d_r (where d_v is the vertex distance and d_r is the distant from the anterior corneal surface to the CR of the eye). The radius of the second lens surface is R_2 and the radius of the first lens surface is R_1.

The goal of the procedure is to find exactly the path of the ray which arrives with a particular eccentricity to the lens and reaches the fovea. For this reason, the starting point of the ray tracing procedure is the CR. It is considered that the eye rotates an angle *v* from the optical axis. The reverse path of a ray which arrives to the posterior surface of the lens passing by the CR is considered to determine the angles of incidence and refraction of the ray at each lens surface and the conjugated object space ray will then be calculated (Fig.2.9). Snell's law will be used for the evaluation of the direction of refraction while trigonometric relationships will be used for translation calculations from one surface to the next one.

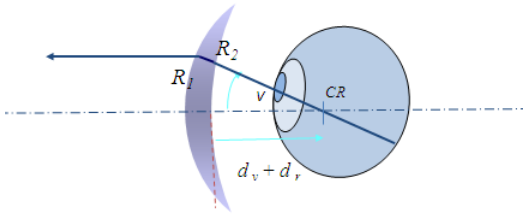

Figure 2.9. The eye is rotating an angle *v*. The reverse path of the ray which passes through the pupil and the center of rotation of the eye is used to evaluate lens performance at a given angle.

This first step delivers the exact path of a ray which defines a particular direction of gaze. This ray crosses the ophthalmic lens through some refraction and translation operations and arrives to the object space. In a second, final step, the path of the ray is reversed and considered from the object to the image space, and then classical Coddington's equations are used surface by surface.

The use of the Coddington's equations (developed in the early 19th Century (23) is suitable because when the eye rotates about its CR and looks for eccentric points of the lens the configuration for the application of these equations is matched. Coddington's equations are used to calculate the analytical solutions for the tangential and sagittal foci derived from OA generated by a spherical refracting surface whose surface normal is tilted relative to the principal ray of the incoming bundle of rays (15). In this case, there is a narrow incoming bundle of rays created by an eccentric object point which arrives to the anterior refracting surface of the lens with a relative tilt.

Coddington's equations may be written as:

$$\frac{n'}{s'} - \frac{n}{s} = \frac{n'\cos i' - n\cos i}{r} \tag{2.1}$$

$$\frac{(n'\cos^2 i')}{t'} - \frac{(n\cos^2 i)}{t} = \frac{(n'\cos i' - n\cos i)}{r} \tag{2.2}$$

Where r is the radius of curvature of the refracting spherical surface, n the refractive index in the incident medium, n' the refractive index in the refracted medium, i the angle of incidence of the chief ray and i' its angle of refraction, with all angles calculated relative from the normal to the surface. s and t are the object distances and s' and t' are the image distances to the sagittal and tangential foci, respectively. Coddington's equations are a two-dimensional, analytical approximation which goes far beyond the assumptions which need be taken if paraxial optics was used. These equations have typically been used in classical ophthalmic lens design, limited to 2D surfaces, and usually taking avantage of symmetry to describe rotationally symmetrical surfaces.

The method we propose in this thesis to evaluate the ophthalmic lens performance will be comparable, but it will involve a finite ray tracing (FRT) procedure for the first step and a generalized ray tracing (GRT) procedure for the second one (Fig. 2.10). These are the general methods used in modern ophthalmic lens design and are not limited by the geometry of the surface, and enable three-dimensional tracing without the requirement of symmetry assumptions. In FRT, each direction of gaze is characterized by a so-called finite ray in 3D space, again traced backwards from image to object space of the lens. Finite rays are those traced exactly in 3D according to Snell's law. FRT becomes one of the essential tools of the optical designer, and is essentially an iterative sequence of two operations: transfer and refraction. Transfer takes a ray from where it leaves one optical surface to where it meets the next one, so in homogeneous media it is little more than linear propagation. Refraction finds the new direction of the ray once it has passed through the surface of interest taking into account the difference in refractive indexes (24). It is an established technique which fundamentally uses the vector form of Snell's law. Analytical expressions for FRT in an ophthalmic lens may be found explicitly developed in Section 4.2.

Once we have traced the direction of the principal ray using FRT, the path of the ray will be inverted and the system will be rotated backwards. Then GRT tracing algorithms will be applied. GRT deals with the effects on the geometry of a local wavefront associated to the principal ray as it travels across each surface of the lens. The FRT concept is associated with

the ray which crosses the optical system, while the GRT concept is associated with a beam of light. GRT procedure will be explained in detail in the state of the art and in Section 4.3.

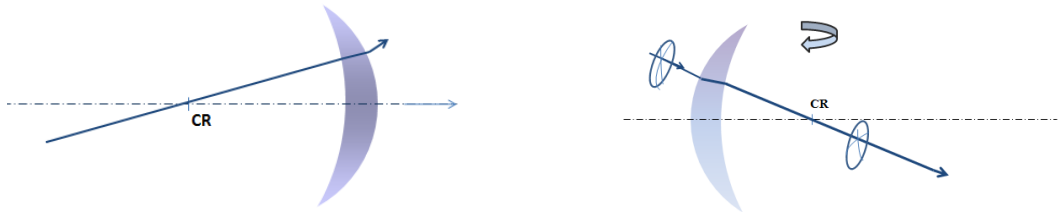

(a) (b)

Figure 2.10. (a) FRT for the calculation of the reverse path of a principal ray starting at the center of rotation of the eye and (b) GRT is used when the path of the ray is inverted and the system is rotated backwards, so each principal ray has a wavefront associated in its vicinity.

2.4. Power vectors

The description of the refractive error is a basic element in optometry. Usually, sphero-cylinder refractions are described in terms of sphere, cylinder and axis (S, $C\times\theta$). This notation is used for prescription and is very useful in clinical practice, although sphere and cylinder components are not independent of each other. This lack of independence arises because a cylinder lens carries on a form of spherical power, called the mean spherical equivalent.

However, when a combination of sphero-cylinder refractions is required, several methods can be used. In this thesis the power vectors proposed by Thibos (25) are used, where a sphero-cylinder refraction is represented as the sum of a spherical lens (M) and two cross-cylinders, one at axis 0º(J_0) and the other at axis 45º(J_{45}). The power of these three component lenses may be interpreted as (x,y,z) coordinates of a power vector in a dioptric space (Fig. 2.11). This representation has advantages when problems involving the combination of refractive errors, the comparison of different lenses and the statistical distribution of refractive errors, are involved, as it is based in a Fourier decomposition, and, in difference with the spherocylindrical expression, the components may be interpreted as independent of each other.

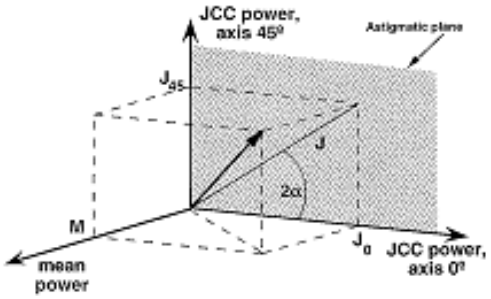

Figure 2.11. A three-dimensional dioptric space for representing refractive error as a power vector (25)

The relationship between component power vectors and sphere, cylinder and axis is, in addition, extremely simple, as:

$$M = S + \frac{C}{2} \tag{2.3}$$

$$J_0 = -\frac{C}{2}\cos 2\theta \tag{2.4}$$

$$J_{45} = -\frac{C}{2}\sin 2\theta \tag{2.5}$$

And subsequently the inverse relationships are:

$$C = -2\sqrt{{J_0}^2 + {J_{45}}^2} \tag{2.6}$$

$$S = M - \frac{C}{2} \tag{2.7}$$

$$\theta = -\arctan\left(\frac{C/2 + J_0}{J_{45}}\right) \tag{2.8}$$

This notation will be extremely useful in this Thesis for the calculation IPR by an ophthalmic lens, as the calculation method will be based in the combination of the refractive errors of the eye and the lens three-dimensionally, at all retinal eccentricities.

3. State of the art

Several different topics need be considered to cover the full state of the art of this project, from ray tracing techniques to optometric analysis on the reasons of progression of myopia. We have divided the state of the art in three main parts. In the first one, we will present the different procedures used to trace rays and beams of light through optical systems. We are interested in this issue because we need to evaluate the performance of ophthalmic lenses, which are the optical systems of our interest, to understand their performance and improve it. Ophthalmic lenses are extremely simple optical systems and their peculiarities of use will allow the choice of GRT as the optimal ray tracing procedure.

The second part of this state of the art reviews the issue of peripheral refraction. Studies that relate peripheral refraction and the progression of myopia are exposed, and the relevance of such hypothesis analyzed. We will then be interested in the different methods to measure patterns of peripheral refraction in humans.

In the last part of this State of the art, we will establish the link between the two first ones, by presenting how ophthalmic lenses affect peripheral refraction, and the different attempts made up to date to design ophthalmic lenses which in addition serve the purpose to prevent the progression of myopia. The main limitations of the present methods will be outlined and the basis of the work developed will be settled.

3.1. Generalized ray tracing

One of the simplest ways of tracing beams of light through an optical system is via an off-axis extension of paraxial optics using narrow beams. Although this is an exact ray tracing procedure in the sense that Snell's law is applied without approximations in the principal ray of the beam, the marginal rays of the beam are so close to the principal ray that they are considered paraxial in nature (26) and are traced as paraxial rays. Fig. 3.1 shows a narrow beam of light that illuminates a tangential small vertical segment centered on the optical axis on the Y axis. A similar sagittal beam illuminates a small horizontal segment. Tracing rays using classical Coddington's equations is based on this concept. Classical Coddington's equations (Eq.2.1 and Eq.2.2) can be applied then in spherical surfaces and if the surfaces are rotationally symmetrical.

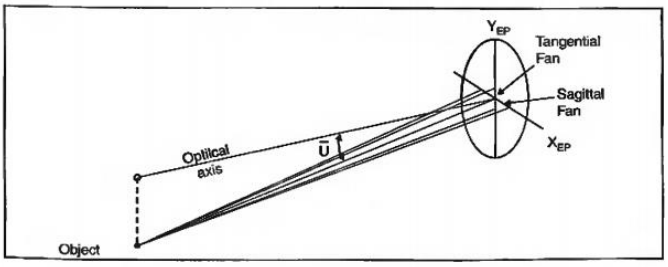

Figure 3.1. Paraxial tangential beam and sagittal beam relative to the entrance pupil (26)

However, the light beam can also be traced using parabasal rays, which are real rays which form a small angle with the principal ray of the beam. These rays are real in the sense that every ray of light interacts with the real curvature of the surface, not with a plane of equivalent power, as in classical Coddington's equations. Parabasal rays lose the computational advantages of paraxial rays, but represent better the performance of the system. These rays can be applied on decentered, tilted, or non-rotationally symmetrical surfaces, diffractive surfaces, or surfaces with refractive index gradients... This is the ray tracing process used in most commercial optical design software packages, like Zemax (27)

In an alternative approach, it has been proposed to trace rays using different strategies of generalization of classical Coddington's equations, initially proposed for spherical surfaces in a plane, in order to adapt them to 3D surfaces with arbitrary shapes(28,29), yielding what has been known as generalized Coddington's equations (GCE).

The main contributions leading to this point have been related to the inclusion of differential geometry aspects in Coddington's approach, which has enabled alternative derivations of the classical equations (30–32). Stavroudis (33,34) purposes that each ray traced through the optical system should be associated to a local perpendicular wavefront which propagates through the optical system accompanying the principal ray, so the previous "narrow beam" present in Coddington's equations is substituted by a principal ray and its local wavefront on the element of surface of interest. Thus, the propagation of the local wavefront in the neighborhood of the principal ray through an optical system is used for the evaluation of the optical system. This introduces the concept of GRT, where the heights and slopes of incidence of the ray are no longer the parameters of interest. Instead, the shape and orientation of the local wavefront in the vicinity of the principal ray becomes the subject of study. GRT

equations provide the change of the curvatures and torsions of a surface (the associated wavefront) at the point of incidence of the principal ray of the beam at the refracting surface.

Landgrave et al. refer to Stavroudis equations as "intrinsic generalized Coddington equations" (35). Their work proposes a matrix version of the GCE combined with the introduction of the propagation matrix. The equivalence of this approach with classical equations is also established. Eqs (2.1) and (2.2) have been reconsidered to fix the tangential and sagittal focal length of any ray contained in the tangential plane, and not just that of the main beam, deriving formulas for more efficient evaluation of the aberrations (36). Campbell (37) has considered the refraction of a wavefront by a powered element as the action of an operator acting on the wavefront introducing the concept of vergence operators. The local area of the wavefront to be refracted is given in terms of a vergence operator that takes the form of the product of the refractive index of incoming media and a 2x2 matrix whose elements are the local curvature components of that wavefront. The local area of the refracting surface that interacts with the wavefront is given in terms of a refraction operator, which is a type of vergence operator which consists in the product of the change in the effective optical path length across the surface and a 2x2 matrix whose elements are the local curvature components of that refracting surface. The creation of the refracted vergence operator, which gives the properties of the local area of the refracted wavefront, can take place in a simple way if both the incoming vergence operator and the refraction operator are expressed in the same coordinate system, normally that of the refraction operator.

Lately, a general method to generate equations for refraction from wavefront aberrations of any order for any incidence condition has been proposed (38). These results include Coddington's equations as a special case, and extend them to refractive aberrations of any order, by defining local aberrations in detail using their expansion in power series coefficients which describe the surface local coordinate systems aligned with the principal rays from the surface normal. Equations of refraction become then a sequence of analytical relationships between these sets of coefficients.

Coddington's equations have played a central role in ophthalmic lens design and are still subject of active research. In this Thesis we will implement the GRT approach proposed by Stavroudis, where a local wavefront is associated to a particular ray to evaluate lens performance. Analytical expressions for GRT may be found in Section 4.3, and its application to ophthalmic lenses is developed in detail along Section 4.4.

3.2. Peripheral refraction

Eye refraction in diopters is defined as the inverse of the distance, expressed in meters, from the corneal apex to the remote point of the eye. This refraction usually refers to the refractive central power of the eye, i.e, the remote point is conventionally associated to the conjugate point of the fovea in object space.

If instead of limiting to the point of greatest visual acuity of the retina we take into account the behavior of eccentric points around the fovea, the concept of peripheral refraction can be defined in a comparable way. It is obviously a 3D concept which in the general case may attain different values depending on the direction being considered. Fig. 3.2 shows an emmetropic eye with blur due to peripheral hyperopia.

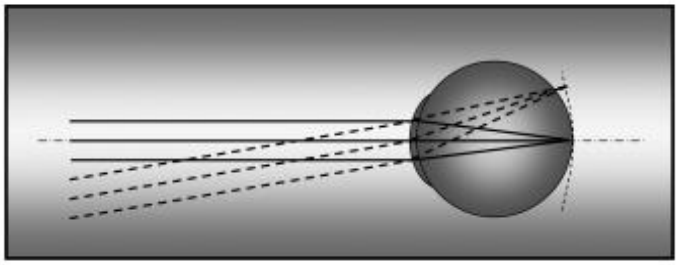

Figure 3.2. Emmetropic eye with blur due to peripheral hyperopia blurring (39).

3.2.1. Peripheral refraction and myopia

In recent years, peripheral refraction has gained importance by its alleged relationship with the emmetropization process and the development of myopia. Studies on animals have provided evidence that post-natal visual experience and non-foveal areas of the retina can affect refractive error development. The eye's growth is regulated by a homeostatic control mechanism but, unlike any other organ, vision is the principal input to guide ocular growth (10). Both growth and refractive development are regulated by visual feedback, which is associated with the refractive state of the eye. Present findings show that ocular growth evolves trying to keep images focused on the retina. Thus, as depicted in Fig. 3.3, if a negative lens places the ocular image behind the retina, and axial myopia will be induced by eye growth. Similarly, positive lenses, which place the image in front of the retina, reduce the ocular growth rate (40).

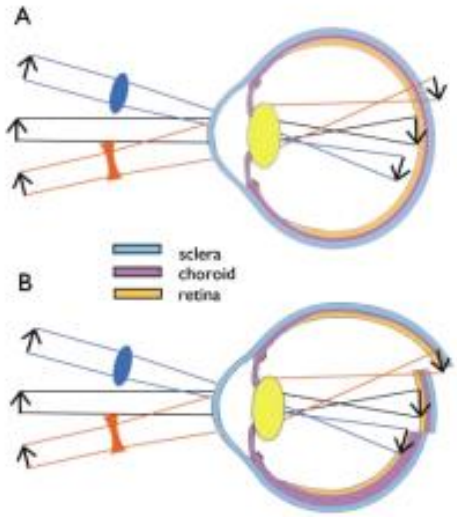

Figure 3.3. Ocular compensation for lens-induced defocus (10)

Emmetropization does not occur in animals which are left in total darkness (41,42), yielding a phenomena termed form-deprivation myopia. If instead of being defocused by lenses, the images on the retina are obscured by diffusers or lid suture, eyes tend to elongate. This response implies a direct relationship of ocular image quality with eye growth. An important aspect is that mechanisms involving the development of both form-deprivation myopia and lens-induced myopia are regulated locally within the eye. However, it should be mentioned that some studies have also found that the progression of axial myopia in children is not linked to peripheral optical quality (43,44), so the relationship of peripheral refraction and myopia should still be considered an hypothesis subject of active research.

Historically, it had been assumed that visual signals from the fovea dominate refractive development (45), but they are not essential for the phenomenon of form-deprivation myopia(46). However, the foveal area forms only a small fraction of the overall visual field and several studies show that eye growth can be regulated by different local regions of the retina(40). Visual signals from the periphery can override visual signals from the central retina and alter central refractive development. If there is integration of growth signals across the posterior globe, spatial summation factors may allow the peripheral retina to dominate central refractive development(10).

A recent study (47) corroborates the hypothesis that peripheral vision can influence eye shape and potentially central refractive error in a manner that is independent of central visual

experience. They determined if the effects of myopic defocus were integrated in a local manner in primates. Seven rhesus monkeys were reared with monocular spectacles that produced 3 diopters (D) of relative myopic defocus in the nasal visual field of the treated eye but allowed unrestricted vision in the temporal field. These monkeys exhibited compensating hyperopic changes in refractive error that were greatest in the nasal visual field. Other seven monkeys were reared with monocular +3D lenses that produced relative myopic defocus across the entire field of view which developed compensating hyperopic anisometropia, the degree of which was relatively constant across the horizontal meridian.

The key study that suggested a link between the pattern of peripheral refraction and development of myopia in humans was made by Hoogerheide (48). They found that the majority of pilots that developed myopia had skiagrams (peripheral refraction patterns) in which both sagittal and tangential oblique astigmatic image surfaces in either one or both of the horizontal semi-field meridians were relatively hyperopic (types I and III) in comparison to axial refraction (Fig. 3.4). This implies that the image surface corresponding to the mean spherical equivalent was also relatively hyperopic. Hoogerheide only studied late-onset myopia.

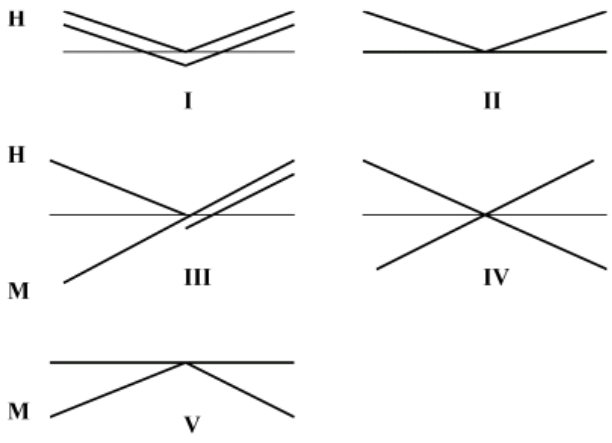

Figure 3.4. The common patterns of peripheral refraction across the horizontal meridian. On each skiagram, the thick lines show schematically the radial and tangential image fields across the horizontal meridian, H and M indicating whether the peripheral fields are hyperopic or myopic with respect to the axial refraction. (11).

However, Mathur and Atchison (49) studied skiagrams using the Hartmann-Shack technique for hypermetropes, myopes and emmetropes across 60º along the horizontal visual field. Thirty percent of eyes studied showed a pattern that was a combination of type IV and type I (Fig.3.4) which shows the characteristics of type IV (relative hypermetropia along the vertical meridian and relative myopia along the horizontal meridian) out to an angle of between 40 and 50 degrees before behaving like type I (both meridians show relative hypermetropia). They classified this pattern as type IV/I. A considerable portion of emmetropes with the IV/I pattern suggests that it is unlikely that refraction at visual field angles beyond 40 degrees from fixation contributes to myopia development.

Mutti et al. (50) proposed that a relative hyperopic refractive error may be a risk factor to be given a start and further development of myopia in children. Thus, if the image that occurs outside the visual axis is hyperopic respect to the peripheral retina, the growth of the eye will be accelerated to match the optical image with the peripheral retina, which will increase the axial length of the eye causing peripheral emmetropia but also foveal myopia (10,45,51–53). Conversely, if a relatively myopic peripheral refraction exists, the effect is a maintenance or development of a foveal hyperopia.

However, some studies also have found that relative peripheral refraction does not have a consistent effect on the risk of myopia onset (54,55)and it has been proposed that the development of peripheral hyperopia seems to be a consequence, rather than a cause, of myopia.

Although the basic hypothesis that a relatively hyperopic peripheral refractive error can lead to the development of human myopia remains subject of active discussion, the available data support the possibility of an interaction between the states of focus on the axis and in the periphery, and a reasonable doubt is set. Thibos(56) in a more recent study suggests that hyperopic blur is a risk factor only when the eye has a negative spherical aberration, because that is the combination leading to relatively low contrast in the defocused retinal image.

The hypothesis that a peripheral hyperopic refractive error is a risk factor for the development of myopia implies that the peripheral retina is sensitive to defocus and its sign and can generate a signal to control ocular growth. The ability of the peripheral visual system to detect focus change has been evaluated by studies of both depth-of–focus (57,58)and accommodation(59,60). There is good evidence to suggest that accommodation can be

induced by stimuli lying several degrees outside the central fovea, although with progressively reduced efficiency with eccentricity, and there is some evidence that peripheral accommodation may be less effective in myopes than emmetropes. Accommodation studies suggest that stimuli falling on the peripheral retina can alter the accommodation response of the eye and, in the presence of an axial accommodation target, can affect the response to the latter.

It is known that under-correction of myopia produces a greater degree of myopic progression than full correction(4,61). A recent study has reported the effect of over-, under- and full correction on peripheral refraction using contact lenses(62). It would be expected that contact lenses would change the peripheral refraction profile in a myopic or hyperopic direction compared with full correction. However, the shift between full and over-correction was slightly less than full and under-correction in both low and moderate myopes. This is probably due to accommodation with over-correction resulting in a slightly more myopic refraction measurement.

Smith (63) highlights five main reasons to focus on peripheral refraction to design treatments to control development of refractive error:

- Ocular growth and refractive development are regulated by visual feedback.
- The vision dependent mechanisms that regulate refractive development operate in a regionally selective manner.
- Visual signals from the fovea are not essential for many aspects of vision dependent growth.
- When conflicting signals exist between the central and peripheral retina, peripheral visual signals can dominate central refractive development.
- Refractive errors can vary with eccentricity and peripheral optical errors can alter central refractive development.

He also proposes an optical treatment based on providing optimal central vision while, at the same time, the field curvature of the image shell is increased in order to eliminate hyperopic peripheral visual signals while producing myopic peripheral signals to reduce axial growth (Fig. 3.5). This proposal represents a big difference with traditional ophthalmic lenses for myopia, which in general increase the degree of relative hyperopic peripheral defocus in myopic eyes pushing towards further progression of central myopic error (12,13) as will be

detailed in a next section. Traditional lenses are designed to provide perfect foveal vision for all directions of gaze, and their effect on peripheral refraction has never been taken into account until the very last years.

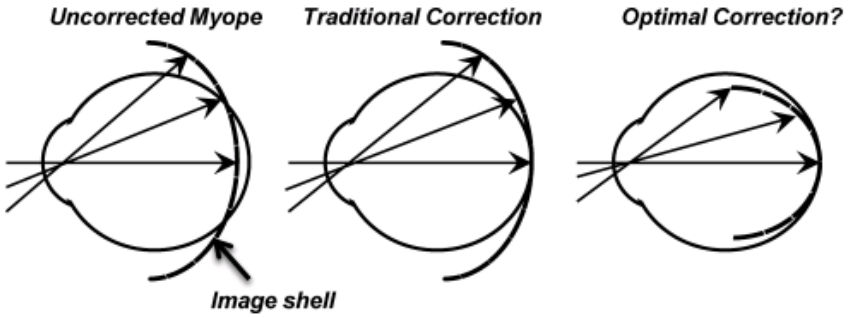

Figure 3.5. Schematic of the optical goals of a potential peripheral treatment strategy to slow the progression of myopia. The left image illustrates the position of the image shell for a distant object in a typical unaccommodated myopic eye. The middle image shows the image shell that traditional correcting lenses provide. The right image emphasizes that a fundamental goal of a peripheral treatment strategy would be to provide optimal central vision while at the same time eliminate peripheral visual signals that may stimulate the growth of the eye (63).

3.2.2. Measures of peripheral refraction

Multiple techniques have been proposed and used for the evaluation of peripheral refraction: subjective refraction, retinoscopy, manual optometers, the double-pass technique, photorefraction, wavefront sensors... Yet, from all the methods reviewed, the Shin-Nippon NVision K5001 open field autorefractor and the Hartmann-Shack wavefront sensor technique seem to be the most outstanding and useful commercially available instruments to measure peripheral refraction (39). But in recent years, faster instruments requiring no off-axis fixation, instrument rotation, or numerous realignments across one meridian have been proposed(64,65). One major advantage of these new instruments is the speed in measuring peripheral refraction and, based on the Hartmann Shack principle, they are able to assess both refractive errors and higher-order ocular aberrations across the visual field to assess the optical quality of the eye.

The concept of relative peripheral refraction (RPR) has been usually used in different studies and it refers to the difference between the refractive error measured in a point of the periphery

of the retina and the refractive error that exist in the fovea(52,67,68, 69,70). A positive RPR reflects an eye with more hyperopia in the periphery than in central vision. A negative RPR reflects an eye more myopic in the periphery.

Measures of peripheral refraction have usually been restricted to the horizontal visual field. Along this meridian different studies have demonstrated that the peripheral refractive error for a moderately myopic eye is a hyperopic shift relative to the fovea (positive RPR), while hyperopic eyes showed a myopic shift (negative RPR), and emmetropic eyes showed no relevant differences(50,66,68,69). However, Atchison et al.(66) measured peripheral refraction along the horizontal and vertical visual field for emmetropic and myopic eyes, finding that peripheral refraction profiles for the spherical equivalent (M) were different for the vertical visual field and for the horizontal visual field. For the horizontal field and for temporal visual angles beyond 20º to 25º and for nasal field angles beyond 5º the differences between peripheral and central refraction were significantly affected by the different values of M for central vision, while for the vertical field these differences were significantly affected by the central refraction M for a few visual angles only.

Another study by Chen at el(70) measured relative peripheral refractive errors at nasal, temporal, superior and inferior meridians of retina. Horizontally, they found a hyperopic shift for the myopic eyes studied, with a nasal-temporal asymmetry, with temporal retina showing greater shifts in comparison to nasal retina. For the vertical meridian, groups of people with different refractive errors demonstrated myopic defocus relative to the fovea, and there were no appreciable differences between the groups.

In a more recent study, Lee and Cho (67), measured eyes without correction biannually by an open-view autorefraction under cyclopegic. Peripheral refraction were measured along 10°, 20° and 30° from central fixation in both nasal and temporal fields. They found that hyperopic eyes showed relative peripheral myopia while myopic eyes had relative hyperopia across the central 60° horizontal field. Emmetropic eyes had relative myopia in the more central field, but showed relative hyperopia beyond the central 30° field. Emmetropic eyes demonstrate individual variations, ascribing symmetrical and asymmetrical patterns with different signs of RPR in different hemifields.

A study of the relationship between peripheral defocus and the progression of myopia using single lenses or progressive lenses (8), and a database of the refraction values in central vision

and in peripheral eccentricities of 30º for temporal, nasal and superior fields, and of 20º for the inferior field was obtained for uncorrected subjects. A significant difference was found between RPR values measured in the horizontal meridian of the eye when compared to RPR values in the vertical meridian of the eye. The mean RPR at each peripheral location was significantly different from zero, and in the horizontal meridian of the eye, the mean RPR was hyperopic in nasal and temporal retina, while the mean RPR was myopic in superior and inferior retina.

Recently, patterns of relative peripheral astigmatic refraction between progressing and stable myopes have been compared (14). Progressing myopes showed a hyperopic relative sagittal focus at 35 degrees in the nasal retina and stable myopes showed a myopic relative sagittal focus at the same eccentricity.

Although most studies measure peripheral refraction at discrete points across the retina, Tabernero et al developed an angular scanning photorefractor which allowed a continuous peripheral refractive error measurement.(64). Tabernero et al. obtained continuous refractions along the horizontal field for myopes and emmetropes, finding that myopic people appear to have a more irregular profile of refractive error than emmetropic individuals do.

Tabernero et al. used the angular scanning photorefractor to obtain refraction profiles on the horizontal field for the refractive error in the vertical pupil meridian. These refraction profiles were fitted with four different models proposed for the variation of refraction along the horizontal field. The peripheral refraction profile was best described by the so-called "box model" which considered a central area with a linear change in refraction from a certain peripheral angle (71).

Ehsaei et al.(72)measured peripheral refraction across the horizontal, vertical, and two oblique meridians in a group of myopic and emmetropic adults to obtain a more comprehensive understanding of the relation between peripheral and central refractive errors. Their experimental measures for myopic and emmetropic eyes will be considered in the development of this Thesis as example to obtain a model of the peripheral refractive error of the eye.

Mutti et al (9) also measured peripheral refraction, and then described ocular shapes on the basis of relative peripheral refraction. Relative peripheral hyperopia was measured in myopic children and interpreted as indicating prolate eye shapes, relative peripheral myopia was

measured in emmetropic children and interpreted as indicating near spherical or oblate eye shapes, and finally relative peripheral myopia was measured for hyperopic children and interpreted as oblate eye shapes. These inferences of eye shape based on peripheral refraction have appeared in many papers since.

Other studies have investigated eye shape by imaging techniques. Eye shape in these studies was mainly a comparison of one or both of height H and width W of the eye with the length L. Some referred to the eye shape in terms of ellipsoids, using prolate and oblate shapes to describe each particular case. Atchison et al (73) described the linear dimensions of emmetropic and myopic eyes using a clinical magnetic resonance imaging (MRI) scanner. Eye length was measured from anterior cornea to retina, and height and width were measured from retina to retina. There was a considerable intersubject variation, but the length of most emmetropic eyes (23.0±0.7 mm) was larger than its height (22.4±1.0mm) or width (22.7±0.9mm). As myopic refractive corrections increased, eyes became larger in all three dimensions, but more so in length (with a mean value of 0.35mm/D) than in height (0.19mm /D) and more so in height than in width (0.10 mm /D). Atchison (68) fitted nonrotationally symmetrical ellipsoids to retinal surfaces for emmetropic and myopic eyes using transverse axial and sagittal images derived from MRI data.

We have seen that different studies have evaluated patterns of peripheral refraction, parameters of ocular shape and parameters of retinal shape for different states of refraction (emmetropia, myopia, hyperopia). However, these concepts need be used with caution (74). Eye shape and eye retinal shape concepts are often used indiscriminately and are not equivalent. Deductions and inferences on the shape of the retina based on measurements of peripheral refraction need be taken with care. It is obvious that both the optics of the eye and the retinal shape will contribute simultaneously and significantly to peripheral refraction.

From all these studies, however, a number of conclusions can be obtained and are generally accepted. In summary:

- Myopic eyes usually have a relative hyperopia in the periphery of the fovea when compared to the central refractive error (positive RPR) although most measurements were taken only in the horizontal meridian.

- In the horizontal meridian there is an asymmetry with a relative hyperopia more pronounced on the temporal side compared to the nasal side. Myopic eyes usually have a more irregular profile of peripheral refraction than emmetropic eyes.

- It is difficult, if not impossible in practice, to establish a common pattern of peripheral refraction for all patients, due to a very large inter-subject variability, included patients with the same central refractive error.

- For our purpose, we will be interested in patterns of peripheral refraction, which have a relationship with ocular shape, but also with the performance of the optics of the eye.

Next section shows a review of studies where the effect of ophthalmic lenses in the periphery of the visual field was considered. New designs of ophthalmic lenses are proposed and some studies have evaluated their effect on the progression of myopia.

3.2.3. Peripheral refraction and ophthalmic lenses

The previous conclusions based on peripheral refraction as cause of progression of myopia push to reconsider the traditional method of ophthalmic lens design, which neglects the peripheral vision of the eye. It's now generally acknowledged that ophthalmic lenses have a very direct effect on both central and peripheral refraction, but generally, only the first one has been considered in traditional ophthalmic lens design.

The concept of correcting peripheral refraction with ophthalmic lenses is not new. Atchison (22) in his review of ophthalmic lens design refers briefly to a principle proposed which consists in designing ophthalmic lenses to correct the peripheral image of the eye and not only the foveal one. However, he suggests that due to the low peripheral resolution of the eye the effect may not be very relevant. However, recently, Atchison (75) designed and manufactured lenses to correct peripheral refraction along the horizontal meridian to determine if there were noticeable improvements in visual performance. He concluded that it is possible to design and manufacture lenses to give near-optimum peripheral visual performance to at least ± 30º along one visual field meridian.

Smith proposed a first method to design ophthalmic lenses which correct the peripheral refractive error of the eye (76). He also states that designing lenses to correct for peripheral

refractive errors is much more complicated that designing them to correct for foveal vision. For foveal vision, the designer wants to keep the true power of the lens over a range of angles and the design is not affected by differences between people (apart from fitting factors such as vertex distance and the center of rotation of the eye). To properly correct peripheral vision, a large number of effective powers will be required within the lens. Moreover, obviously there will be significant differences between people with the same foveal refractive error but with differences in the peripheral shape and optics of the eye.

In the same line, Smith presents that human eyes have very large refractive errors corresponding to large angles of peripheral vision, and presents data from a number of studies for mean sagittal and tangential error curves (Fig. 3.6).

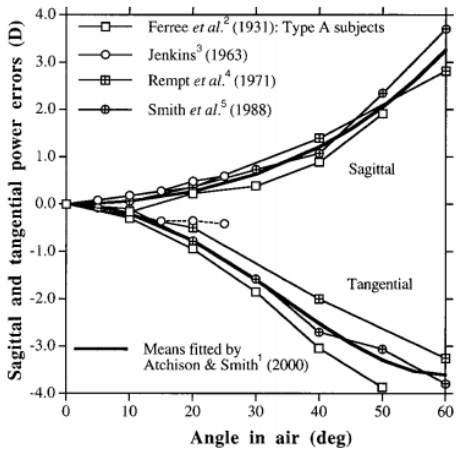

Figura 3.6. Mean values of sagittal and tangential power errors. Solid curves are mean values fitted by Atchison and Smith (77)

Thus, he proposes an ophthalmic lens design procedure based on the compensation of peripheral tangential and sagittal refractive errors of the eye on a meridian. For correcting tangential power errors, the surface shape is considered in Y-Z section only. To correct the sagittal power error the surface is considered in three dimensions. The lens obtained is in every local area equivalent to an astigmatic lens. Fig. 3.7 shows the interpretation of peripheral refractive error by tangential and sagittal focus in image and object spaces. Fig. 3.8 shows an ideal and an imperfect tangential correction by a lens.

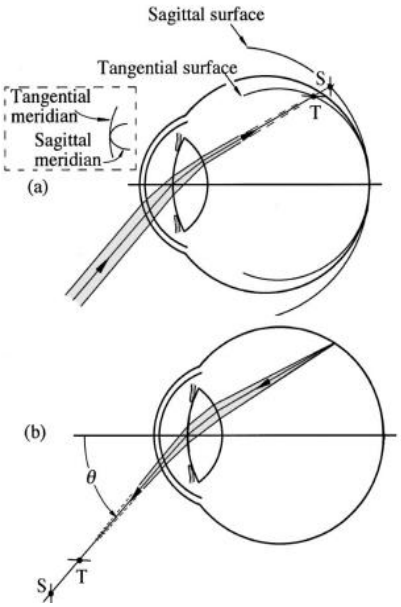

Figura 3.7. a) Sagittal and tangential errors. b) The sagittal and tangential object positions that would place the image at the retina. The vergences corresponding to these positions are the sagittal and tangential power errors as measured in object space. Both power errors are negative in this figure(76)

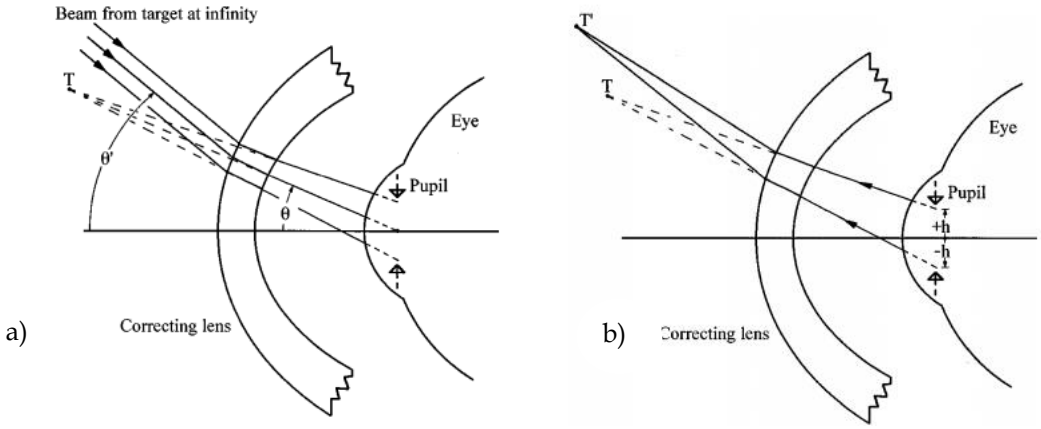

Figura 3.8. a) Ideal tangential compensation by a lens. A thin beam from infinity is refracted and imaged by the lens to the point T, which is conjugate to the retina in the tangential section. b) Imperfect compensation in the tangential section by the lens. The lens does not have the correct power at the refraction point. The point conjugate to T is T'. T' is at a finite distance but should be at infinity (76).

Smith considers that designing lenses to correct peripheral power errors is of little value if other aberrations are introduced. Thus, a good performance of the lens for an object field relatively wide (10º) around the design meridian is considered a requirement. The schematic eye developed by Navarro (78) is used to provide peripheral refractive-error values and

examples of lenses for the correction of the off-axis power errors of emmetropic, myopic and hyperopic eyes are proposed.

Besides, peripheral refractive error has gained relevance recently by the fact of the relationship between peripheral refraction and myopia and the proposal of Smith lenses has been taken one step beyond.

Some studies link peripheral defocus and compensatory methods of refractive error. New strategies for the prevention of the progression of myopia propose to manipulate focus off-axis to obtain the desirable amount of defocus in order to control eye growth as refractive treatments of orthokeratology and laser refractive surgery that produce peripheral myopic refractions for myopes (79–81). Other studies link contact lenses and peripheral refraction effects (62,82–84). However, neither contact lenses nor laser surgery are the most usual solutions for compensation of one very relevant group of population. Ophthalmic lenses are still (now and reasonably for many years) the most common method used in the compensation of myopic children and teenagers, which is the population where actions on eye growth to prevent the progression of myopia may be more relevant. Traditional ophthalmic lenses are designed to provide a perfect foveal vision for all directions of gaze, but their effect on peripheral refraction hasn't been taken into account until very recently(85–87).

The objective is not to obtain a perfect correction of the peripheral errors of the eye, as before; but to induce a myopic defocus in the periphery of the eye. It is intended to control the progression of myopia using systems which provide to the eye a stimulus which delays the progression of myopia by repositioning properly the peripheral off-axis focal points relative to the retina.

Different studies show that traditional ophthalmic lenses generally induce a hyperopic defocus in the periphery of myopic eyes. Tabernero et al.(12) use an optimized photorefractor to measure peripheral refractive errors in the vertical pupil meridian on the horizontal visual field (from -45º to 45°) in patients with myopia both with and without ophthalmic lenses correction (Fig. 3.9). They found significant hyperopia when patients used their conventional lenses in the periphery of their visual field. This induced hyperopia was variable, but there was hardly ever observed a case of lens-induced myopia.

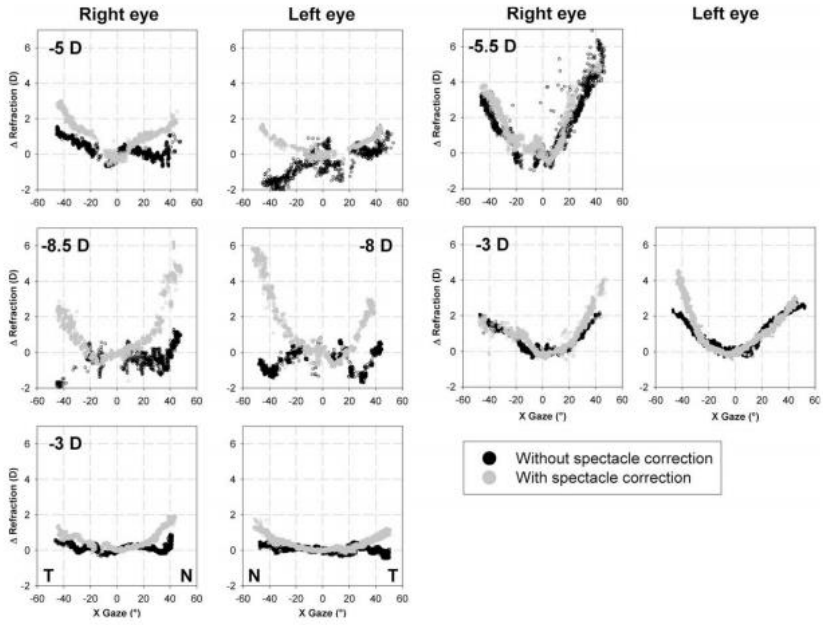

Figure 3.9. Refraction in the vertical pupil meridian measured at different angular positions on the horizontal field correction using ophthalmic lenses (gray symbols) and without them (black symbols). The left eye of patient number 4 could not be measured because of the small pupil diameter(12)

In the same paper another radial refractive gradient lens (RRG lens) which induces myopia in radial directions from the center was presented and tested. This lens was optimized to maintain clear foveal vision in the optical center while presenting a steady increase of positive power in all radial directions. Since the lenses were intended to be used in different subjects with potentially different retinal geometries, the refractive profile was designed and measured in relation to the Far Point Sphere and the Vertex Sphere (10) and not to a given retinal surface. Values of peripheral refraction without lenses and with RRG lenses were obtained and compared. These values can be seen in Fig. 3.10. Lenses may be shown to make subjects more myopic in the periphery of their visual field.

The fact that ophthalmic lenses are the most common method used to correct myopia in children and young adults drove Bakaraju et al.(88) to make a theoretical study of the pantoscopic angle effect on peripheral refraction (Fig.3.11), since this parameter was not taken into account and may have special importance. Using Zemax, they traced finite rays through optical systems that were combinations of ophthalmic lenses and myopic eye models. The three models chosen were myopic eyes of -3.00D, -6.00D and -9.00D constructed out of Atchison's eye model (89). The ophthalmic lenses had a base of 1.00D and a central thickness of 1.5mm. The second lens surface changed to obtain the necessary back vertex power of a vertex distance of 12mm. The refractive index of the lens was equivalent to CR39 polymer.

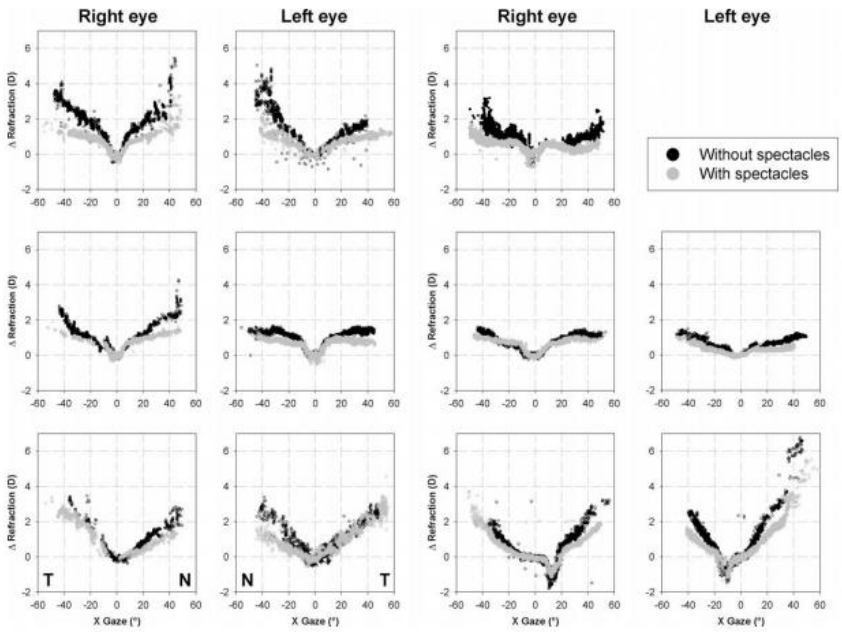

Figure 3.10. Refractions in the vertical pupil meridian measured at different angular positions with horizontal lens correction by RRG (gray) and without it (black) (12)

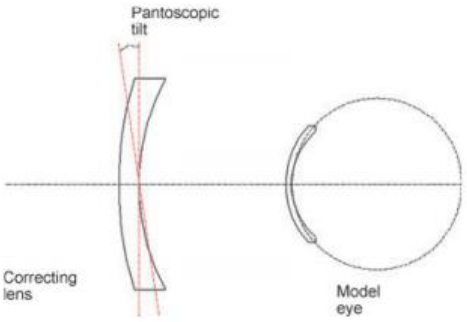

Figura 3.11. Pantoscopic angle for an ophthalmic lens (88)

The proposed models of myopic eyes without correction showed a profile with a spherical equivalent of peripheral refraction towards hyperopia increasing with angle when the eye had moderate or high myopia. For low myopia, the profile was relatively myopic. When the ophthalmic lens is introduced the peripheral refraction profiles recalculated for these models showed that there was a uniform change in spherical equivalent towards hyperopia in both vertical and horizontal meridians. Moreover, when the lens is tilted a pantoscopic angle there is a uniform change in spherical equivalent towards hyperopia. Higher degrees of tilt of high

myopic prescriptions seem to produce considerable non-uniform, hyperopic shifts of up to 1.50D, and reasonable amounts of astigmatism (nearly 2–3D).

Lin et al (13) related the use of single vision lenses to correct myopia and its impact on peripheral blurring. They studied a group of twenty-eight Chinese children aged between 8 and 15 years, with a refraction between -0.75D and -6.00D and astigmatism up to 1.00D. The central and peripheral refraction was measured using an autorefractometer NVision K5001, which was modified to present different fixation eccentricity points. The measures of refraction were made at 0, 20, 30 and 40° in both the nasal and temporal retina. These measurements were made both with and without correction. The base curve of the lenses used is shown in Table 3.1:

Table 3.1 Base curve of the different lenses used to correct refractive error (13).

n 1.595	Lens power	Base curve(D)
Spherical lenses	-1.00	+4.27
	-1.50	+4.27
	-2.00	+3.70
	-2.50	+3.98
	-3.00	+3.70
	-3.50	+3.13
	-4.00	+2.84
Spherocylindrical lenses		+3.41

Children were divided into two groups: those who had low myopia (between -0.75 D to -3.00D included) and those who had moderate myopia (-3.25D to -6.00D included). When children didn't use ophthalmic lenses they showed a relative hyperopia in the horizontal peripheral retina. When the eyes were corrected by monofocal lenses there was an absolute hyperopia in the periphery. If the magnitude of this hyperopia is compared between uncorrected and corrected eyes, monofocal lenses may be seen to increase the amount of blur in hyperopic eyes with moderate myopia (Fig. 3.12).

New designs of ophthalmic lenses to reduce peripheral hyperopic defocus and their effect on the progression of myopia have been tested. Sankaridurget al(86) studied the effect of three novel spectacle lens designs to in children aged 6 to 16 years. These novel designs were intended to reduce peripheral hyperopic defocus. Two designs were rotationally symmetrical. The first design had a progressively ramped zone of increasing positive power surrounded the central aperture with a maximum spherical equivalent of +1.00D relative peripheral power.

The second featured a central aperture of 14mm and a maximum spherical equivalent of +2.00D relative peripheral power. The other design was asymmetric with a clear central aperture of 10mm either side of center along the horizontal meridian and a similar distance below to provide clear vision for convergence and down-gaze.

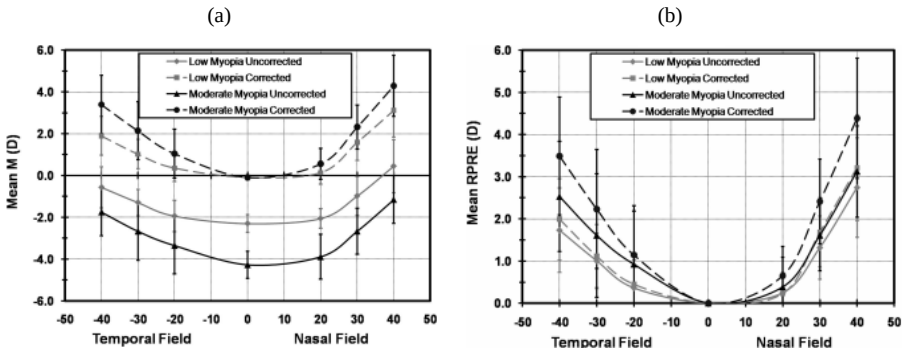

Figura 3.12. a) Spherical equivalent change in the horizontal meridian of the eye with and without compensation according to whether it is low or moderate myopia. b) Relative peripheral refractive error (relative to the fovea) both for low myopia and moderate myopia with and without correction. The hyperopic shift that occurs with eccentricity with and without correction when myopia is low is very small. However, when myopia is high, the change that occurs is as significant in the nasal field(13).

The three new designs and a conventional design were used in the study. There were no statistically significant differences in the rates of progression of myopia between eyes wearing novel designs to those wearing conventional ones. For a subgroup of younger children a reduction of the speed of progression was observed in the asymmetric design. These children had a parental history of myopia, but the mechanism of action by which the novel designs reduced myopia progression is unclear. In this study the manipulation of the peripheral image was not personalized. The peripheral hyperopic defocus considered was the average found in different studies by myopic populations.

Berntsen (8) studied the association between peripheral defocus and the 1-year change in central myopia. They compared effect of hyperopic RPR and myopic RPR using single vision lenses (SVLs) and progressive addition lenses (PALs) on myopic eyes in the evaluation of progression of myopia. They measured that single vision lenses caused a hyperopic shift in peripheral defocus at the four locations measured. Progressive addition lenses caused a myopic shift in peripheral defocus in three of four locations measured with the greatest shift superiorly due to the PALs addition. Measurements were made centrally, 30º nasally, temporally, and superiorly, and 20º inferiorly on the retina using a Complete Ophthalmic

Analysis System for Vision Research (COAS-VR). They found an association between superior retinal defocus and one year change in refractive error showing that children with myopic superior defocus using PALs has a reduction in myopia progression compared with children with a hyperopic superior defocus using SVLs. The Correction of Myopia Evaluation Trial (COMET)(90) was a clinical trial specifically designed to evaluate whether PALs might slow the rate of progression of juvenile-onset myopia, when compared to conventional correction with SVLs. The main hypothesis behind was that increased retinal defocus was a factor in the pathogenesis of myopia, so children with insufficient accommodation in near-work may present a retinal defocus which can be reduced by PALs. However, this defocus was considered as affecting foveal vision, essentially. It should be noted how this very recent study presents an alternative explanation of the pathogenesis of myopia progression, where peripheral defocus plays a key role.

In a different approach to the ophthalmic lens design problem, Atchison (91) used third-order equations to yield lens forms that correct peripheral power errors, either for the lenses alone or in combination with typical peripheral refractions of myopic eyes. Atchison introduced how peripheral refraction could be manipulated by altering the forms of spectacle lenses. The calculations are based on third-order theory to determine off-axis power errors of thin spectacle lenses. Negative lenses are considered as thin lenses and the third-order theory is based on tracing paraxial chief rays through an effective stop situated at the entrance pupil of the eye, and applying classical Coddington equations to these chief rays.

Atchison analyzes two extreme cases: the foveal and the totally peripheral case. They are extreme examples of the situation during spectacle lens wear. Lenses designed to correct peripheral refractive errors produced large errors when used with foveal vision and a rotating eye. It's shown how when only spherical lens forms are used, correction of the relative hyperopic peripheral refraction values observed experimentally is not possible in the vast majority of myopic cases.

He also proposes equations for power errors in peripheral vision which include the eye. The off-axis power errors of lenses for the rotating eye and in foveal vision can be considered regardless of the eye, except for the position of the effective stop. This is not the case for the power errors in peripheral vision, as the peripheral power errors are directly influenced by the retinal surface shape. Peripheral refractions are included in the equations, and the combined refraction obtained from lens and eye is obtained.

The study gets limited to the use of third-order theory, which does not give the same solutions as a finite ray-tracing, with the errors becoming larger as the peripheral angle increases. However, it provides a useful framework for showing how field aberrations are affected by the lens-design parameters.

Latest studies even suggest that the extension of the optical field that is manipulated influences the effectiveness of the treatment (92). Most studies have into account what occurs only on some points of the horizontal field of vision and other points are forgotten.

In the rest of this Thesis, we will propose a method to calculate the exact value of IPR by an ophthalmic lens across the full field of vision for a particular eye, having into account the particular profile of peripheral refraction in each case. To do this, we follow the next steps:

- We will develop, validate and test an exact ray trace procedure to evaluate lens performance using efficient computation methods (Section 4).
- We will propose an exact tracing method for the calculation of the IPR by an ophthalmic lens, based on the concept of RCS, either modeled from experimental data or from theoretical models. Such methods allow to obtain the peripheral refraction of the eye at all directions of gaze, and allows to calculate the IPR when an ophthalmic lens is used to compensate the central refractive error (Section 5).

4. Ray tracing in ophthalmic lenses

This section presents the general theoretical concepts behind the ray tracing procedure used to evaluate the ophthalmic lens performance. These concepts will be implemented and validated to build a solid basis for Section 5, where this methodology will be adapted to the evaluation of peripheral refraction.

The general equations for the propagation of the principal ray (based on FRT) and its associated local wavefront (calculated as GRT) will be introduced. However, we will start this Section with a brief theoretical introduction to the geometry of surfaces and their parameterization, as both the wavefront and the refractive surfaces of the lens need to be precisely described in order to proceed with the GRT procedure. Next, the theoretical approach for FRT and GRT will be exposed. For GRT we will consider the approach proposed by (33) introduced in Section 3, which makes use of the description of a pencil of light composed by a principal ray and the wavefront in its vicinity. This configuration will be useful for our purpose to evaluate the local and global ophthalmic lens performance, that later will be related to peripheral refraction and potentially to the progression of myopia. The classical scheme of ophthalmic lens design, which evaluates the lens performance for different directions of gaze (Fig.2.5) will be used to apply and validate the ray tracing method proposed. Once the theoretical approaches to the ray tracing procedures are presented, they will be implemented under a general programming environment (Matlab), and a detailed example using an astigmatic ophthalmic lens will be developed. Finally, results obtained using the presented methodology for spherical, aspheric and astigmatic ophthalmic lenses will be calculated and discussed.

4.1. Geometric properties of the surfaces. Parametrization of spherical, aspherical and toroidal surfaces.

As commented, both the wavefront which propagates through the optical system and the different surfaces forming the ophthalmic lens need be described locally with precision. We are thus interested in the geometrical properties of the surfaces in the neighborhood of the point of intersection of the ray with the optical surface.

The ray tracing procedures we will apply require (due to Snell's law) to calculate the vector normal to the surface at one of its points, and also the local calculation of the associated

geodesic curves and its directions at this point. The maximum and minimum values of the curvature of a normal section of the surface are called the principal curvatures, or geodesics, of the surface at the chosen point. These two curvatures are oriented in directions termed principal directions and these two directions are perpendicular to each other in all cases(93).

Entering in detail, each surface in the Euclidean space R^3 can be defined locally by an equation with two parameters *u* and *v*. The result is an expression named local parametric representation of the surface (94):

$$\boldsymbol{s}(u,v) = (x(u,v), y(u,v), z(u,v)) \tag{4.1}$$

The normal and differential geometric invariants, such as the first and second fundamental forms of Gauss, can be computed from a given parameterization of the surface (94). These first and second fundamental forms make possible the calculation of the principal curvatures and its directions at a particular point of the surface. Its calculation will be introduced next.

The unit normal vector to the surface at one point of the surface will be given by:

$$\boldsymbol{n} = \left(\boldsymbol{s}_u \times \boldsymbol{s}_v\right) / \left[\left(\boldsymbol{s}_u \times \boldsymbol{s}_v\right)^2\right]^{1/2} \tag{4.2}$$

Where $\boldsymbol{s}_u$ and $\boldsymbol{s}_v$ stand the surface partial derivatives respect to *u* and *v*.

We define

$$E = \boldsymbol{s}_u^2 \quad F = \boldsymbol{s}_u \cdot \boldsymbol{s}_v \quad G = \boldsymbol{s}_v^2 \tag{4.3}$$

so the expression

$$I = Edu^2 + 2Fdudv + Gdv^2 \tag{4.4}$$

is called the first fundamental form, and, *E*, *F*, and *G* are called the first fundamental quantities.

We now can consider

$$e = \boldsymbol{n} \cdot \boldsymbol{s}_{uu}, \quad f = n \cdot \boldsymbol{s}_{uv}, \quad g = \boldsymbol{n} \cdot \boldsymbol{s}_{vv} \tag{4.5}$$

And equivalently define the expression

$$II = edu^2 + 2\,fdudv + gdv^2 \tag{4.6}$$

Which is called the second fundamental form, and e, f and g the second fundamental quantities.

We now can write the matrix

$$\boldsymbol{A} = \frac{1}{EG - F^2}\begin{pmatrix} e & f \\ f & g \end{pmatrix}\begin{pmatrix} G & -F \\ -F & E \end{pmatrix} \tag{4.7}$$

or

$$\boldsymbol{A} = \frac{1}{EG - F^2}\begin{pmatrix} eG - fF & -eF + fE \\ fG - gF & Eg - fF \end{pmatrix} \tag{4.8}$$

This matrix contains a very relevant information on the surface, as far as the principal curvatures of the surface at a given point can be calculated as the eigenvalues of $\boldsymbol{A}$, and the associated principal directions as its eigenvectors (94).

Such expressions make simple to locally analyze any geometry for the lens surface, given the partial derivatives are known. These local partial derivatives may be computed from the parametric form of the surface. We will use them to calculate the normal and principal curvatures and their directions on the refractive surface at the point of incidence of the ray considered, allowing then to apply the GRT equations presented in Section 4.3 to obtain the refracted wavefront. Such wavefront will be also characterized by its principal curvatures and their directions, as the description of the geometry of the wavefront at the neighborhood of the principal ray. How the curvatures of the wavefront change along the transfer and refraction processes will be described by the GRT equations.

Due to the relevance of the topic, we will briefly introduce the description of the surfaces used in this thesis. We will only work with spherical, aspherical and toroidal surfaces, for the sake of simplicity, although the method for free-form surfaces is equivalent once the fundamental forms are obtained. The first two surfaces are axially symmetric, and will be parameterized using a cartesian coordinate system. Toroidal surfaces have not such a degree of symmetry and will be parameterized using polar coordinates.

Centered axially symmetric surfaces generated by revolution around *Z* axis can be described in a parametric equation as (34):

$$z = z(x, y) = z(x^2 + y^2) \tag{4.9}$$

We have selected the two independent coordinates *x* and *y* as parameters. All the equations described before can be applied here, and only *u* and *v* must be replaced by *x* and *y* in this case.

The general equation for an axially symmetric surface then becomes:

$$\boldsymbol{s} = \left[x, y, z\left(x^2 + y^2\right) \right] \tag{4.10}$$

Although *z* is really a function of a single variable

$$z = z(u) \tag{4.11}$$

Where

$$u = \frac{1}{2}\left(x^2 + y^2\right) \tag{4.12}$$

Let us denote the derivative of *z* with respect to *u* by simply *z*'. Then the first and second derivatives of $\boldsymbol{s}$ may be shown to be:

$$\boldsymbol{s}_x = (1, 0, xz') \quad \boldsymbol{s}_y = (0, 1, yz') \tag{4.13}$$

$$\boldsymbol{s}_{xx} = \left(0, 0, z' + x^2 z''\right) \quad \boldsymbol{s}_{xy} = (0, 0, xyz'') \quad \boldsymbol{s}_{yy} = \left(0, 0, z' + y^2 z''\right) \tag{4.14}$$

And we can get the first fundamental quantities from Eq.4.3 as

$$E = 1 + x^2 z'^2 \tag{4.15}$$

$$F = xyz'^2 \tag{4.16}$$

$$G = 1 + y^2 z'^2 \tag{4.17}$$

In addition, we define

$$K^2 = EG - F^2 = 1 + 2uz'^2 \tag{4.18}$$

So the unit vector normal to the surface is:

$$\boldsymbol{n} = -(xz', yz', -1)/K \tag{4.19}$$

And using Eq.4.5, the second fundamental quantities are obtained:

$$e = z' + x^2 z'')/K \tag{4.20}$$
$$f = xyz''/K \tag{4.21}$$
$$g = (z' + y^2 z'')/K \tag{4.22}$$

Using the matrix defined by Eq.4.8, it is straightforward to find the unit vector in the principal directions, and the associated principal curvatures.

In our case the refracting surface can be a special case of the general surface of revolution, as it is a conic surface, where the value of z and its derivatives are known:

$$z = \frac{2cu}{\left\{1 + \left[1 - 2c^2(1-\varepsilon^2)u\right]^{1/2}\right\}} \tag{4.23}$$

$$z' = \frac{c}{\left\{\left[1 - 2c^2(1-\varepsilon^2)u\right]^{1/2}\right\}} \tag{4.24}$$

$$z'' = \frac{c^3(1-\varepsilon^2)}{\left\{\left[1 - 2c^2(1-\varepsilon^2)u\right]^{3/2}\right\}} \tag{4.25}$$

Where ε being the eccentricity of the curve. This eccentricity is related with the parameter p (asphericity) by:

$$\varepsilon = \sqrt{1-p} \quad p \geq 0 \tag{4.26}$$
$$\varepsilon = \sqrt{1+p} \quad p \leq 0 \tag{4.27}$$

And the spherical surface is the special case when p=0.

Finally, for spherical and aspherical surfaces, the value of K (Eq.4.18) may be written as

$$K^2 = (1+2c^2\varepsilon^2 u)/[1-2c^2(1-\varepsilon^2)u] \tag{4.28}$$

Where the parameter *c* is the curvature at the vertex of the surface.

For the case of the toroidal surface, we will use a parameterization based on polar coordinates. A torus centered at the posterior vertex of the lens has been considered (see Fig. 4.1). It has two orthogonal radius of curvature *R* and *r*, situated at 180º and 90º respectively. The difference between these radius expressed in diopters is the cylindrical power of the lens, usually known as its cylinder.

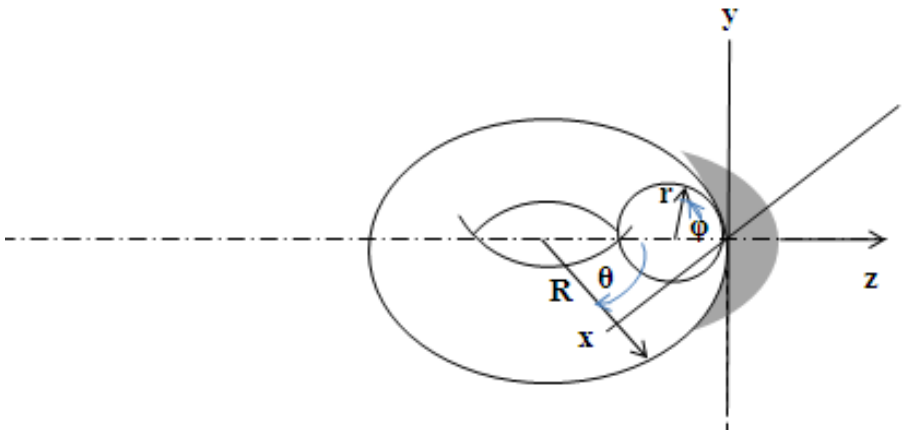

Figure 4.1. For the description of the astigmatic lens, a toroidal surface is situated at the posterior vertex of the lens, with two radius of curvature, R and r. Angles φ and θ will be used in the parametric equation in polar coordinates.

The parametric equation in polar coordinates for this surface may be shown to be

$$s = \begin{Bmatrix} x = (R - r + r\cos\varphi)\sin\theta \\ y = r\sin\varphi \\ z = -R + (R - r + r\cos\varphi)\cos\theta \end{Bmatrix} \tag{4.29}$$

where $0 \le \varphi \le 2\pi$ and $0 \le \theta \le 2\pi$ and *R* and *r* are considered as absolute values. The normal vector to the surface, ***n*** can be calculated using Eq.4.2, where *u* and *v* are now considered as θ and φ. This enables to obtain:

$$\boldsymbol{n} = (\sin\theta\cos\varphi), \sin\varphi, (\cos\theta\cos\varphi)) \tag{4.30}$$

The first and second Gauss fundamental forms of the toroidal surface (Eq.4.3 and 4.5) are, respectively:

$$E = \left(R - r + r\cos^2\varphi\right) \tag{4.31}$$

$$F = 0 \tag{4.32}$$

$$G = r^2 \tag{4.33}$$

and

$$e = -\left(R - r + r\cos\varphi\right)\cos\varphi \tag{4.34}$$

$$f = 0 \tag{4.35}$$

$$g = -r \tag{4.36}$$

Again, the use of these fundamental forms enable to obtain the principal curvatures of the surface and the principal directions of the surface at the point of intersection of the ray using the eigenvalues and eigenvectors of matrix ***A*** (Eq. 4.8). The spherical case is also contemplated here, as a particular case when $r=R$.

4.2. Theoretical approach to finite ray tracing

Let *S* be a surface that separates two media of constant refractive index *n* and *n*'. An incident ray, with a direction vector ***r*** , intercepts the refracting surface at some point *P*, giving rise to a refracted ray whose direction vector is ***r***' (Fig. 4.2).

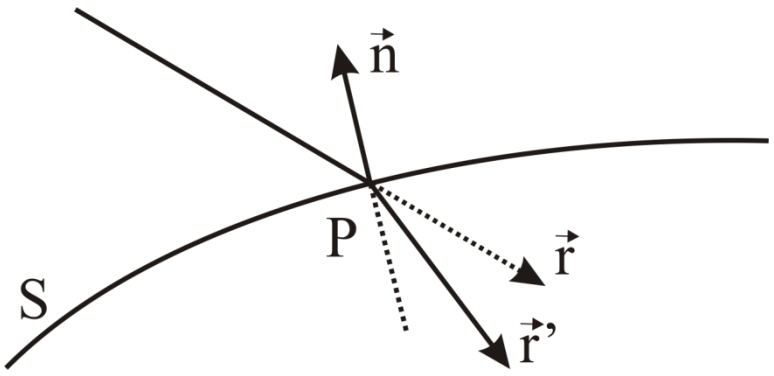

Figure 4.2. Outline for ray tracing.

The relationship of the incident and refracted ray and ***n***, the unit normal to the refracting surface at *P*, is given by the vector form of Snell's law:

$$n'(\boldsymbol{r}'\times\boldsymbol{n}) = n(\boldsymbol{r}\times\boldsymbol{n}) \tag{4.37}$$

or

$$\boldsymbol{r}'\times\boldsymbol{n} = \mu(\boldsymbol{r}\times\boldsymbol{n}) \tag{4.38}$$

Where μ is the ratio of the refractive indexes.

The well-known scalar version is thus simply:

$$\sin i' = \mu \sin i \tag{4.39}$$

Where i and i' are the angles of incidence and refraction.

From the vector form we have

$$(\boldsymbol{r}' - \mu\boldsymbol{r})\times\boldsymbol{n} = 0 \tag{4.40}$$

So the vectors $(\boldsymbol{r}'-\mu\boldsymbol{r})$ and $\boldsymbol{n}$ are parallel. Therefore, a scalar quantity γ such that $(\boldsymbol{r}'-\mu\boldsymbol{r}) = \gamma\boldsymbol{n}$. may be found. The direction of the refracted ray can then be expressed as a linear combination of the incident ray vector and the normal to the surface at *P:*

$$\boldsymbol{r}' = \mu\boldsymbol{r} + \gamma\boldsymbol{n} \tag{4.41}$$

This equation is the vector form for refraction, where γ may be determined as

$$\gamma = \mu(\boldsymbol{r}\cdot\boldsymbol{n}) + \left\{1 - \mu^2[1-(\boldsymbol{r}\cdot\boldsymbol{n})^2]\right\}^{1/2} = -\mu\cos i + \cos i' \tag{4.42}$$

The path through the ophthalmic lens of the different rays will be calculated in this Thesis with FRT using Eq.4.41, both in the concave and convex surface of the lens. This enables the evaluation of the performance of the lens on a ray by ray basis in the three-dimensional space. However, the cumbersome process of tracing a dense ray matrix of rays through the lens is simplified using the concepts behind GRT.

4.3. Theoretical approach to generalized ray tracing

GRT takes advantage of the fact that the wavefront associated with each ray traced though the optical system has well defined geometric properties. Generally speaking, such a wavefront

will have two principal directions and two different principal curvatures at the point where the ray intercepts the wavefront, being thus a surface described in comparable terms to those presented in 4.1. GRT explains what happens to the principal directions and curvatures of such a wavefront after transfer from one surface to the next, and after refraction on a surface such as that on Fig.4.2(33,34,95). For transfer the approach is quite simple, as it can be shown that the principal directions of the wavefront are unchanged and the centers of curvature stay fixed for each position of the wavefront.

Refraction, however, is a more interesting issue. Let *W* and *W*' represent the incident and refracted wavefronts, respectively. Let ***r*** and ***r***' represent the direction vectors of an incident and a refracted ray. Let *P* be the point of intersection of these rays on the refracting surface *S* and let the normal to the refracting surface at that point *P* be ***n***. We next introduce three different coordinate systems associated with the incident wavefront, the refracting surface, and the refracted wavefront (Fig. 4.3).

Let's define a unit vector ***p*** such as

$$\boldsymbol{p} = \frac{\boldsymbol{r} \times \boldsymbol{n}}{\sin i} \tag{4.43}$$

p is thus perpendicular to ***r***, ***n*** and ***r***'. In other words, ***p*** is perpendicular to the plane of incidence. Moreover, since ***r*** is perpendicular to *W*, ***n*** to *S*, and ***r'*** to *W*', ***p*** is a tangent vector to the two wavefronts and also to the refracting surface.

(a) (b)

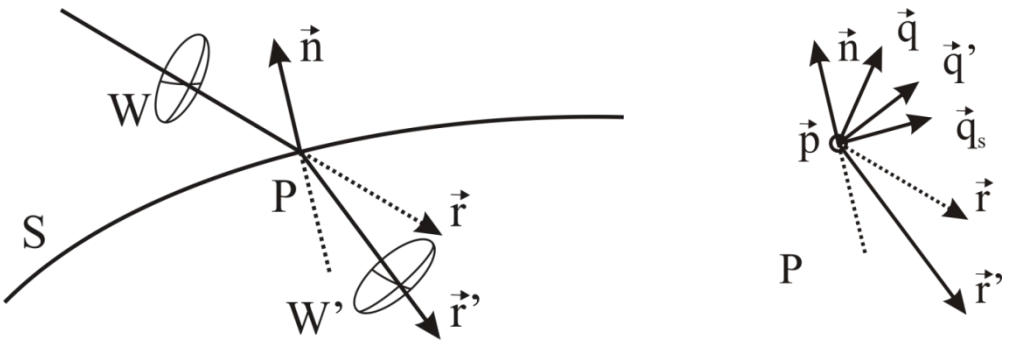

Figure 4.3. GRT basics; a) Representation including the incoming and outgoing wavefronts W and W' of a ray incident at P on a surface with normal **n**; b) Representation of the full set of vectors involved in the calculations at P, the point of incidence. ***p*** is a vector normal to the incidence plane (the paper).

We then define three additional unit vectors,

$$\boldsymbol{q} = \boldsymbol{r} \times \boldsymbol{p} \tag{4.44}$$

$$\boldsymbol{q}_s = \boldsymbol{n} \times \boldsymbol{p} \tag{4.45}$$

$$\boldsymbol{q}' = \boldsymbol{r}' \times \boldsymbol{p} \tag{4.46}$$

each perpendicular to $\boldsymbol{p}$ and each tangent to the appropriate surface (the incident wavefront, the surface, and the refracted wavefront, respectively). We now have three orthogonal unit vectors associated with each surface:

$$W : \boldsymbol{r}, \boldsymbol{p}, \boldsymbol{q} \qquad S : \boldsymbol{n}, \boldsymbol{p}, \boldsymbol{q}_s \qquad W' : \boldsymbol{r}', \boldsymbol{p}, \boldsymbol{q}' \tag{4.47}$$

Each set of vectors are orthogonal, and then, for the vectors in *W*:

$$\boldsymbol{q} = \boldsymbol{r} \times \boldsymbol{p} \qquad \boldsymbol{r} = \boldsymbol{p} \times \boldsymbol{q} \qquad \boldsymbol{p} = \boldsymbol{q} \times \boldsymbol{r} \tag{4.48}$$

and equivalently for the other surfaces of interest. The pair of principal curvatures of the incident wavefront *W*, of the refracted wavefront *W'*, and of the surface *S* are labeled as $\rho_\xi, \rho_\eta, \rho'_\xi, \rho'_\eta, \rho_{\xi s}, \rho_{\eta s}$, respectively. The directions of these principal curvatures are given by the vectors ***t, t'*** and $\boldsymbol{t}_s$, assuming these vectors indicate the direction of the ξ curvature in each surface, while the η curvature will lay in the perpendicular direction to ***t***, ***t***' and $\boldsymbol{t}_s$ in the proper surface. The angles between the vectors ***t, t'*** and $\boldsymbol{t}_s$ and ***p*** are θ, θ' and θ_s, which are given by:

$$\cos\theta = \boldsymbol{t} \cdot \boldsymbol{p} \qquad \cos\theta' = \boldsymbol{t}' \cdot \boldsymbol{p} \qquad \cos\theta_s = \boldsymbol{t}_s \cdot \boldsymbol{p} \tag{4.49}$$

Then, the normal curvatures relative to the defined coordinate systems and the torsion for the incident wavefront are defined by (33,93):

$$1/\rho_u = \left(1/\rho_\xi\right)\cos^2\theta + \left(1/\rho_\eta\right)\sin^2\theta \tag{4.50}$$

$$1/\rho_v = \left(1/\rho_\xi\right)\sin^2\theta + \left(1/\rho_\eta\right)\cos^2\theta \tag{4.51}$$

$$\left(2/\sigma\right) = \left(1/\rho_\xi - 1/\rho_\eta\right)\sin^2 2\theta \tag{4.52}$$

Where ρ_u is the curvature of the incident wavefront along the ***p*** direction, ρ_v is the curvature of the incident wavefront along the ***q*** direction, and σ is the related torsion, that is, a

parameter describing what is missing from the curve to be contained on a plane, i.e, to be a flat curve. Obviously, the inverse relationships may also be obtained. Considering only the incident wavefront, given its curvatures relative to the defined coordinate system and its torsion σ, the principal curvatures of the wavefront and the angle θ between the vector $\boldsymbol{t}$ and $\boldsymbol{p}$ may be calculated from:

$$1/\rho_{\xi} = (1/\rho_u)\cos^2\theta + (1/\rho_v)\sin^2\theta + (2/\sigma)\sin\theta\cos\theta \tag{4.53}$$

$$1/\rho_{\eta} = (1/\rho_u)\sin^2\theta + (1/\rho_v)\cos^2\theta - (2/\sigma)\sin\theta\cos\theta \tag{4.54}$$

$$\tan 2\theta = (2/\sigma)(1/\rho_v - 1/\rho_u) \tag{4.55}$$

The vector $\boldsymbol{t}$ is then:

$$\boldsymbol{t} = \boldsymbol{p}\cos\theta + \boldsymbol{q}\sin\theta \tag{4.56}$$

Likewise, if the curvatures of the refracting surface ρ_{us} and ρ_{vs} are known the principal curvatures of the surface may be computed from than expression equivalent to Eqs (4.53) to (4.55). The same situation occurs in the refracted wavefront, where ρ'_u and ρ'_v enable the calculation of θ' and ρ'_{ξ} ρ'_{η}.

Now, the set of generalized ray tracing equations can be presented. These equations are obtained from the directional derivative of the vectorial form of Snell's law and from the Frenet equations for space curves (34). GRT equations provide the refracted wavefront curvatures along $\boldsymbol{p}$ (ρ'_u) and on the $\boldsymbol{q}$ direction (ρ'_v) and σ', the torsion of the refracted wavefront, starting from the equivalent values in the incident wavefront:

$$1/\rho'_u = \mu/\rho_u + (\gamma/\rho_{us}) \tag{4.57}$$

$$\cos i'/\sigma' = (\mu\cos i/\sigma) + (\gamma/\sigma_s) \tag{4.58}$$

$$\cos^2 i/\rho'_v = (\mu\cos^2 i/\rho_v) + (\gamma/\rho_{vs}) \tag{4.59}$$

Thus, calculation of the geometrical properties of the refracted wavefront may be computed from known input values. The main benefit of the procedure is its ability to involve a region around each ray (a pencil of rays), so local optical properties around the point of incidence are obtained in a faster and simpler manner than when using intensive ray tracing approaches, while describing the parameters in a manner very familiar to ophthalmic lens designers.

4.4. Step by step ray tracing procedure in an ophthalmic lens

Let's now take a look onto the global ray tracing procedure used in ophthalmic lens design, introducing the concepts of FRT and GRT described in Sections 4.2 and 4.3. We will present first the general procedure, without assumptions on the shape of the surfaces of the lens. Later, the detailed procedure for a particular case will be exposed as an example, implemented in Matlab® code and, in a final subsection, validated. The case of ophthalmic lenses with a toroidal surface has been chosen as example as it is not generally described in the literature, which usually stays limited to rotationally symmetrical surfaces.

4.4.1. General procedure

As explained in Section 2.2, the evaluation method used in ophthalmic lens design ignores the optical system of the eye, replacing it by a surface containing the remote points of the eye at all directions of gaze, and an aperture situated at the center of rotation of the eye. Such remote surface is the continuous surface where the best focus of the lens should ideally be placed for all directions of gaze (Fig. 2.5).

Generally speaking, the lens is considered to have two refractive surfaces, the anterior or convex surface and the posterior or concave surface. A particular coordinate system at the vertex of each surface is considered, so each surface of the lens is defined by a parametric equation in its particular coordinate system. A ray characterized by its director cosines (L, M, N) with origin at the center of rotation of the eye is chosen to start the procedure. The center of rotation is assumed to be at a distance d from the posterior vertex of the lens. This ray arrives to the posterior surface of the lens at point P_1, whose coordinates may be found using the equation of the line defined by (L, M, N) and the parametric equation of the surface. This process is the first transfer process of the design. Note the ray is propagating in opposite direction to that of the real situation, with light crossing the ophthalmic lens and then impinging the eye.

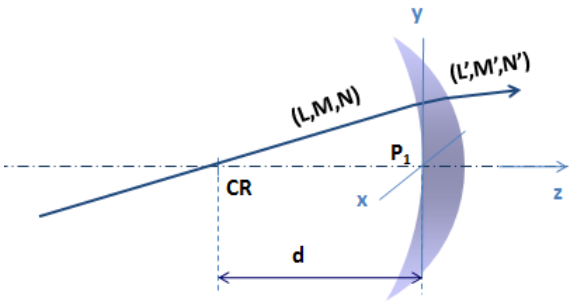

Figure 4.4. First step of the ray tracing process. The ray passes through the center of rotation of the eye with director cosines (L, M, N) to reach the posterior surface of the lens at point P_1. After refraction its director cosines are (L',M',N').

The next step is the refraction of the ray on the posterior surface of the lens using the vectorial form of Snell's law (Eq. 4.41); as described in previous sections, $\boldsymbol{r}$ and $\boldsymbol{r}'$ are unit vectors along the incident and refracted rays, and $\boldsymbol{n}$ is a unit vector along the normal to the interface between media of refractive indices n and n'. The normal at P_1 is calculated by Eq. 4.2. The components of $\boldsymbol{r}$ are (L, M, N), and using Eq.4.41 the director cosines for the refracted ray (L', M', N) are obtained (Fig. 4.4).

The next step is a new transfer and refraction process for the ray, crossing the lens and being refracted at the anterior surface of the lens. The ray will hit the anterior surface at point P_2, with coordinates (x_2, y_2, z_2), and there it will be refracted with director cosines (L'', M'', N''). Both processes are entirely equivalent to the ones described in the previous paragraph (Fig. 4.5).

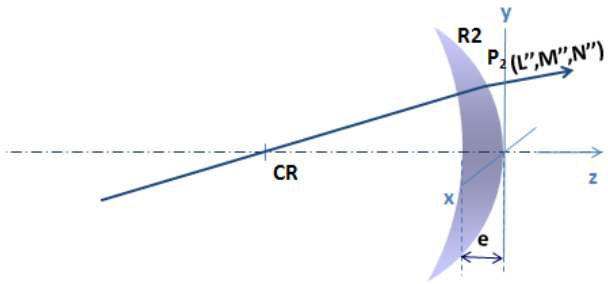

Figure 4.5.The ray emerges from the anterior surface of the lens at point P_2 with director cosines (L'', M'', N'')

The FRT procedure equations have now been completed, so the complete path of the ray across the lens is now known. We can now proceed to apply the GRT procedures once we know the direction of the principal ray in each case. We will now turn the lens-eye system

backwards to its real position and send narrow bundles of light towards the ophthalmic lens to evaluate its performance. We are interested in bundles with central point of incidence on the anterior surface of the lens determined by P_2 and director cosines determined by (L'', M'', N''). The fact of turning the system and changing the direction of incidence involves some changes in sign in the affected coordinate systems. The radius of curvature of the lens changes its sign, too. All these changes are detailed in Fig.4.6:

GRT starts with an incident wavefront which has $\rho_{\xi 2}$ and $\rho_{\eta 2}$ as principal curvatures, and $\boldsymbol{t}_2$ as principal direction corresponding to $\rho_{\xi 2}$, with the direction for $\rho_{\eta 2}$ perpendicular to $\boldsymbol{t}_2$. The ray with director cosines (L'', $-M''$, N'') is orthogonal to the incident wavefront at the point of incidence P_2.

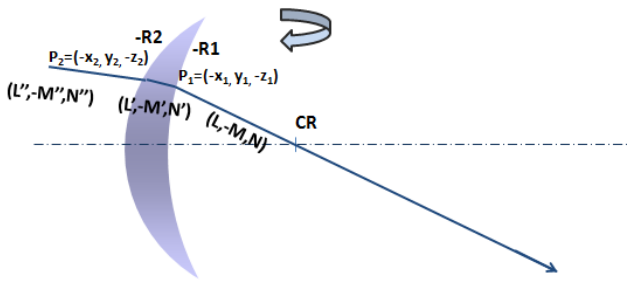

Figure 4.6. Changes in sign in coordinates and director cosines when the system is turned back to its original position

For the anterior surface of the lens the relation between indexes μ_2 is:

$$\mu_2 = \frac{1}{n'} \tag{4.60}$$

Being n' the refractive index of the lens. The incidence and refraction angles are those previously calculated using FRT, with the roles of refracted and incident angle now interchanged. γ_2 can thus be calculated as

$$\gamma_2 = -\mu_2 \cos i + \cos i' \tag{4.61}$$

In order to apply the GRT equations it is required to calculate the principal curvatures of the refractive surface and their directions at the point of incidence of the ray (P_2). If the refractive surface is defined by a parametric equation, the first and second fundamental quantities can be

calculated and then principal curvatures and directions can be obtained. Let us call $\rho_{\xi S2}$ and $\rho_{\eta S2}$ to the principal curvatures of the surface, and vector $\boldsymbol{t}_{S2}$ to the one which will describe the principal direction of curvature $\rho_{\xi S2}$.

To find $\boldsymbol{p}_2$ we use:

$$\boldsymbol{p_2} = \frac{\boldsymbol{r} \times \boldsymbol{n}}{\sin i} \tag{4.62}$$

Then, a rotation is performed using equations (4.50), (4.51) and (4.52) adapted to the surface:

$$1/\rho_{uS2} = \left(1/\rho_{\xi S2}\right)\cos^2\theta_s + \left(1/\rho_{\eta S2}\right)\sin^2\theta_s \tag{4.63}$$

$$1/\rho_{vS2} = \left(1/\rho_{\xi S2}\right)\sin^2\theta_s + \left(1/\rho_{\eta S2}\right)\cos^2\theta_s \tag{4.64}$$

$$\left(2/\sigma_{2S}\right) = \left(1/\rho_{\xi S2} - 1/\rho_{\eta S2}\right)\sin^2 2\theta_s \tag{4.65}$$

Where θ_s is given by

$$\cos\theta_s = \boldsymbol{t}_{S2} \cdot \boldsymbol{p}_2 \tag{4.66}$$

This way we will get the normal curvatures of the refractive surface relative to the defined particular coordinate system and the torsion at P_2 (which correspond to the quantities ρ_{uS2}, ρ_{vS2}, and σ_{S2}). An equivalent process is applied to the principal curvatures of the incident wavefront to find the normal curvatures and torsion of the incident wavefront relative to the coordinate system at P_2 (which correspond to ρ_{u2}, ρ_{v2}, σ_2).

With this information, using Eq. (4.57) to (4.59) the curvatures of the refracted wavefront are obtained at the direction of $\boldsymbol{p}_2$, ρ'_{u2} and ρ'_{v2}. Then, a new rotation is necessary to find the principal refracted curvatures and directions $\rho'_{\xi 2}$, $\rho'_{\eta 2}$ and $\boldsymbol{t}'_2$ using equations (4.53, (4.54) and (4.55).

This way the curvatures of the refracted wavefront at the anterior surface of the lens have been calculated in a general manner. The next refracting surface is the posterior surface of the lens, so first we need to perform a transfer operation to know how the curvature of the refracted wavefront changes when the ray we traced travels from the anterior to the posterior surface of

the lens, i.e., from P_2 to P_1. The distance between these points can easily be calculated using their coordinates. Let this distance be e'. Then, when the wavefront travelling with the considered ray arrives to P_2 these principal curvatures are:

$$\rho_{\xi 1} = \rho'_{\xi 2} + e' \tag{4.67}$$

$$\rho_{\eta 1} = \rho'_{\eta 2} + e' \tag{4.68}$$

Our next step is to calculate vector $\boldsymbol{p}$ for the posterior surface of the lens at point P_1 ($\boldsymbol{p}_1$). We will use again

$$\boldsymbol{p_1} = \frac{\boldsymbol{r} \times \boldsymbol{n}}{\sin i} \tag{4.69}$$

where $\boldsymbol{r}$ = (L', $-M'$, N'), being $\boldsymbol{n}$ the vector normal to the surface at P_1 and i the incidence angle of the ray.

The angle between $\boldsymbol{t}_1$ and $\boldsymbol{p}_1$ can then be found, as $\boldsymbol{t}_1 = \boldsymbol{t}'_2$:

$$\cos\theta = \boldsymbol{t}_1 \cdot \boldsymbol{p}_1 \tag{4.70}$$

The same process is applied again: a rotation is performed to find the curvatures of the incident wavefront relative to the new coordinate system at the posterior surface of the lens, i.e, $\rho_{\xi 1}$ and $\rho_{\eta 1}$ are already known from Eq. 4.67 and Eq. 4.68, and the present objective is to find ρ_{u1}, ρ_{v1}, and the related torsion σ_1. If the refractive surface is defined again by a parametric equation, the first and second fundamental quantities can be calculated and then principal curvatures and directions can be obtained ($\rho_{\xi S1}$, $\rho_{\eta S1}$ and the vector $\boldsymbol{t}_{S1}$), and a new rotation is performed to get the normal curvatures of the refractive surface relative to the defined particular coordinate system and the torsion at P_1 ($\rho_{uS1}, \rho_{vS1}, \sigma_{S1}$).

From the refraction at the posterior surface of the lens:

$$\mu_1 = n' \tag{4.71}$$

and

$$\gamma_1 = -\mu_2 \cos i + \cos i' \tag{4.72}$$

With this information, using Eqs.4.57 to 4.59 the refracted wavefront curvatures are obtained at the direction of $\boldsymbol{p}_1$. The values obtained (ρ'_{u1} and ρ'_{v1}) are the refracted curvatures of the wavefront in the directions of $\boldsymbol{p}_1$ and $\boldsymbol{q}_1$ (eq. 4.48) respectively. The principal curvatures of the refracted wavefront through the lens can be obtained from Eqs. 4.53, 4.54 and 4.55. The angle between $\boldsymbol{p}_1$ and $\boldsymbol{t}'_1$ is first obtained using Eq.4.9. Then, the principal curvatures ($\rho'_{\xi 1}$ and $\rho'_{\eta 1}$) are obtained from Eqs. 4.53 to 4.55. The direction of $\boldsymbol{t}'_1$ is obtained from Eq. 4.56.

It should be noticed that the curvatures of the wavefront refracted across the lens have to be defined relative to some reference surface, which will always be the same regardless the geometry of the posterior surface of the lens, to avoid potential ambiguities. This reference surface is the vertex sphere, defined at Section 2.2, a spherical surface centered at the center of rotation of the eye whose radius is the distance from the back vertex of the lens to the center of rotation of the eye, as depicted in Fig. 2.4.

The refracted wavefront curvatures are thus calculated when they intersect this vertex sphere, so a final transfer operation is needed to bring the refracted wavefront to the reference sphere using the distance from the back surface of the lens to the vertex surface for each ray, so the refracted wavefront curvatures may be modified properly. For a particular ray, the position of the centers of curvature for each principal curvature of the refracted wavefront are the equivalent to the classical sagittal and tangential foci images.

4.4.2. Detailed case for an astigmatic lens

Let's consider now a particular case in detail. We have chosen the case of the astigmatic lens although it uses equivalent procedures to that of rotationally symmetric surfaces. We will use an astigmatic lens with a toroidal concave surface and a spherical convex surface (96).

As commented, we will perform first a FRT procedure in order to know the path of the principal ray at the considered direction of gaze. For the parametrization of the posterior surface of the lens, a torus situated at the posterior vertex of the lens has been considered (see Fig. 4.1 and Eq. 4.29). The ray with origin at the center of rotation of the eye which arrives to the posterior surface of the lens is parameterized relative to a coordinate system situated at the posterior vertex of the lens by:

$$x = \lambda L \qquad y = \lambda M \qquad z = \lambda N - d \tag{4.73}$$

Where *L*, *M* and *N* are the director cosines of this ray.

The point P_1 defined by the intersection of the ray and the posterior surface of the lens is common to the line and the toroidal surface, so:

$$\lambda L = (R - r + r\cos\varphi)\sin\theta \tag{4.74}$$
$$\lambda M = r\sin\varphi \tag{4.75}$$
$$\lambda N - d = -R + (r - r + r\cos\varphi)\cos\theta \tag{4.76}$$

becomes a system of nonlinear equations to be solved. Although different solutions may be found, we will only be interested in the minimum absolute z_1 value, as it is the solution with physical meaning. Then, the intersection point of the incident ray with the posterior surface of the lens is obtained.

The refraction of the ray at the toroidal surface of the lens is calculated from the vector form of Snell's law (Eq. 4.41), taking ***r*** and ***r***' as the unit vectors along the incident and refracted rays and ***n*** as the unit vector along the normal to the surface at P_1.

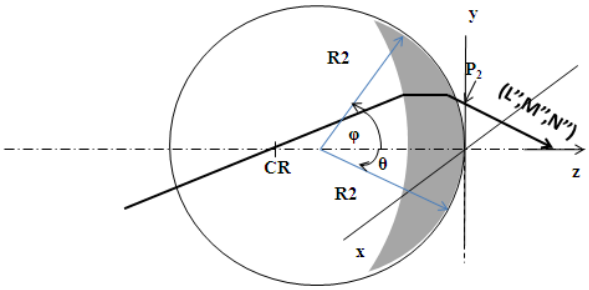

Figure 4.7. The anterior surface of the lens is a sphere with radius R_2 which is parametrized with spherical coordinates φ and θ. The refracted ray leaves the lens at P_2 with director cosines (L'',M'',N'').

Now, a transfer and refraction process for the ray crossing the lens at the anterior surface of the lens need be applied. Both processes are entirely equivalent to the ones described before except for the fact that now the refractive surface is spherical (see Fig.4.7). Now the

parametric description used may be equivalent to the one used for the toroidal surface but with $r=R=R_2$:

$$s=\begin{Bmatrix} x=R_2\cos\varphi\sin\theta \\ y=R_2\sin\varphi \\ z=-R_2+R_2\cos\varphi\cos\theta \end{Bmatrix} \tag{4.77}$$

With normal at the point of intersection described by:

$$\boldsymbol{n}=\left[\sin\theta\cos\varphi,\sin\varphi,\cos\theta\cos\varphi\right] \tag{4.78}$$

The path of the principal ray has been determined so the FRT procedure has finished, and we can now proceed to the application of the GRT procedure. We start with an object at infinity, corresponding to a flat wavefront. The ray with director cosines (L'', $-M''$, N'') and point of incidence $P_2=(-x_2, y_2, -z_2)$ is orthogonal to the incident wavefront. As the wavefront is plane:

$$\rho_{u2}=\rho_{v2}=1/\sigma_2=0 \tag{4.79}$$

The refracting surface is a sphere, so it has not any principal direction, and $1/\sigma_{s2}=0$. Moreover, if the sphere radius is $-R_2$, we may set

$$\rho_{us2}=\rho_{vs2}=-R_2 \tag{4.80}$$

With this information, using Eqs.4.57 to 4.59 we obtain:

$$1/\rho'_{u2}=\left(\gamma_2/-R_2\right) \tag{4.81}$$

$$\cos i'/\sigma'_2=0 \tag{4.82}$$

$$\cos^2 i/\rho'_{v2}=\left(\gamma_2/-R_2\right) \tag{4.83}$$

with ρ'_{u2} and ρ'_{v2} the refracted wavefront curvatures on the anterior surface of the lens at point P_2. The value of $1/\sigma'_2$ is zero, but the two curvatures are not equal in the general case. The fact that $1/\sigma'_2$ is zero tells us that we are already oriented relative to the principal

directions and that the $\boldsymbol{p}_2$ vector is coincident in with one of them. In this case $\boldsymbol{p}_2 = \boldsymbol{t}_2$ so $\rho'_{u2} = \rho'_{\xi 2}$ and $\rho'_{v2} = \rho'_{\eta 2}$.

It's now necessary to perform a transfer operation to know how the wavefront curvatures change when the ray travels from the anterior to the posterior surface of the lens, i.e., from P_2 to P_1. (Eqs. 4.67 and 4.68).

The parameterization of the toroidal surface once the path of the ray has been reversed will be

$$s = \begin{Bmatrix} x = -(R - r + r\cos\varphi)\sin\theta \\ y = r\sin\varphi \\ z = R - (r - r + r\cos\varphi)\cos\theta \end{Bmatrix} \tag{4.84}$$

where again $0 \le \varphi \le 2\pi$ and $0 \le \theta \le 2\pi$ and R and r are considered as absolute values.

The fundamental forms are now used to obtain the principal curvatures of the surface and the principal directions of the surface at the point of intersection of the ray. The principal curvatures are calculated as the eigenvalues of $\boldsymbol{A}$ (Eq.4.8) and the principal directions as its eigenvectors.

With this information of the surface it is now possible to complete the entire GRT process described in Section 4.4., to find the principal refracted wavefront curvatures and directions associated at each direction of gaze ($\rho'_{\xi 1}$, $\rho'_{\eta 1}$, and $\boldsymbol{t}'_1$). The position of the centers of curvature of the principal curvatures of the refracted wavefront can be interpreted as the sagittal and tangential focal images, once they are referenced to the vertex sphere.

The vertex sphere can be expressed as:

$$x^2 + y^2 + (z + d)^2 = d^2 \tag{4.85}$$

Where d is the distance from posterior vertex of the lens to the center of rotation of the eye. The refracted rays that emerge from the posterior surface of the lens have these components:

$$x = -x_1 + \Delta L \tag{4.86}$$
$$y = y_1 - \Delta M \tag{4.87}$$
$$z = -z_1 + \Delta N \tag{4.88}$$

Where Δ is a parameter. When the objective is to obtain the intersection point between the refracted ray and the vertex sphere we find the value of Δ which satisfies vertex sphere equation. A second order equation must be solved. Generally we obtain two solutions and we choose which makes *z* close to zero. At this point, the distance between the vertex sphere and P_1 can be calculated and the principal curvatures properly modified.

Fig. 4.8. shows the three-dimensional off-axis performance of an astigmatic lens. This figure shows the power in all directions of gaze for a lens of 180º-4.00-2.50 BVP, center thickness of 1,60mm, refractive index of 1.579, radius of the anterior surface 298,50mm and principal radius at the posterior toroidal surface of 132,44mm and 70,17mm. The center of rotation of the eye is located 27mm away from the posterior surface of the lens. The vertical axis contains the power values expressed in diopters. The horizontal plane contains the X and Y direction cosines for a particular direction of gaze. The large difference between power values reflects the presence of a large cylinder.

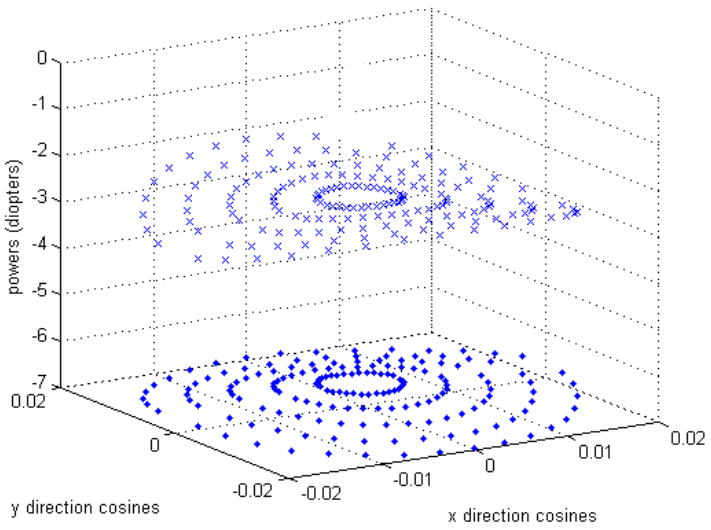

Figure 4.8. Maximum (diamond) and minimum (cross) absolute value power for an astigmatic 180º-4.00-2.50 back vertex power lens described in the text. The vertical axis contains the power values expressed in diopters. X and Y director cosines determine a particular direction of gaze in space. The difference between power values reflects the presence of cylinder.

Once known, these tangential and sagittal powers in each direction can be expressed in different ways, either as sphere, cylinder and axis or as the M, J_0 and J_{45} power vectors described in Section 2.4 (Eq. 2.3, 2.4, and 2.5). Fig. 4.9 represents refracted surfaces for this same lens in terms of power vectors. A matrix of rays and its related matrix of wavefronts are sent to the ophthalmic lens to build these refracted surfaces. For the representation, an

imaginary plane situated on the vertex of the concave surface of the lens is considered (Fig.4.10). Each ray that passes though the concave surface of the lens intersects with this plane at the point *(x, y)*. This point defines a given direction of gaze, determined by the ray that crosses this point and the center of rotation of the eye.

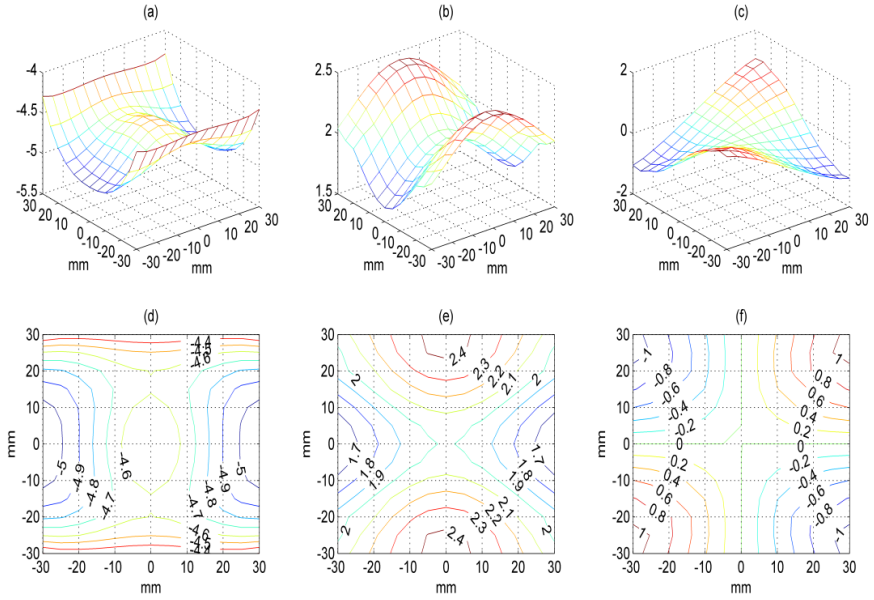

Figure 4.9. Refracted surfaces for M (a), J_0(b) and J_{45}(c) and contours for M (d), J_0(e) and J_{45}(f)for an ophthalmic lens with back vertex power of 180º-4.00-2.50 described in the text.

Fig.4.9 shows that M increases the horizontal meridian and decreases in the vertical meridian. J_0 presents symmetry respect to the horizontal and vertical axis and J_{45} has symmetry respect oblique axis. J_0 has bigger values than J_{45}, which is logical as the axis selected for the astigmatic lens is situated at 180º.

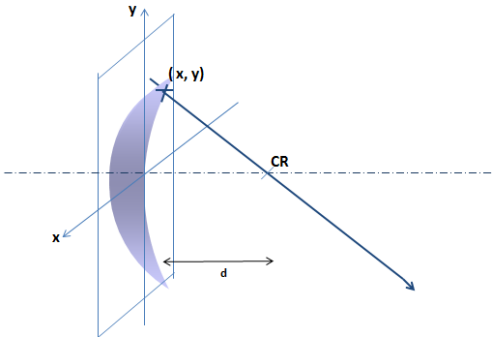

Figure 4.10. Imaginary plane situated on the vertex of the concave surface of the lens is considered for the representation of M, J_0 and J_{45} presented in figure 4.10. Each ray that passes though the concave surface of the lens intersects with this plane at the point *(x, y)*. This point defines a given direction of gaze, determined by the ray that crosses this point and the center of rotation of the eye.

It may be noticed how the procedure proposed enables a fast, easy implementation of the code in programming environments in order to produce 3D power maps of the optical properties of interest.

4.5. Validation of results

The validation of the equations and its software implementation is divided in two parts, following the tracing scheme depicted. Firstly we will validate the principal ray path of the wavefront when the inverse path of the ray is considered. The validation of the principal ray path is performed by the comparison of the code implementation done using Matlab® with results obtained using Beam4®, a commercial exact ray tracing software from Stellar® software, which enables ray by ray slope calculation and the exact calculation of the intersection point of the surface for each ray. A similar validation could be performed using any usual software optical design package, like Zemax® or OSLO®. The second part is the validation of the values of the refracted wavefront curvatures once the wavefront has passed through the lens. The validation of the wavefront curvatures is compared with PRIMER, a software for ophthalmic lens design based on the classical 2D version of Coddington equations (Eq. 2.1, 2.2). The author wants to stress that the full coding and testing of FRT and GRT procedures has been one very demanding task developed from zero along this Thesis. The validation step was thus implemented to test the accuracy of the code developed, to ensure the results obtained were correct and, if required, debug the code.

a) Finite ray tracing

The 180º-4.00-2.50 lens presented in Section 4.4 as an example will be used for validation, although, obviously, equivalent results are obtained for other geometries. The reverse path of a ray that crosses the center of rotation of the eye is considered. This ray reaches first the posterior surface of the lens, which is toric and presents two principal radius of curvature (-132,44mm and -70,17mm), and afterwards the anterior surface of the lens, with a radius of -298,50mm. The director cosines of the ray and the parameters of the lens are introduced in the software tool developed to obtain the point of incidence of any ray on each surface of the lens and the director cosines for this ray after each refraction.

An equivalent optical system is introduced into BEAM4® to compare the results obtained in our implementation in Matlab® with the values of the coordinates of the point of incidence on

each surface and the director cosines of the ray after refraction. Figure 4.11 shows the values obtained with both approaches, when the ray arrives to the convex surface of the lens and is refracted. The comparison of the refracted director cosines in X and Y (Fig.4.11(a)) and the coordinates of the point of incidence of the ray on the convex surface of the lens (Fig.4.11(b)) calculated using both applications are presented, showing full coincidence.

(a) (b)

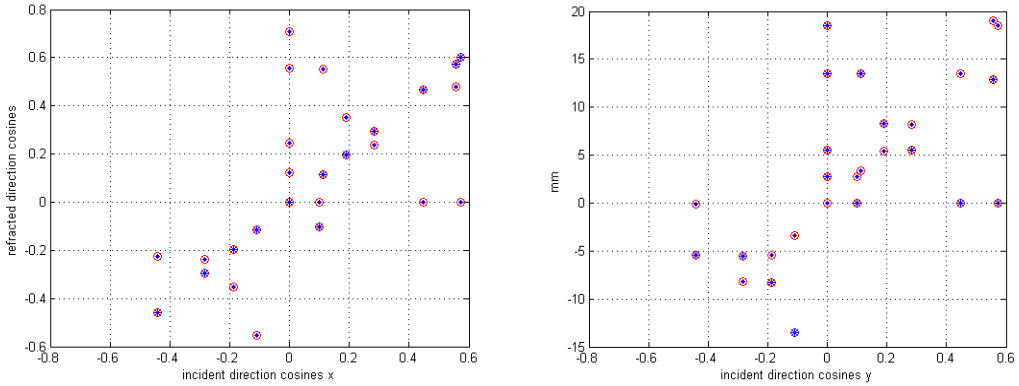

Figure 4.11. (a). Values obtained from our implementation in Matlab® (red circle) and from Beam4 (blue dots) for the X director cosines of the refracted ray on the convex surface of the lens. Values obtained from our code (red circle) and from Beam 4 (blue star) for the Y director cosines of the refracted ray on the convex surface of the lens. (b) X local coordinate values obtained from our code (red circle) and from Beam4 (blue dots) for the point of incidence of each ray on the anterior or convex surface of the lens. Y local coordinate values are shown also from our code (red circle) and Beam4 (blue star). Coincidence is complete.

b*) Generalized ray tracing*

To validate the implementation of GRT algorithms, wavefronts with principal rays contained on the tangential plane at first, and on the sagittal plane at second, are sent to the used lens to make possible the validation of power at the principal meridians, in our case the vertical and horizontal meridians. The associated wavefronts are chosen to validate the results using the classical version of Coddington's equations, where only a 2D problem is considered. Table 4.1 shows the values obtained by generalized ray tracing for different vertical angles of rotation of the eye in the vertical meridian for the tangential and sagittal powers, compared to the values obtained by an application based on classical Coddington's equations. Table 4.2 shows the values obtained for the horizontal meridian for the tangential and sagittal powers for different angles of horizontal rotation of the eye. Calculated values using our Matlab® implementation

are at the left in the pair of values of each column, while values from classical Coddington's equations are placed at the right. Fig. 4.12 presents these solutions

Table 4.1. Tangential and sagittal powers obtained by GRT (left of each pair of values) and by classical Coddington's equations (right of each pair of values), when calculated along the vertical meridian of the lens.

Vertical rotation angle of the eye	Tangential power (diopters)	Sagittal power (diopters)
5º	-6.516/-6.51	-2.506/-2.50
10º	-6.552/-6.55	-2.486/-2.49
15º	-6.613/-6.61	-2.472/-2.47
20º	-6.701/-6.70	-2.439/-2.44
25º	-6.791/-6.79	-2.399/-2.40
30º	-6.873/-6.87	-2.352/-2.35
35º	-6.944/-6.94	-2.271/-2.27
40º	-6.962/-6.96	-2.162/-2.16

Table 4.2. Tangential and sagittal powers obtained by GRT (left of each pair of values) and by classical Coddington's equations (right of each pair of values), when calculated along the horizontal meridian of the lens.

Horizontal rotation angle of the eye	Tangential power (diopters)	Sagittal power (diopters)
5º	-2.518/-2.51	-6.509/-6.50
10º	-2.553/-2.55	-6.527/-6.52
15º	-2.613 /-2.61	-6.546/-6.54
20º	-2.692/-2.69	-6.573/-6.57
25º	-2.808/-2.80	-6.610/-6.61
30º	-2.937/-2.93	-6.645/-6.64
35º	-3.085/-3.08	-6.673/-6.67
40º	-3.242 /-3.24	-6-699/-6.70

(a)

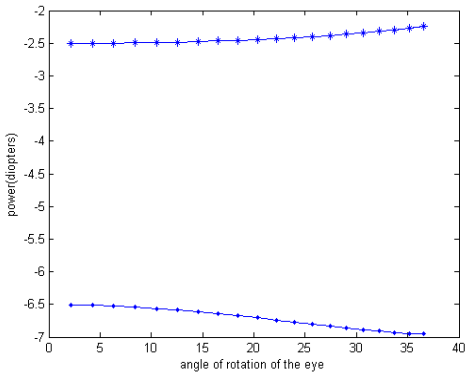

(b)

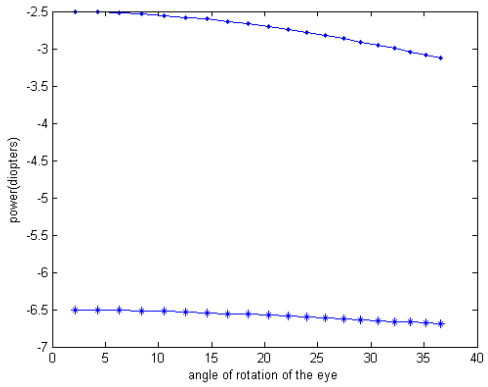

Figure 4.12. Tangential power (.) and sagittal power (*) obtained by classical Coddington equations and tangential power and sagittal power (lines) obtained by generalized ray tracing against the different directions of gaze (degrees) (a) Vertical meridian, and (b) Horizontal meridian.

graphically, with the values obtained in our implementation plotted as continuous lines, and the discrete values obtained by applying classical Coddington's equations plotted as symbols. Full coincidence may be seen to be obtained, validating the raytracing approach and the software tool developed.

4.6. Implementation of ray tracing code. Results.

Once the software implementation procedures for the FRT and GRT for ophthalmic lenses (in our case, in the shape of Matlab® functions) have been validated, a study of some results on ophthalmic lens performance for spherical, aspherical and astigmatic lenses will be presented to show briefly the capabilities of the computation method and the associated 3D representation of the results. We analyze these lenses for different directions of gaze and present results graphically, both as discrete points for tangential and sagittal powers, and as refracted surfaces for the associated power vectors. This type of representations will be used often in Section 5 to evaluate peripheral refraction.

4.6.1. Spherical lenses.

In this case, both surfaces of the lens are spherical. The next figures show two examples. Fig. 4.13(a) shows the power distribution in all directions of gaze for a positive lens with +2.00D BVP, suitable for moderate hypermetropia, with center thickness of 3mm, refractive index of 1.5, radius of the anterior surface 71,44mm and radius of the posterior surface 98.05mm. The center of rotation of the eye is located on axis at 27mm from the posterior surface of the lens. Fig. 4.13(b) represents the tangential and sagittal powers for a lens with a BVP of -8.00 D, suitable for a myopic patient, with central thickness of 1mm, index of refraction 1.7, radius of the anterior surface of the lens 215.38mm and radius of the posterior surface 62.19mm; the center of rotation of the eye has now been situated on-axis at 30mm from the posterior surface of the lens. The vertical axis contains the power values expressed in diopters. The horizontal axis contains X and Y direction cosines for a particular direction of gaze.

(a) (b)

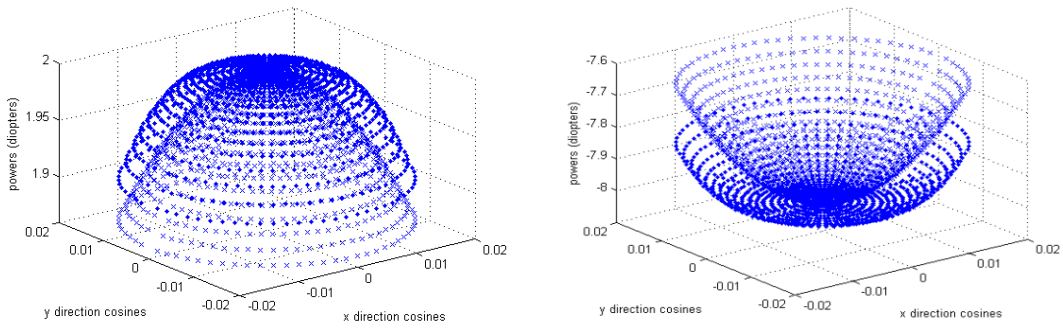

Figure 4.13: Tangential (exterior cup, dots) and sagittal (interior cup, crosses) refracted powers for the (a) +2.00D BVP lens described in the text; and (b) -8.00D BVP lens described in the text. X and Y axes contain the x and y director cosines which define each direction of gaze in space.

The negative lens of -8.00 D is also presented in Fig.4.14 using the representation of power vectors M, J_0 and J_{45}, in the form of refracted surfaces (upper plots) and their corresponding contour maps (lower plots). It can be observed how the two astigmatic components (J_o and J_{45}) are virtually zero, as it is an spherical lens, although the effects of oblique astigmatism may be observed in the different directions of gaze.

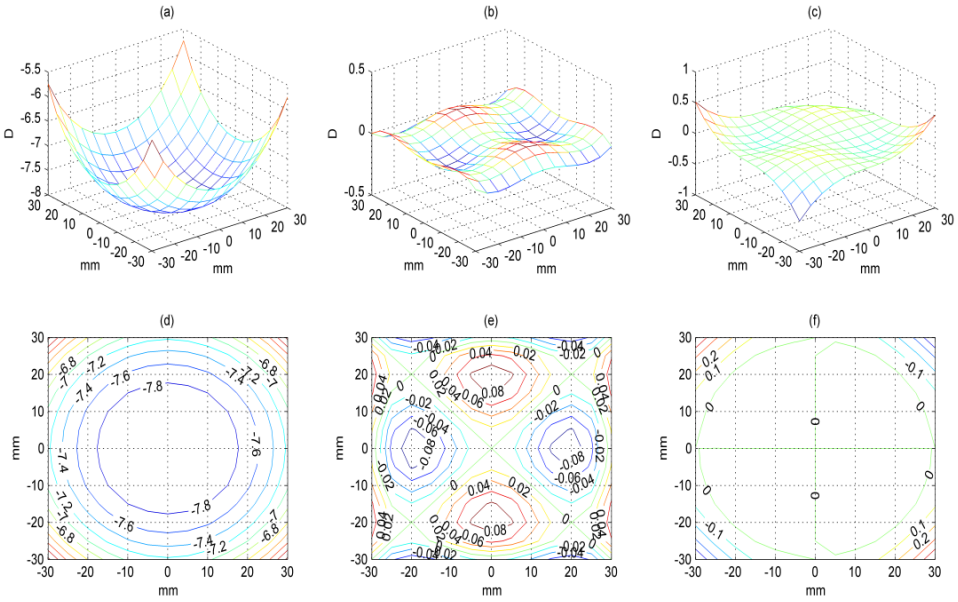

Figure 4.14. . Refracted surfaces for M (a), J_0(b) and J_{45}(c) and contours for M (d), J_0(e) and J_{45}(f) for an ophthalmic lens with back vertex power of -8.00 D described in the text.

4.6.2. Aspherical lenses

Figure 4.15 shows a three-dimensional representation of the tangential and sagittal powers for different directions of gaze of an ophthalmic lens with a convex spherical surface and a concave aspherical surface. Figure 4.15(a) represents the tangential and sagittal powers for a myopic lens with back vertex power of -8.00D with the parameters used for the spherical lens case and presented in figure 4.13(b), but now including a concave aspherical surface with a conic constant p=0.9. Figures 4.15(b), 4.15(c), 4.15(d), and 4.15(e) show lenses with the same parameters but with conic constants p=0.7, p=0.5, p=0.3, and p=0.1 respectively.

The progression of the tangential and sagittal powers with the evolution of the conic constant can be observed. At first, the sagittal powers are in the interior cup (p=0.9) as in the spherical case, while for smaller conic constants gradually the sagittal and tangential power "cups" eventually become inverted.

We present also the cases of Fig.4.15(b) and Fig.4.15(e) in the shape of power vector plots in Fig. 4.16 and Fig. 4.17 respectively. The differences of values for all components (M, J_0 and J_{45}) in these two lenses different only in the conic constant value of the posterior surface may be observed. The lens with p=0.7 may be seen to minimize OA better than the lens with

concave surface of p=0.1, something we can see in the values of J_0 and J_{45}. The lens with p=0.7 presents less difference between M in the optical center and M in different direction of gaze.

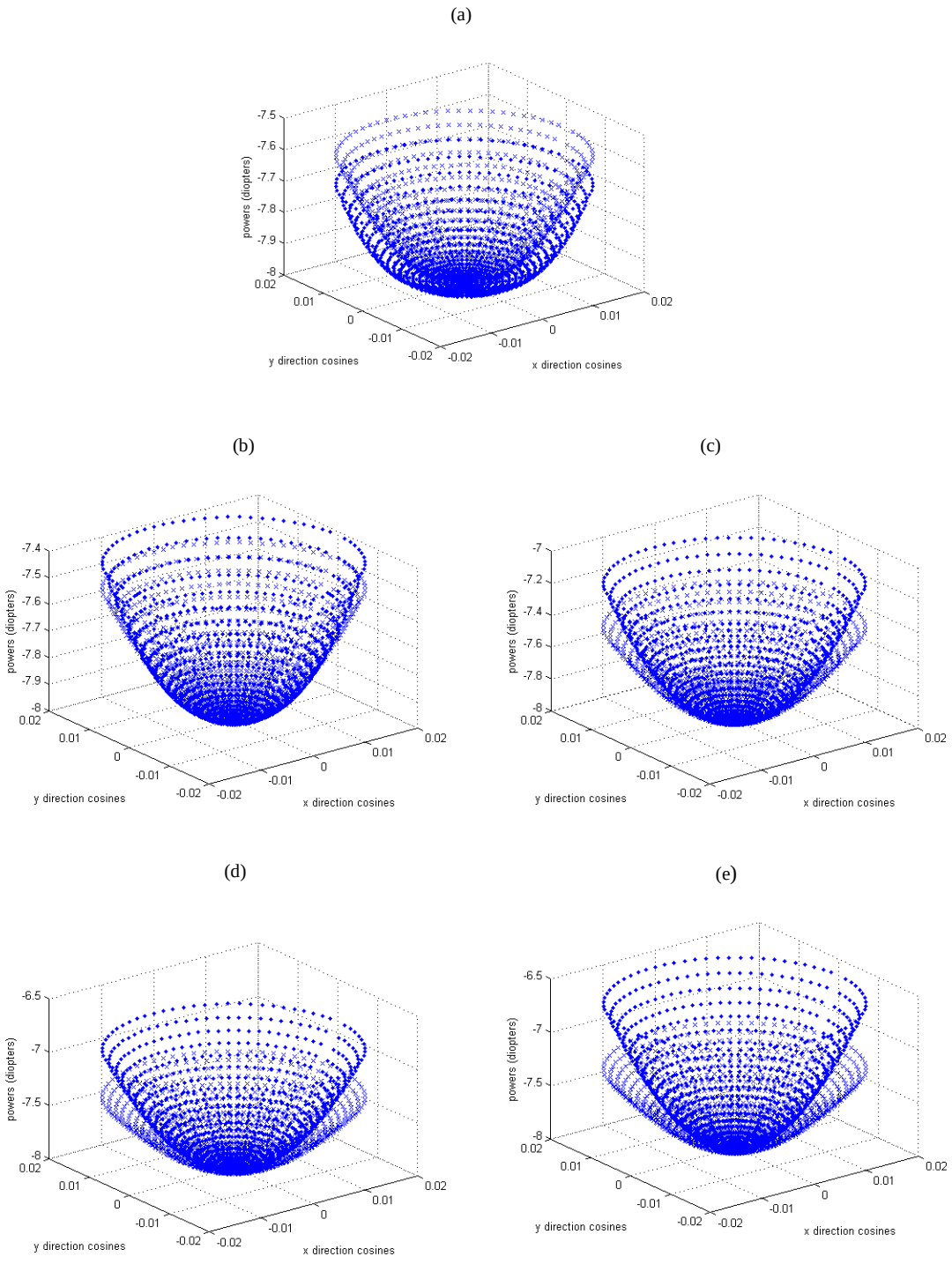

Figure 4.15. Effect of changing the conic constant in the concave surface in off-axis performance. Results show tangential (dots) and sagittal (crosses) refracted powers for the -8.00D BVP lens described in the text. (a) Conic constant p=0.9; (b) Conic constant p=0.7; (c) Conic constant p=0.5; (d) Conic constant p=0.3; (e) Conic constant p=0.1.

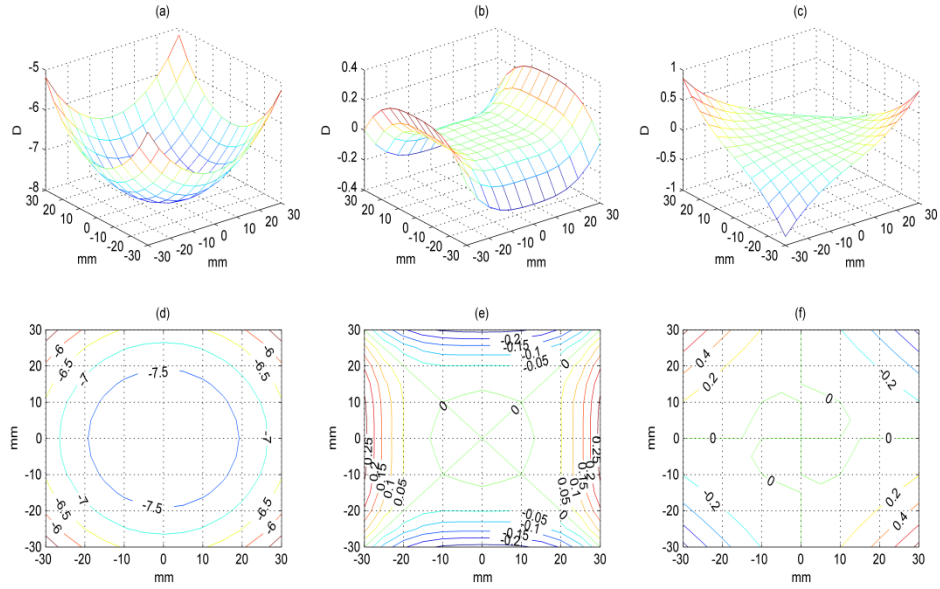

Figure 4.16. . Refracted surfaces for M (a), J_0(b) and J_{45}(c) and contours for M (d), J_0(e) and J_{45}(f) for the aspheric lens described in the text with conic constant of the posterior surface p=0.7

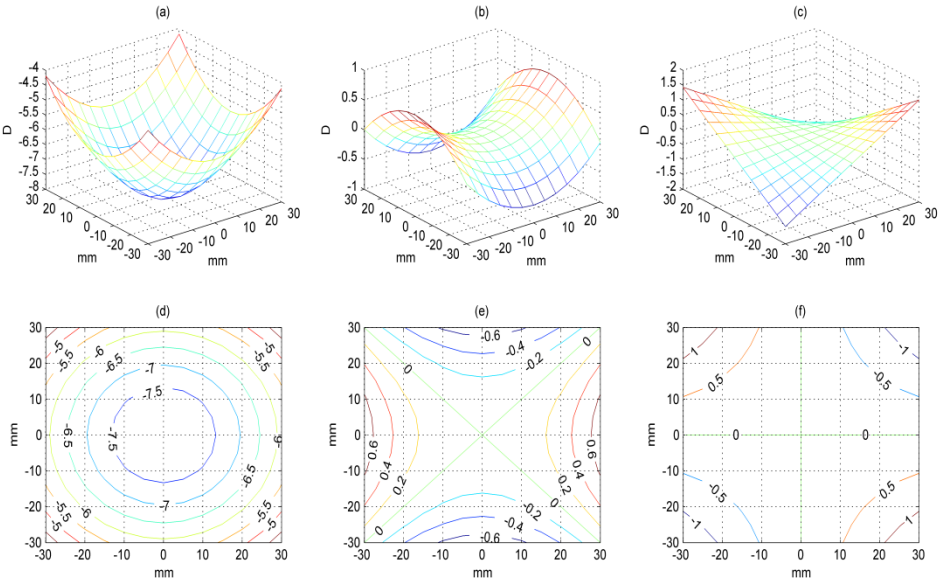

Figure 4.17. Refracted surfaces for M (a), J_0(b) and J_{45}(c) and contours for M (d), J_0(e) and J_{45}(f) for the aspheric lens described in the text with conic constant of the posterior surface p=0.1

4.6.3. Astigmatic lenses

As final example, Fig.4.18a shows the three-dimensional off-axis performance of an astigmatic lens of BVP -5.76-2.50×180º, with a toric concave surface, center thickness of 1,60mm, refractive index of 1.579, an spherical anterior surface of +5.00D and distance from the posterior surface of the lens to the center of rotation of the eye of 27mm. Fig.4.18b shows the same lens when the spherical anterior has a base curve of +3.00 D. The figure presents the maximum and minimum power values in a three-dimensional patterns final example, Fig.4.18a shows the three-dimensional off-axis performance of an astigmatic lens of -5.76-2.50×180º BVP, with a toric concave surface, center thickness of 1,60mm, refractive index of 1.579, an spherical anterior surface of +5.00D and distance from the posterior surface of the lens to the center of rotation of the eye of 27mm. Fig.4.18b shows the same lens when the spherical anterior has a base curve of +3.00 D. The figure presents the maximum and minimum power values in a three-dimensional pattern.

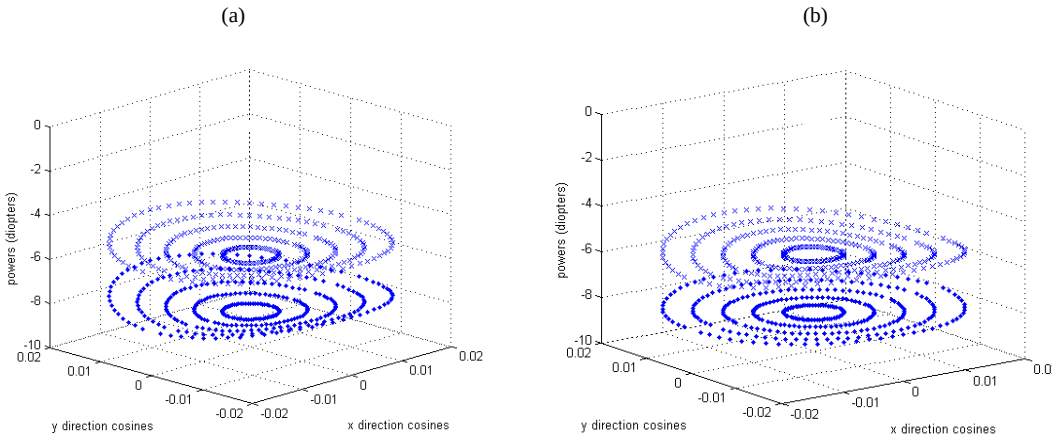

Figure 4.18. Maximum (diamond) and minimum (cross) power values for the astigmatic lens described in the text (a)Anterior surface of +5.00D; (b) Anterior surface of +3.00D.

The presence of cylinder is appreciated as tangential and sagittal powers are not coincident in the main direction of gaze. Although both plots look quite similar, even for the small change introduced the performance of the lens is quite different, and can be better observed in the contour plots of the power vectors presented in Fig.4.19 and 4.20, where the refracted powers of the lenses are expressed in terms of M, J_0 and J_{45}. Different behaviours in all components are expressed, being J_{45} the most stable one, while differences between the lenses are concentrated in the distribution of M and specially of J_0.

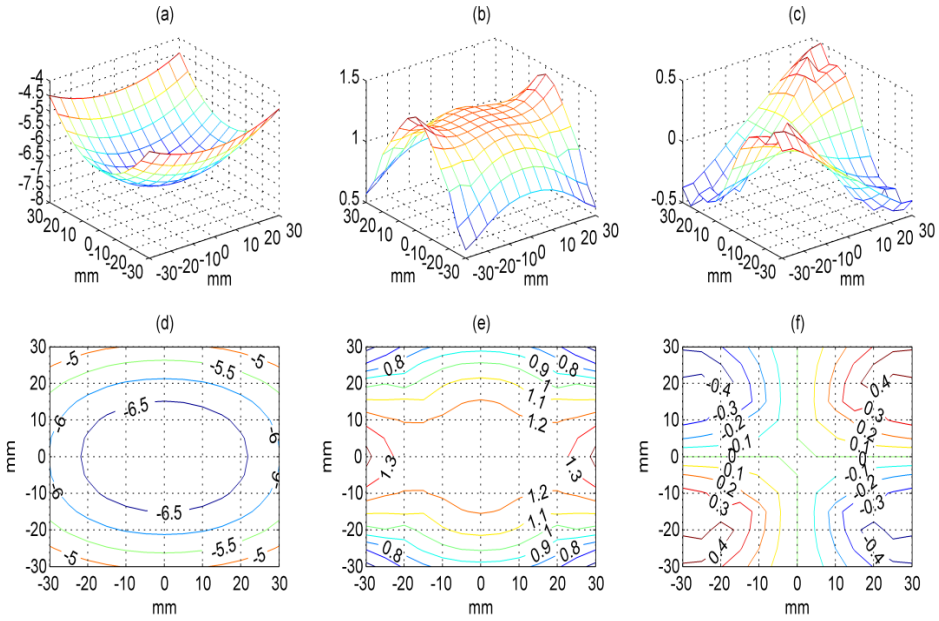

Figure 4.19. Refracted surfaces for M (a), J_0(b) and J_{45}(c) and contours for M (d), J_0(e) and J_{45}(f) for the astigmatic lens described in the text with anterior curve of +5.00D

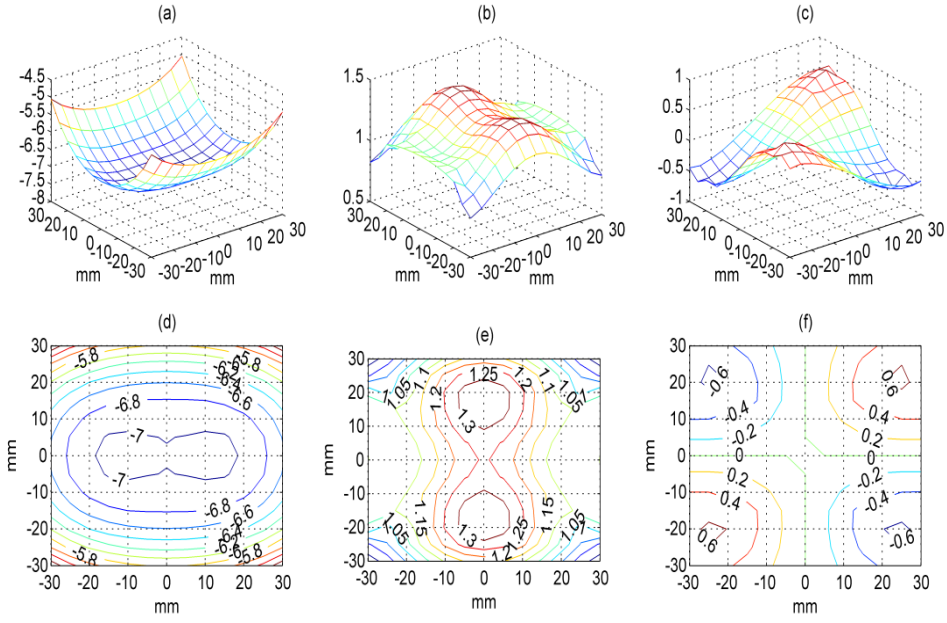

Figure 4.20. . Refracted surfaces for M (a), J_0(b) and J_{45}(c) and contours for M (d), J_0(e) and J_{45}(f) for the astigmatic lens described in the text with anterior curve of +3.00D

Along this Section we have described the general concepts of FRT and GRT. We have shown in detail their application to the ophthalmic lens design problem and their implementation into a general software tool. We have also validated the tool developed using comparable (but more limited) software tools. Finally, we have shown the capabilities of the tool developed by applying it to calculate the performance of the ophthalmic lenses of different geometries, showing consistent results. Three-dimensional representations of the power distribution along all directions of gaze, both in the shape of effective power values at all directions of gaze and as power vectors have been obtained for lenses of different geometries, showing the capability of our tool to perform precise evaluations of the off-axis performance of ophthalmic lenses using the principles of FRT and GRT.

5. Evaluation of peripheral refraction in ophthalmic lenses.

Given the hypothesis of peripheral hyperopic defocus as cause of the progression of myopia was confirmed, it should be taken into account when a compensation element is used or designed for a myopic eye. No methodology for the evaluation of the peripheral refraction induced by an ophthalmic lens (the IPR) has been set, except for the use of conventional ray tracing software packages. In this Section we will propose a method for such evaluation when an ophthalmic lens is situated in front of an eye to compensate its refractive error. Such IPR will be the combination of the effects of the power of the ophthalmic lens and the peripheral refraction of the eye without compensation.

In Section 3 we saw how the design of the compensatory element has been shown to have an effect on the peripheral refraction of the eye. Besides, it has been demonstrated that it is difficult in practice to establish a common pattern of peripheral refraction valid for all patients, even for those with equivalent central refractive error. Thus, we propose a method for the evaluation of IPR which takes into account the personalized pattern of peripheral refraction of the eye of a given patient. This potentially enables to optimize ophthalmic lenses for each particular individual. This final goal, however, would require to consider the effects of the rotation of the eye in-the performance of the lens in all directions of gaze, which has been left as future research work. For our purposes, we will stay focused in the proposal of a method for the calculation of the peripheral refraction of the lens-eye system working as a centered system, that is, with the eye not tilted and looking through the optical center of the lens. This will be shown to assess whether conventional lens designs are the most appropriate or to evaluate the effect of changes in the geometry of the lenses to better control the progression of myopia.

Along Section 4 the essential theory and methods of ray tracing for ophthalmic lens design have been introduced. In conventional ophthalmic lens design theory lenses are designed for foveal vision and rays are traced through the centre of rotation of the eye. The remote sphere removes from the lens design problem the optical elements of the eye, while enabling a full-field evaluation of the performance of the lens. For peripheral vision, however, the approach needs to change as now the interest is the behavior of the lens at a fixed retinal eccentricity around the main direction of gaze, that is, around the fovea and not at the fovea. We will use FRT and GRT to evaluate peripheral refraction, using a new simple scheme similar to that used in conventional ophthalmic lens design (Fig.2.5). In our approach, the center of rotation

of the eye will be replaced by the nodal point of the eye, and the remote sphere will be replaced by a surface which will be the conjugate of the retina through the optics of the eye, which we will designate as the retinal conjugate surface (RCS)(Fig.5.1). This scheme will be used to find the positions for the tangential and sagittal foci of a pencil of light that arrives to a particular eccentric point of the retina. The combination of these foci and the dioptric power of the RCS at that point will allow to calculate the IPR at a given retinal eccentricity (97).

Section 5.1 will present two different methods for building the RCS of a given patient, the first one based on the assumption of a theoretical shape of the retina, and the second based on fitting experimental data. Then, Section 5.2 will present the methodology for the calculation of the peripheral refracted powers of a given ophthalmic lens using FRT and GRT. Finally, Section 5.3 will show the calculation of IPR of a given eye-lens system, showing how changes in the geometry of the lens or in the refractive condition of the compensation affect the IPR values.

5.1. Modeling a retinal conjugate surface

In conventional ophthalmic lens design different directions of gaze are evaluated using the remote sphere as the reference for power errors. The tangential and sagittal foci obtained by each direction of gaze have a relative position relative to the remote sphere which is directly related to the power error. To assess peripheral refraction we will establish a parallel to the remote sphere in the shape of a new surface we will call the retinal conjugate surface (RCS), which in each of its points presents the equivalent refraction of a point of the retina with the same eccentricity. Thus, any arbitrary point P situated on the retinal surface of the eye, has a conjugate point P' through the optics of the eye on the retinal conjugate surface (Fig.5.1(a)). RCS is the reference of measure for the peripheral power error for a particular eccentricity, and will allow us to define an induced peripheral refraction (IPR), obtained from the combination of the peripheral refracted surface out of the lens and the RCS refraction at each retinal eccentricity. The scheme of the arrangement showing the concept of RCS (Fig.5.1.a) and the general schematics for the calculation of IPR (Fig.5.1.b) is presented in Fig.5.1.

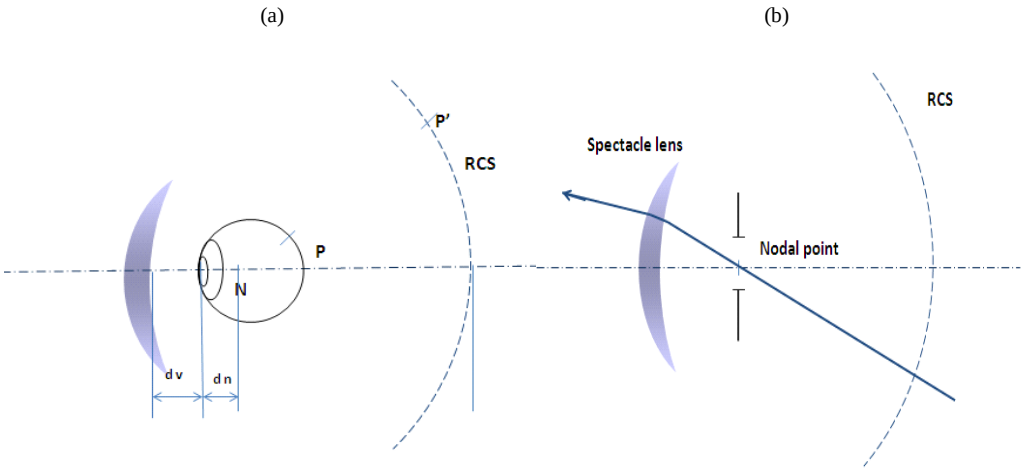

Figure 5.1. Scheme proposed to assess IPR. a) An arbitrary point P situated on the retinal surface of the eye will have a conjugate point through the optics of the eye on the RCS (P'). The ophthalmic lens is situated a distance *dv* from the anterior corneal surface. The nodal point of the eye is situated a distance *dn* from the anterior corneal surface. b) Schematics of the ray tracing approach used to compute IPR.

As discussed in the state of the art, different studies suggest it is very difficult to obtain a common pattern for peripheral refraction for myopic eyes, due to the considerable individual variability observed. Our purpose is to build an ideal RCS where the refracted peripheral rays at the lens will be projected to evaluate the global performance of the lens-eye system. The RCS thus should be defined by the peripheral power error of the subject before the introduction of the lens. Such surface could be modeled in the shape of some axially symmetric surface (like an ellipsoid or an hyperboloid (68), or measured on the subject with some of the methods discussed before (12,39,65) . We present here the two different approaches: At first, we will model a theoretical RCS expressed in terms of power vectors, based on the trends observed in the state of the art and using equations of 3D surfaces. Next, we will build a RCS based on experimental data in which interpolation methods will be necessary, but which will enable to cope with intersubject variability issues and personalization of the lens design.

5.1.1. Theoretical RCS model

We present here a theoretical model for a RCS in terms of power vectors(25) which, according to the trends discussed in the state of the art, should take into account a number of issues:

- Myopic eyes usually have a hyperopic relative peripheral refraction. That is, they are less myopic in the periphery than in the fovea. This hyperopia increases faster in the horizontal meridian that in the vertical meridian(9,68). This effect is reflected in the M component in the RCS.

- The study reported by Mathur (44) shows that the astigmatic components J_{45} and J_0 increase following an approximate quadratic pattern along the 135º-315º meridians and the 90º–270º meridians, respectively, and that they decrease along the perpendicular meridians.

Taking these trends into account we have modeled a theoretical RCS for a -5.76D myopic eye as example (Fig.5.2). The imaginary plane of reference situated in the posterior vertex of the concave surface of the ophthalmic lens is considered as reference for defining retinal eccentricities. We have used an ellipsoid for M, an hyperbolic paraboloid for J_0, and the sable equation for J_{45}, which are surfaces that allow us to model the characteristics exposed before. The equations used are:

$$M = a \cdot \sqrt{16 - \left(\frac{y^2}{100b^2}\right) - \left(\frac{x^2}{100c^2}\right)} \tag{7.1}$$

$$J_0 = \frac{y^2 - x^2}{100} \tag{7.2}$$

$$J_{45} = \frac{-xy}{100} \tag{7.3}$$

Where x,y are expressed in mm and a, b and c are constant values for each surface represented. We have modeled a theoretical RCS for a -5.76D myopic eye using the next values:

a= BVP/4 b=0.9 c=0.7

This values of a, b and c have been chosen trying to obtain a desired pattern for M in this particular example, obtaining values which follow the trends exposed before. However, these

values can be redefined to obtain bigger o smaller changes of refraction in different meridians and for each BVP, but maintaining the ellipsoid pattern for M. The hyperbolic paraboloid for J0, and the sable equation for J45 allow us to obtain the trends for the astigmatic components. Fig. 5.2. shows the representation of these three surfaces. It can be observed how M becomes more hyperopic in the periphery, but faster in the horizontal than in the vertical meridian. J0 and J45 may be seen to increase along the 90º–270º and the 135º-315º meridians, respectively, and to decrease along the orthogonal directions, as proposed in the bibliography. Different values for *a*, *b*, *c* produce different progressions for M in different meridians. For the astigmatic components, a multiplication constant can be introduced if a larger or smaller progression wants to be modeled.

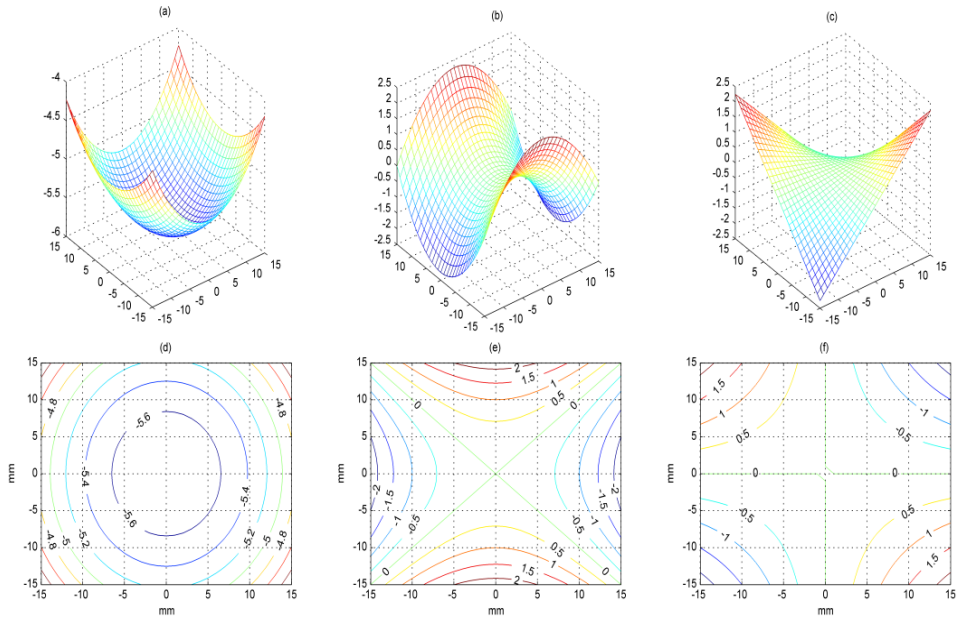

Figure 5.2. Theoretical RCS for a myopic eye of -5.76D expressed in power vectors. (a), (b) and (c) are the surfaces for M, J_0 and J_{45} respectively. (d), (e) and (f) are the corresponding contour plots.

5.1.2. Experimental RCS model

An alternative and more interesting approach is to build a RCS based on real experimental data, obtained from measurements on a particular eye of a given patient. This approach

contains the additional value of opening the door to personalization of lens designs, tailoring them to the needs of each particular user.

An experimental RCS model involves three major steps:

1. Different measurements of peripheral refraction at different angles of eccentricity need be taken in terms of sphere, cylinder and axis (S, C, θ), or directly as component vectors (M, J_0 and J_{45}) (25) using some of the techniques described in the state of the art. Values for discrete angular directions on different meridians should be measured. Ideally, horizontal, vertical and some oblique meridians will be measured.

2. The measured values of refraction will be expressed as component vectors, as described in Eqs.2.3, 2.4 and 2.5.

3. As last step, a polynomial function can be interpolated for M, J_0 and J_{45} to these experimental data for each meridian and, finally, a surface fitted to the data from the results obtained by these polynomial fitting. Direct surface fitting to the data may also be used. A RCS is thus defined in terms of M, J_0 and J_{45} against position on the plane tangent to the back vertex of the lens.

To show the potential of the method, we have built a sample RCS using the experimental values obtained by Ehsaei et al.(72). They measured peripheral refraction at different eccentricities (10º, 20º and 30º) for vertical, horizontal and oblique meridians for myopic and emmetropic eyes using the ShinNippon autorefractor, one of the commercial instruments most frequently used. It should be stressed that such an instrument has not been designed specifically for the measurement of peripheral refraction, so accuracy of the results may be enhanced by using some other techniques. However, the data obtained will be useful for our purposes, as it is used to demonstrate the method described and contains peripheral refraction data in four meridians covering the full extent of the visual field.

Obviously, this measurement approach does not consider high-order aberrations which degrade optical quality and are not taken into account in the autorefractor data. It needs to be stressed here that the role of higher-order aberrations remains the subject of discussion, although some authors have pointed out that the progression of axial myopia in children is not linked to them, as commented in the state of the art(44,66).

The mean values of this measured data will be used to calculate the RCS. For completeness, the values we have used to calculate the RCS are detailed in Table 5.1 (myopic eyes) and 5.2 (emmetropic eyes) respectively.

Table 5.1. Mean values of peripheral refraction for myopic eyes used to build the RCS. Data from (72)

	Temporal Retina			Central	Nasal Retina		
	-30º	-20º	-10º	0	+10º	+20º	+30º
A.	**Horizontal meridian**						
M	-3.71±2.09	-4.97±1.78	-5.62±1.84	-5.76±1.82	-5.54±1.96	-4.96±2.43	-3.69±2.89
J_0	0.14±0.94	-0.05±0.39	0.07±0.18	0.17±0.16	0.23±0.30	0.23±0.33	0.47±0.59
J_{45}	0.31±0.64	0.13±0.40	0.10±0.26	0.04±0.14	-0.01±0.30	-0.02±0.34	0.01±0.65
B.	**Vertical Meridian**						
M	-3.32±3.10	-4.96±2.32	-5.50±1.83	-5.76±1.82	-5.56±1.91	-5.22±2.12	-4.36±2.68
J_0	-0.21±1.29	0.16±0.68	0.27±0.45	0.17±0.16	0.26±0.24	0.40±0.37	0.71±0.82
J_{45}	-0.09±0.67	-0.12±0.35	0.01±0.30	0.04±0.14	0.09±0.25	0.21±0.33	0.45±0.58
C.	**Oblique Meridian: Superior Temporal-Inferior Nasal**						
M	-4.47±2.34	-5.11±2.06	-5.63±1.87	-5.76±1.82	-5.71±2.08	-5.18±2.32	-3.85±2.79
J_0	0.28±0.72	0.21±0.35	0.14±0.23	0.17±0.16	0.21±0.32	0.26±0.41	0.11±0.59
J_{45}	0.51±0.94	0.19±0.46	0.18±0.26	0.04±0.14	-0.09±0.24	0.09±0.41	-0.27±0.70
D.	**Oblique Meridian: Superior Nasal-Inferior Temporal**						
M	-3.95±2.96	-4.89±2.37	-5.40±2.17	-5.76±1.82	-5.81±1.95	-5.03±2.05	-3.94±2.11
J_0	0.62±0.51	0.43±0.40	0.21±0.29	0.17±0.16	0.02±0.28	-0.05±0.51	-0.21±0.69
J_{45}	-0.11±0.69	0.00±0.38	-0.03±0.21	0.04±0.14	0.02±0.21	-0.01±0.53	-0.14±0.94

Table 5.2. Mean values of peripheral refraction for emmetropic eyes used to build the RCS. Data from (72)

	Temporal Retina			Central	Nasal Retina		
	-30º	-20º	-10º	0	+10º	+20º	+30º
A.	**Horizontal meridian**						
M	-0.18±1.34	-0.26±0.95	-0.34±0.62	-0.32±0.44	-0.34±0.63	0.09±0.74	0.40±01.12
J_0	-0.59±0.79	-0.23±0.38	-0.06±0.23	0.06±0.16	-0.03±0.34	-0.06±0.41	-0.09±0.75
J_{45}	0.10±0.65	-0.04±0.52	-0.08±0.18	0.05±0.13	0.05±0.31	0.04±0.31	-0.09±0.46
B.	**Vertical Meridian**						
M	0.63±1.45	-0.40±1.03	-0.54±0.79	-0.32±0.44	-0.49±0.61	-0.58±0.62	-0.99±1.15
J_0	-0.02±0.98	0.24±0.48	0.30±0.29	0.06±0.16	0.15±0.24	0.32±0.40	0.97±0.87
J_{45}	-0.10±0.32	-0.03±0.33	0.02±0.21	0.05±0.13	0.10±0.24	0.19±0.46	0.23±0.54
C.	**Oblique Meridian: Superior Temporal-Inferior Nasal**						
M	-0.76±1.45	-0.58±0.90	-0.57±0.68	-0.32±0.44	-0.36±0.87	-0.31±0.77	0.13±1.06
J_0	0.01±0.66	0.04±0.33	0.01±0.22	0.06±0.16	0.26±0.37	0.34±0.34	0.19±0.62
J_{45}	0.44±1.40	-0.22±0.50	0.11±0.30	0.05±0.13	0.04±0.26	0.03±0.49	-0.11±0.61
D.	**Oblique Meridian: Superior Nasal-Inferior Temporal**						
M	-0.10±0.97	-0.18±0.87	-0.39±0.77	-0.32±0.44	-0.46±1.07	-0.50±1.32	-0.09±1.60
J_0	0.34±0.40	0.21±0.27	0.14±0.23	0.06±0.16	0.01±0.24	0.05±0.46	-0.17±0.60
J_{45}	-0.26±0.47	-0.06±0.29	-0.01±0.23	0.05±0.13	0.00±0.17	-0.05±0.35	-0.11±0.55

We will develop in detail the RCS for the myopic case (Table 5.1). The experimental values described for M, the mean spherical equivalent for myopic eyes, are plotted in Fig 5.3(a). Values obtained for the mean spherical equivalent on each meridian (vertical, horizontal and oblique meridians) are interpolated by a polynomial function which provides continuous values for RCS in terms of M in the four main meridians (Fig 5.3(b)). A final simple interpolation method for surfaces enables to build the RCS for M (Fig.5.4).

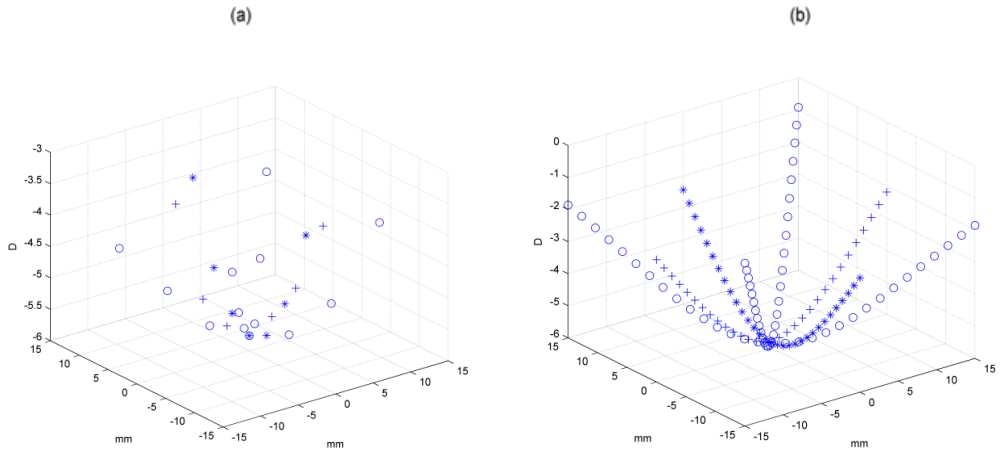

Figure 5.3. a) Experimental values obtained for mean spherical equivalent for myopic eyes (vertical meridian(+), horizontal meridian(*) and oblique meridians(o)); b) Values obtained for mean spherical equivalent on each meridian (vertical(+), horizontal(*) and oblique meridians(o)) once interpolated by a polynomial function.

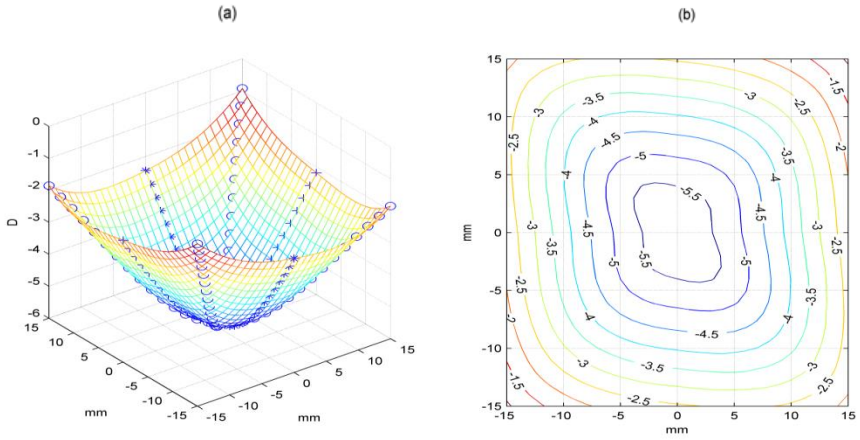

Figure 5.4. RCS for M fitted out of polynomial functions from experimental data (a) Surface; (b) Contour plot.

Equivalent procedures enable to obtain surface maps for the other vector components, J_0 and J_{45}. Fig. 5.5 shows the complete RCS in terms of M, J_0 and J_{45} for the considered experimental average myopic eye. A contour representation of the values on the *x*-*y* plane is presented too.

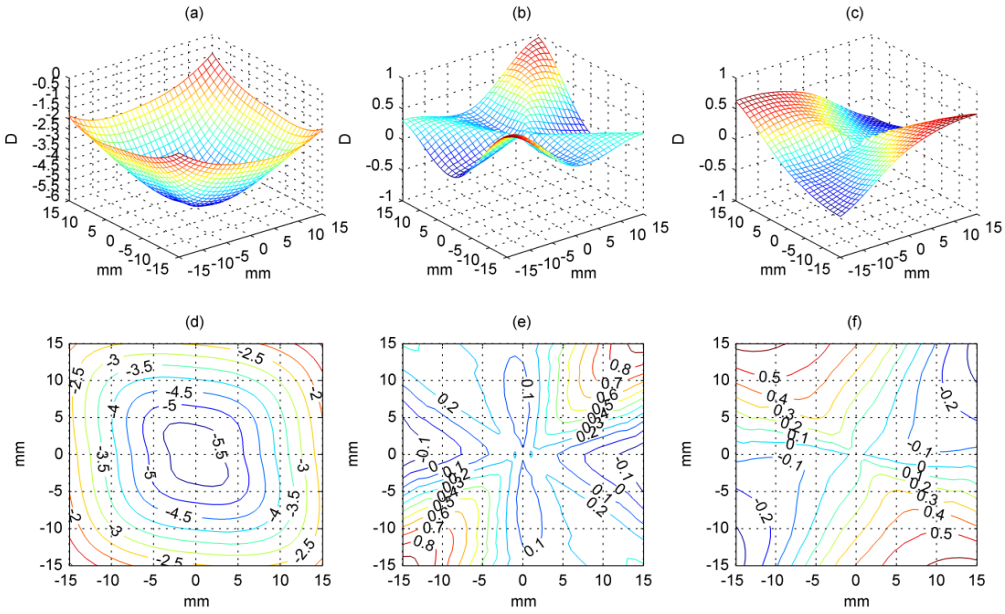

Figure 5.5. RCS for M, J_0 and J_{45} for myopic eyes, from the data in Table 5.1. Top, surfaces for M(a), J_0(b) and J_{45}(c); Bottom, corresponding contour plots for M (d) J_0,(e), J_{45} (f)

Data in Table 5.2, corresponding to emmetropic eyes, may be used to model a RCS for a corresponding average emmetropic eye. Fig. 5.6 shows the RCS obtained for this case. It can be seen how the M value changes less than one diopter from the foveal refraction, with different areas with light hyperopic and myopic peripheral refraction. A different behavior of the RCS for these experimental results in myopic and emmetropic eyes may be easily appreciated.

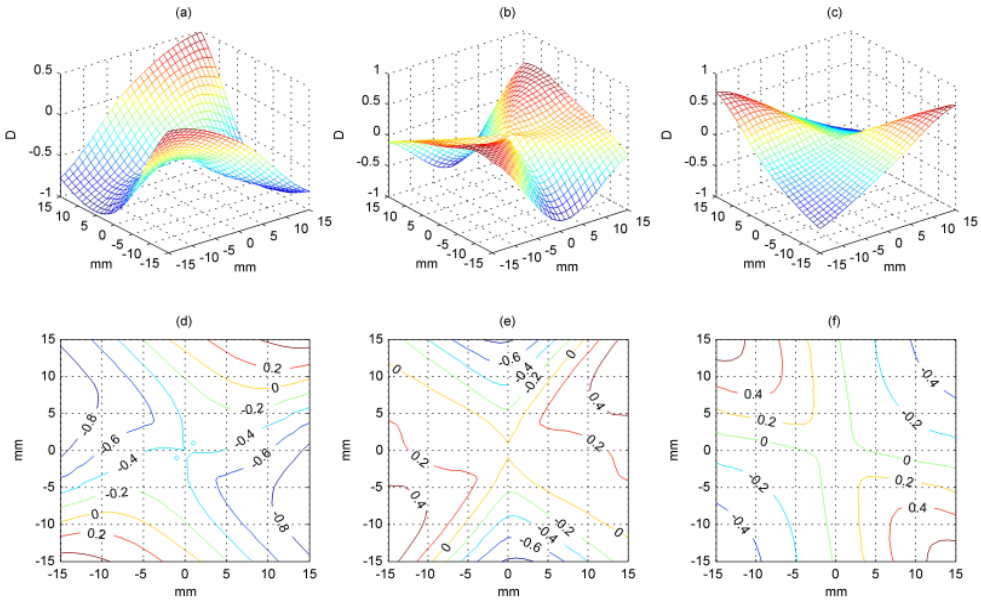

Fig. 5.6. RCS for M, J_0 and J_{45} from an average emmetropic eye using the data from Table 5.3. Top, surfaces for M(a), J_0(b) and J_{45}(c); bottom, contour plots for the respective surfaces: M (d) J_0,(e), J_{45} (f).

5.2. Peripheral refracted surface of an ophthalmic lens.

To assess peripheral refraction, the eye and its parameters are obviously of high relevance. It is required to calculate the layout of the rays passing through the ophthalmic lens which affect a point of the retina with a given eccentricity. This means tracing through the lens, but also through the eye. This usually has been solved by the use of detailed models of the eye in optical design environments, assuming that the results will depend on the eye model used. In addition, the optical constants of the eye (radius, refractive indexes, intraocular distances...) present relevant differences among individuals.

Eye models are schematic descriptions of a typical adult eye as an optical system where its parameters are determined using statistics on a more or less large number of eyes. This can be done at different levels of sophistication. Basically we can refer to paraxial schematic eyes (Emsley's reduced eye, Gullstrand–Emsley simplified eye, the Le Grand exact eye and Gullstrand's No. 1 eye), where the refractive surfaces are spherical and centered on a common optical axis, and the refractive indices are constant within each medium(except the last one) and to finite schematic eyes, which can include non-spherical refractive surfaces, not

alignment along a common axis and a lens gradient refractive index (Lotmar , Drasdo and Fowler, Kooijman , Navarro, Santamarıa, and Besco´s and Liou and Brennan). (77,78)

Paraxial schematic eyes are only accurate within the paraxial region. They do not accurately predict aberrations and retinal image formation for large pupils or for angles at more than a few degrees from the optical axis, but they serve as framework for examining a range of optical properties and allows a study of the cardinal points of the eye. In our approach, we are interested in the nodal points of the eye because of the convenience of their definition to our problem: a ray that travels in the object space with a given slope and passes through the object nodal point, will travel in image space with the same slope passing through the image nodal point.

Fig. 5.7 shows examples of three typical types of paraxial model eyes. In each case F, F'; P, P';N, N' represent the object and image focal, principal and nodal points, respectively. Fig.5.7(a) represents an unaccommodated schematic eye with four refracting surfaces (Le Grand and El Hage). Fig 5.7(b) represents a simplified schematic eye with three refracting surfaces (Emsley). Fig. 5.7 (c) represents a reduced eye with a single refracting surface (Emsley). It can be note that progressive reduction in the number of surfaces used in the model produces only minor changes in the positions of the cardinal points. The close proximity of the two nodal and two principal points has encouraged the use of reduced eye models consisting of a single refracting surface(98)

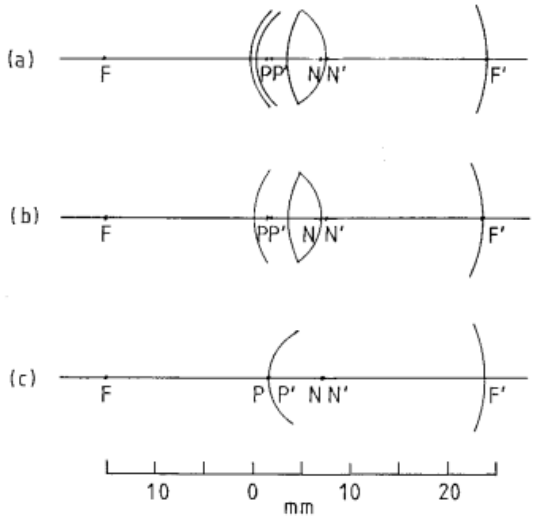

Figure 5.7. (a) Unaccommodated schematic eye with four refracting surfaces (Le Grand and El Hage). (b) simplified schematic eye with three refracting surfaces (Emsley).(c) reduced eye with a single refracting surface (Emsley) (98)

In a reduced model eye, nodal object and image points may be seen to be so close that they may be assumed to merge into one. Moreover, most eye models have object and image nodal points situates in nearby positions(99) and for models without accommodation the difference is below 0.313 mm(77). Table 5.3. shows some values for the position of object and image nodal point from the anterior surface of the cornea in different eye models. Using the proximity of these points, we may assume the coincidence of the object and image nodal points, which we will refer simply as nodal point in the following. Thus, in our approach rays passing through the nodal point of the eye will not deviate (Fig. 5.8).

Table 5.3. Values of positions of object nodal point and image nodal point from the anterior surface of the cornea in different eye models

Model eye	Object nodal point	Image nodal point
Schematic eye	7,20 mm	7,51 mm
Simplified schematic eye	7,06 mm	7,36mm
Reduced eye	5,55mm	5,55mm
Robbert- Bennetts	7,11mm	7,42mm

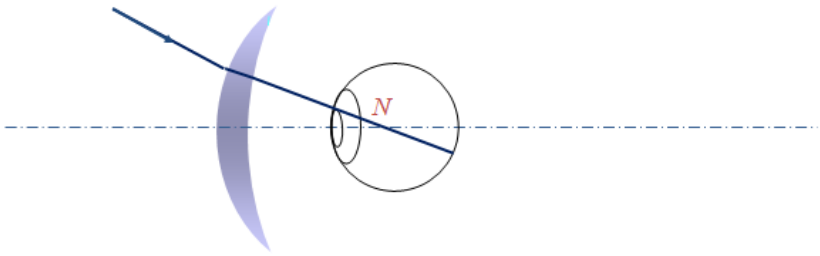

Figure 5.8. Scheme for a reduced eye model where the nodal point N, combining the object and image nodal points is presented. Any ray crossing N does not deviate.

Harris has developed a general theory of nodes for optical systems in general, including eyes, where astigmatism and relative decentration of refracting elements in the system are considered (100). Nodal points are special cases of nodes. He exposes a numerical example for a simplified eye with the features of Table 5.4.

Table 5.4. Values used by Harris for the calculation of the nodes of his model eye(100).

Single surface cornea power	**48(180)/43(90º)**
Lens front surface powers	6(30)/9(120)
Lens back surface powers	11(60)/15(150)
Reduced distance between cornea-lens	2.7 mm
Reduced distance between lens-retina	12.5 mm
Lens reduced thickness	2.6 mm
Index of the lens	1.416
Index of the rest of the eye	1.333

He assumes that all refracting surfaces are centered on axis Z, except for the cornea which is decentered 1mm. Acording to Harris, the point halfway between the incident and emergent nodal centers has a longitudinal position of 6.975 mm from the cornea. For our purposes, on one hand, we consider a simple nodal point *N* as discussed before, and on the other hand, we will consider a value of 7mm away from the cornea for the position of the nodal point. This value agrees well with most of the values in Table 5.3, while reflects one of the most developed theories for nodes in optical systems including eyes.

The geometrical properties of a simple nodal point *N* are very useful to select rays traveling inside the eye in a given direction, so we can control at which point of the retina they arrive. At this point we can trace the reverse path for rays with origin at the nodal point of the eye that arrive to the posterior surface of the lens and later to the object space using a FRT procedure, as described in Section 4. Then, using GRT we can find the curvatures and directions of the neighboring wavefront associated to the ray once it has been refracted by the lens.

A matrix of rays and its associated matrix of wavefronts are sent to an ophthalmic lens to build refracted surfaces in terms of M, J_0 and J_{45} at all retinal eccentricities, using the software tool presented and validated along Section 4. All principal rays pass now through the nodal point of the eye. Fig. 5.9. shows the refracted peripheral surfaces by a spherical lens with BVP of -5.76D, radius of the convex surface 298mm (base +2.00D), radius of the concave surface of 76.9mm, thickness of 1.6mm and refractive index of 1.597. The lens is situated 12mm in front of the anterior corneal surface. An imaginary plane of reference at the posterior vertex of the concave surface of the lens is considered. (*x*,*y*) coordinates for a given point on this plane describe a given retinal eccentricity, defined by the ray that crosses (*x*,*y*) point and the nodal

point of the eye. Such a plane accounts for retinal eccentricities over ±40º around the main direction of gaze, when dimensions of ±15mm centered at the optical axis are considered.

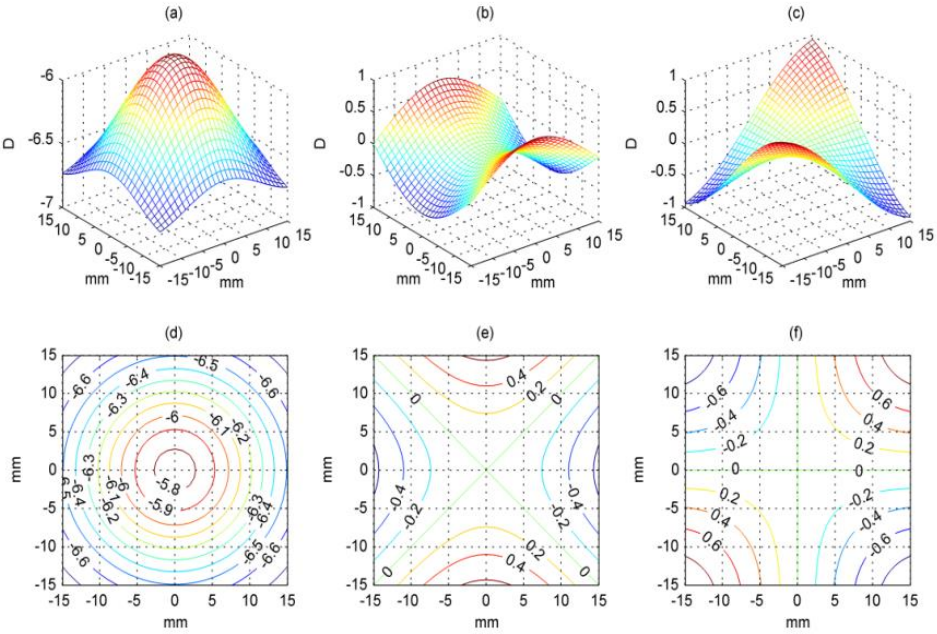

Figure 5.9. Peripheral refracted surfaces for M (a), J_0(b) and J_{45}(c) and corresponding contour plots for M (d), J_0(e) and J_{45}(f) for the ophthalmic lens with BVP of -5.76D and base curve +2.00D described in the text.

In this case the M refracted surface shows an increase in myopic power from the center to the periphery. J_0 presents symmetrical negative values at 180º and positive values at 90º, and J_{45} symmetrical positive values at 45º and negative values at 135º.

Obviously, these surfaces change when geometrical and optical parameters of the lens are changed. A lens with the same BVP but with a different base curve, or including some aspherical surface, will produce different peripheral refracted surfaces. As an example, Fig.5.10. shows the peripheral refracted surfaces by a lens with the same BVP used in Fig.5.9, but with a radius of the convex surface of 74.62mm (base + 8.00D). In this case, M turns more hyperopic from the optical center to the periphery and astigmatic components are minimized.

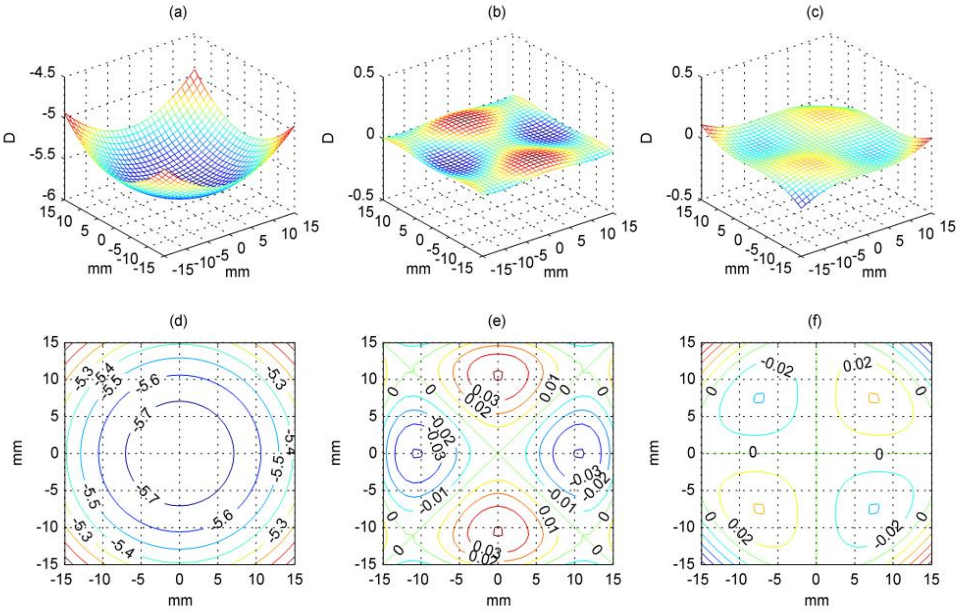

Figure 5.10. Peripheral refracted surfaces for M (a), J_0(b) and J_{45}(c), and corresponding contour plots for M (d), J_0(e) and J_{45}(f) for a ophthalmic lens with BVP of -5.76D and base curve +8.00D described in the text.

When an aspherical surface is introduced, the peripheral error introduced by the lens can be obtained in an equivalent manner. As example, the concave surface of the lens presented in Fig. 5.10 (with base +8.00D) is changed to have an asphericity of p=-1.5, and the associated refracted surfaces are presented in Fig. 5.11. Compared to Fig.5.10, M becomes more hyperopic in the periphery and a large amount of OA is introduced (represented by J_0 and J_{45}).

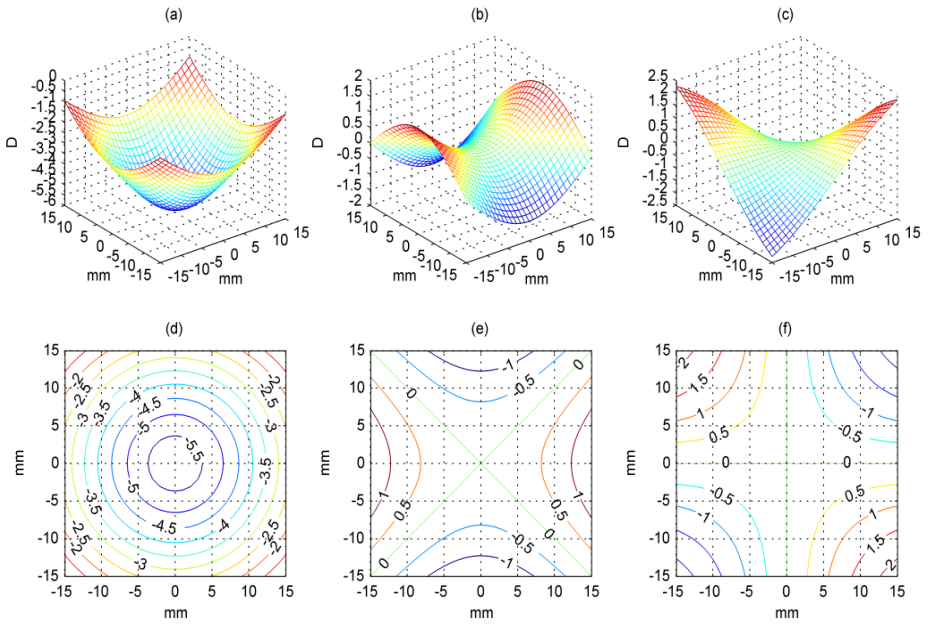

Figure 5.11. Peripheral refracted surfaces for M (a), J_0(b) and J_{45}(c) and corresponding contour plots for M (d), J_0(e) and J_{45}(f) for a ophthalmic lens with BVP of -5.76D, base curve +8.00 and asphericity in the concave surface of p=-1.5.

5.3. Calculation of induced peripheral refraction

Once we have expressed the peripheral refracted surfaces by the lens and the RCS in terms of power vectors, the induced peripheral refraction (IPR) is simply the sum of both. IPR results from the combination of refractions provided by the eye without correction and the peripheral refractions provided by the lens calculated as explained in Section 5.2.

We present as examples of IPR calculation the combination of the peripheral refracted surfaces for the lens of BVP of -5.76D with spherical surfaces and base curve +2.00D (Fig.5.9), spherical surfaces and base curve +8.00D (Fig.5.10) and aspheric concave surface p=-1.5 and base curve +8.00D (Fig. 5.11) with the myopic RCS obtained by experimental values (and presented in Fig.5.5). Finally, we will further analyze the behavior of the lens-eye system regarding peripheral refraction to show an example of the calculation of IPR when under or over-correction is present. We will use experimental RCS for myopic (Fig.5.5) and emmetropic eyes (Fig. 5.6).

5.3.1. Calculation of IPR for an experimental RCS

Fig 5.12 shows the IPR expressed in terms of M, J_0 and J_{45} obtained when a spherical ophthalmic lens of BVP of -5.76 D base curve +2.00D (presented in Fig. 5.9) is situated in front of a myopic eye with central refraction of -5.76D, and pattern of peripheral refraction defined by the RCS represented in Fig. 5.5. This lens obviously is perfectly fitted to compensate the central refractive error, but our interest is in the analysis of what happens in the periphery.

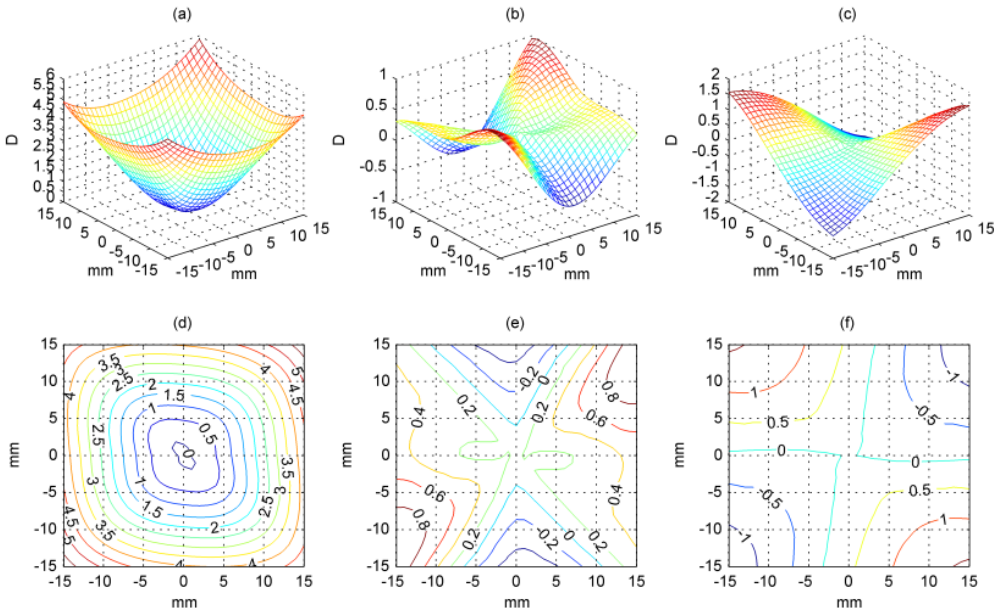

Figure 5.12. Lens-induced peripheral refraction (IPR) of the analyzed case for M, J0, and J45, using the RCS of Fig.. 5.5 and the peripheral refracted surfaces described in Fig. 5.9. Top, surfaces for M (a), J0 (b), and J45 (c). Bottom, corresponding contour plots for these surfaces [(d), (e), and (f).

Those IPR values expressed in terms of M, J_0 and J_{45} can now be expressed as sphere, cylinder and axis using Eqs. 2.6 to 2.8, yielding the maps of spherocylindrical components shown in Fig. 5.13.

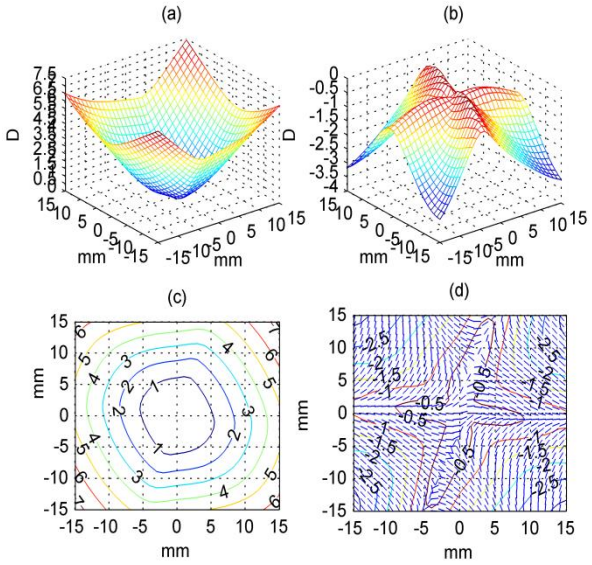

Figure 5.13. IPR surfaces expressed in terms of sphere (a) and cylinder (b), and corresponding contour plots for sphere (c) and cylinder (d) including local axis orientations (spherical lens with BVP -5.76D and base +2.00D).

Let's now take a look at the effect on IPR of a change in the base curve of the lens. Fig. 5.14 shows IPR in terms of sphere, cylinder and axis for a lens with BVP -5.76D and a base curve of +8.00D. RCS has been kept the same of the previous case, so only the base curve of the lens has been changed when compared to Fig.5.13. It may be appreciated how the induced spherical component is severely reduced. Significant changes, in special in the region around the fovea, may also be appreciated following the same trend in the cylinder plot. Peripheral refraction becomes less hyperopic and thus better suited to avoid the progression of myopia. As could be expected, a very relevant role for ophthalmic lens design in the control of myopia is shown.

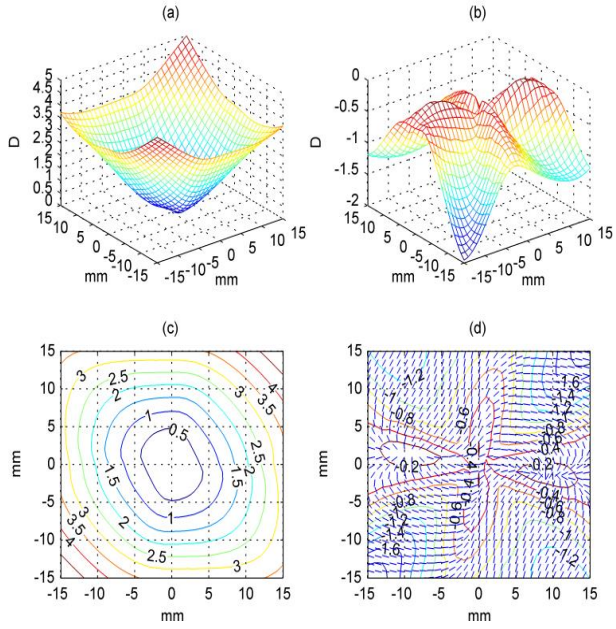

Figure 5.14. IPR surfaces expressed in terms of sphere (a) and cylinder (b), and corresponding contour plots for sphere (c) and cylinder (d) including local axis orientations (spherical lens with BVP -5.76D and base +8.00D).

Following with our analysis, when the concave surface is set to have an asphericity of p=-1.5 and the base curve is +8.00 the IPR obtained is presented in Fig. 5.15, showing a slightly different pattern:

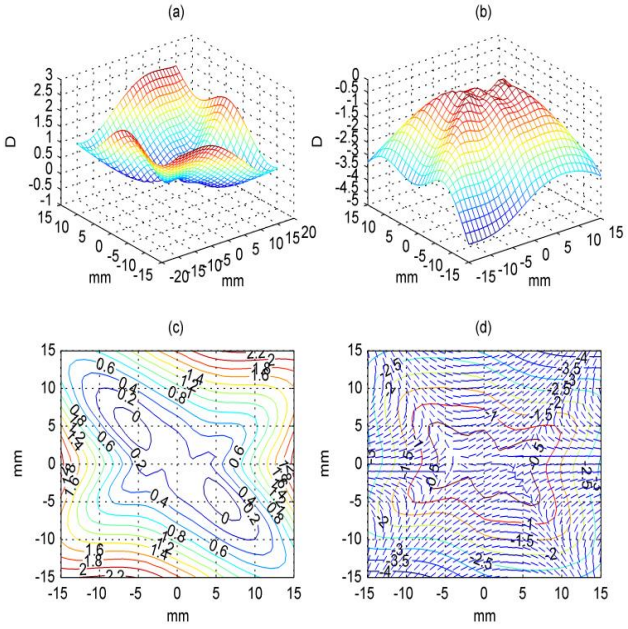

Figure 5.15. IPR surfaces expressed in terms of sphere (a) and cylinder (b), and corresponding contour plots for sphere (c) and cylinder (d) including local axis orientations (spherical lens with BVP -5.76D, and concave aspherical surface with base +8.00D and p=-1.5).

It was observed how the induced sphere decreases significantly when the base curve increases. By iterating this calculation for different base curves it may be observed how an increase in the curvature of the convex surface decreases the mean sphere in IPR in the area considered (Fig.5.16), showing the potential for an optimization of the curvature to minimize the value of IPR.

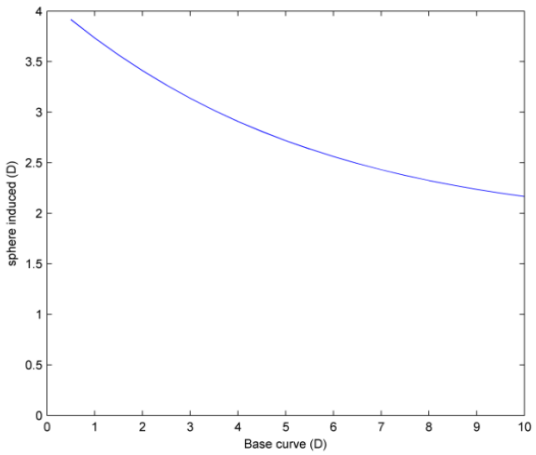

Fig. 5.16. RMS value of the induced sphere against base curve of a lens of BVP -5.76D, index 1.597 and thickness 1.6mm, and the experimental RCS used in all cases. The increase in power of the base curve decreases the induced sphere

Finally, Fig. 5.17 presents the changes on IPR when the concave surface of the lens becomes aspherical. A fixed base curve of +2.00D at Fig. 5.17 a) and +8.00D at Fig.5.17 b), and different values of asphericity set at the concave surface keeping the RCS defined at Fig. 5.5. The effect of the aspherization of the concave surface on peripheral refraction may be clearly appreciated, in special when the base curve of the lens has larger power.

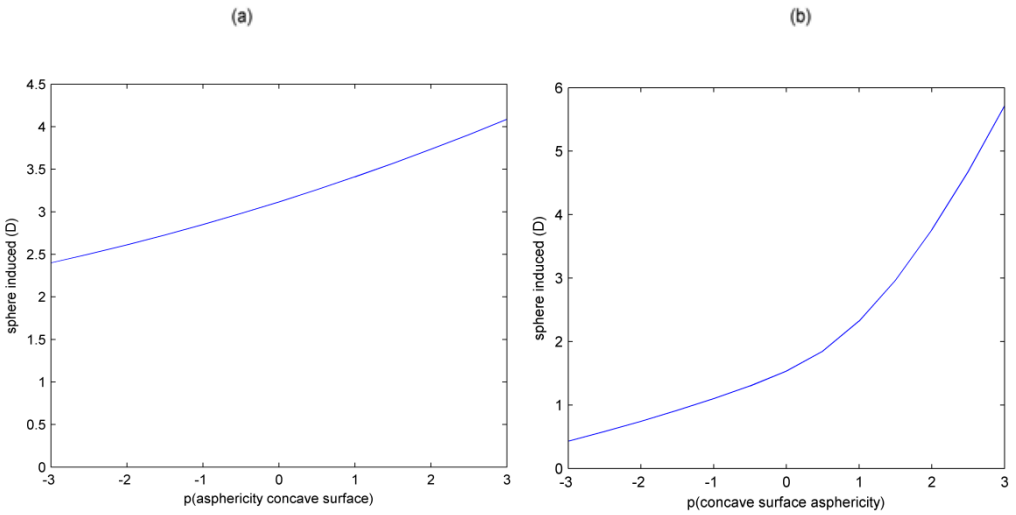

Fig.5.17. Effect on sphere induced when asphericity for concave surface is changed, when base curve is +2.00D(a) and when base curve is +8.00D(b). The lens is that defined in the text and the RCS is that represented in Fig.5.5.

5.3.2. Calculation of IPR in over-correction and under-correction.

The hypothesis that a peripheral hyperopic refractive error is a risk factor for the development of myopia implies that the peripheral retina is sensitive to defocus and its sign and can generate a signal to control ocular growth. The ability of the peripheral visual system to detect focus change has been evaluated by studies of both depth-of–focus(57,101) and accommodation(59,60) There is good evidence to suggest that accommodation can be induced by stimuli lying several degrees outside the central fovea, although with progressively reduced efficiency with eccentricity, and there is some evidence that peripheral accommodation may be less effective in myopes than in emmetropes. Accommodation studies suggest also that stimuli falling on the peripheral retina can alter the accommodation response of the eye and, in presence of an axial accommodation target, can affect the response to the latter.

It is widely accepted that under-correction of myopia produces a greater degree of myopic progression than full correction(4,61). A recent study has reported the effect of overcorrection, undercorrection and full correction on peripheral refraction using contact lenses (62). It would be expected that contact lenses would change the peripheral refraction profile in a myopic or hyperopic direction compared with full correction. However, the shift between full and overcorrection was slightly less than full and undercorrection in both low and moderate myopes. This is probably due to accommodation with overcorrection resulting in a slightly more myopic refraction measurement. The approach proposed in this section easily obtains

theoretical peripheral refraction profiles when over or undercorrection is proposed using an ophthalmic lens, using the tools and strategies presented. These profiles can be used as a reference for the prescription when experimental values are obtained and accommodation is occurring.

Next figures show peripheral refraction profiles for the RCS proposed for myopic eyes (Fig.5.5) when the central refractive error is over (Fig. 5.18) or undercorrected (Fig. 5.19) in a value of 1.00D, and the base curve of the lens is maintained at +2.00D. As could be expected, with over-correction a more hyperopic peripheral refraction profile is obtained when compared to full correction, and a less hyperopic peripheral refraction profile is obtained when undercorrection is used. No significant changes are observed in cylinder.

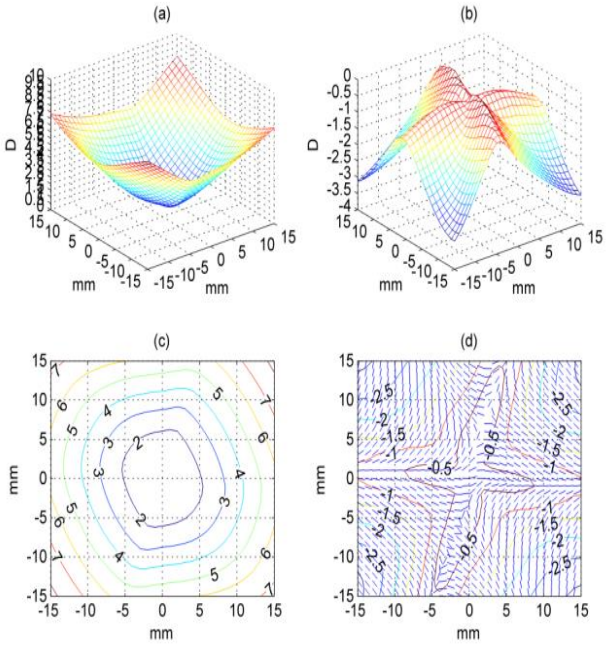

Fig. 5.18. Overcorrection case. IPR surfaces expressed in terms of sphere (a) and cylinder (b), and corresponding contour plots for sphere (c) and cylinder (d) including local axis orientations (spherical lens with BVP -6.76D and base +2.00D).

.

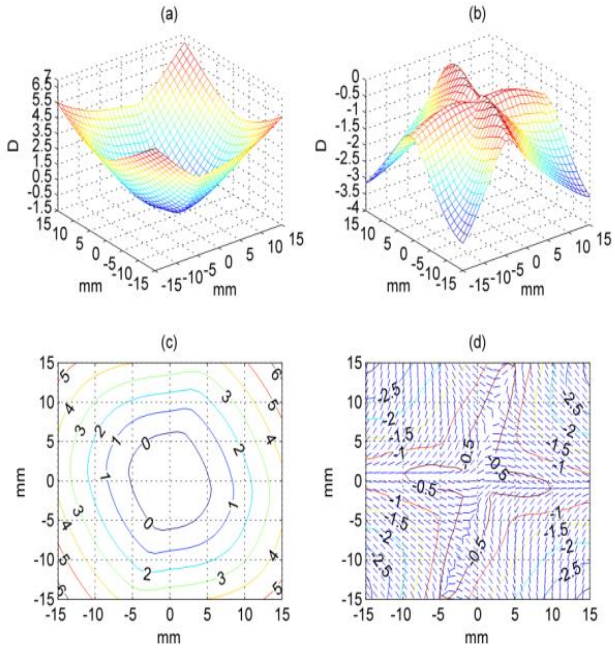

Fig. 5.19. Undercorrection case. IPR surfaces expressed in terms of sphere (a) and cylinder (b), and corresponding contour plots for sphere (c) and cylinder (d) including local axis orientations (spherical lens with BVP -4.76D and base +2.00D).

Finally, we will present results for under and overcorrection using the presented RCS for emmetropes as reference to calculate IPR on full, over and undercorrection. We will consider a lens with back vertex power of -0.32 D (the mean foveal value for emmetropic eyes in the study) to consider the case where the refractive error is fully corrected (Fig.5.20). Overcorrected and undercorrected conditions are shown in Fig, 5.21 and 5.22 respectively with lenses of -1.32D and +0.68D. These lenses have a base curve of +2.00D, index of refraction of 1.597, a thickness of 3mm and are situated 12mm in front of the anterior corneal surface. The feasibility of the method for the calculation of the induced peripheral refraction conditions for an ophthalmic lens, including an easy modeling of the effects of under and overcorrection cases for different central refractive conditions becomes thus demonstrated, showing the potential of the technique.

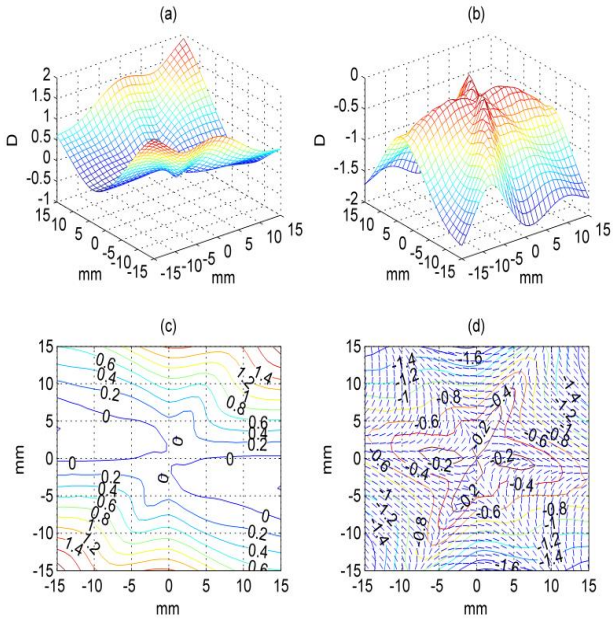

Fig. 5.20. Emmetropic central refraction case at full correction condition. IPR surfaces expressed in terms of sphere (a) and cylinder (b), and corresponding contour plots for sphere (c) and cylinder (d) including local axis orientations (spherical lens with BVP -0.32D and base curve +2.00D).

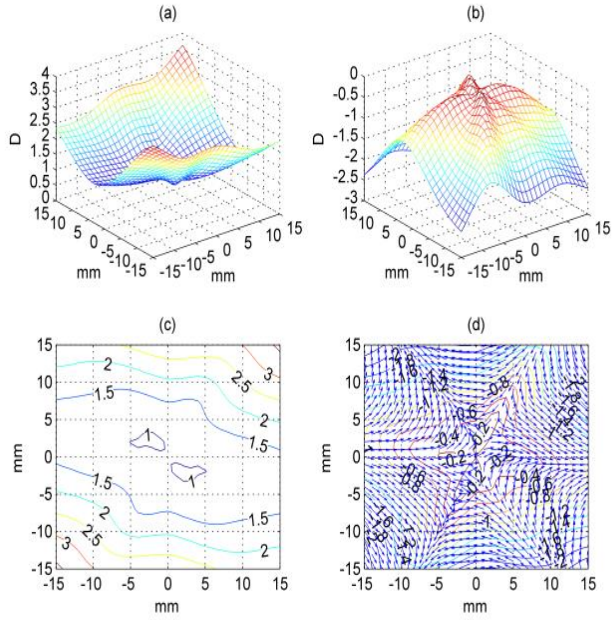

Fig. 5.21. Emmetropic central refraction case in overcorrection condition. IPR surfaces expressed in terms of sphere(a) and cylinder (b), and corresponding contour plots for sphere (c) and cylinder (d) including local axis orientations (spherical lens with BVP -1.32D and base curve +2.00D).

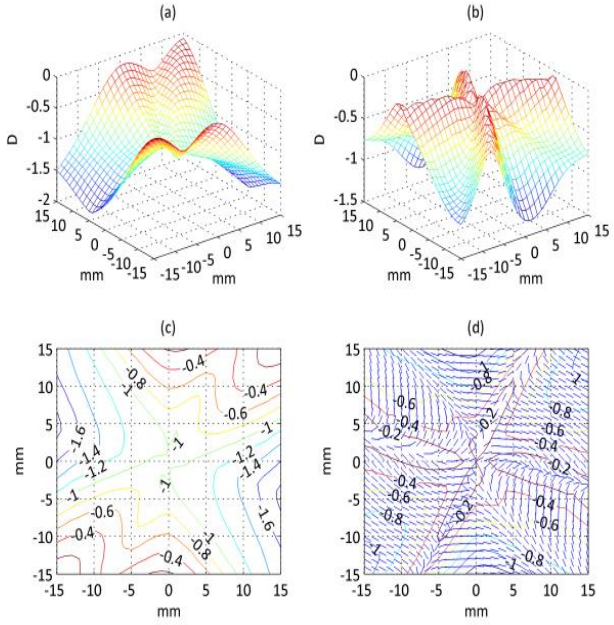

Fig. 5.22. Emmetropic central refraction case in undercorrection condition. IPR surfaces expressed in terms of sphere (a) and cylinder (b), and corresponding contour plots for sphere (c) and cylinder (d) including local axis orientations (spherical lens with BVP +0.68D and base curve +2.00D).

Only in the last case (undercorrected emmetropic eye) it has been possible to induce a negative value for the sphere of the IPR. Other examples are far away to introduce a myopic defocus in the periphery of the eye. This is probably an effect of the RCS taken as example, which includes a large amount of relative peripheral hyperopia.

In this Section we have presented several examples on how different designs of lenses with the same BVP introduce different effects on IPR, plus the potential of personalizing ophthalmic lenses for a given measurement of the myopia of the user. For the RCS used as example for myopic eyes, ophthalmic lenses with a high base curve decreased significantly hyperopic defocus. A negative asphericity for the concave surface also decreased hyperopic defocus, and its effect was seen to be larger for larger surface curvatures. The effect to give asphericity to the concave surface is bigger when the base curve increases. Aspherical surfaces can help to reduce hyperopic defocus. Changes in the geometry of the ophthalmic lens produce significant changes in the IPR. Thus, the introduction of freeform surfaces based on the current methodology is expected to allow personalized ophthalmic lens surfaces to obtain the desired pattern of IPR on all fields of view for a particular eye with a modeled RCS.

In this section we have shown that we can use the methodology based on GRT for the calculation of the IPR for different central refractive conditions modeling a RCS in each case. Moreover, theoretical values of IPR can be a reference when under or overcorrection is used by an ophthalmic lens.

The fact to model a RCS opens the possibility of personalized designs for ophthalmic lenses. Section 6 shows that we dispose of necessary tools to work this aspect, although it isn't the objective of this thesis future works could be addressed following this way.

6. Conclusions.

The main goal of this Thesis has been the development of a method to quantify the induced peripheral refraction (IPR) by an ophthalmic lens. Our approach has been proposed taking into account both ophthalmic lens performance and patient's peripheral refraction data, and based in the general principles of conventional ophthalmic lens design. These are the two basic concepts that we have dealt in detail to obtain a reliable method: the analysis of ophthalmic lens performance, using and implementing a reliable, accurate and validated ray tracing procedure, and the patient's personalized peripheral refraction data, modeling a retinal conjugate surface (RCS). Both have allowed the evaluation of the IPR induced by an ophthalmic lens as the combination of lens features computed by ray tracing through the nodal point of the eye and the values of peripheral refraction assumed for the patient.

Regarding the analysis of ophthalmic lens performance, the main contribution of this work is the detailed description of the implementation and validation of a theoretical ray tracing procedure based in the combination of finite (FRT) and generalized ray tracing (GRT). A detailed description of the implementation of such GRT methodology is presented step by step and, to our knowledge, for the first time for the case of astigmatic lenses. We want to emphasize here that the implementation was made strictly from zero and has delivered a reliable and fast tool with great potential. As a second, and in our opinion most original contribution, we have modified this conventional ray tracing to propose a procedure for the evaluation of the IPR, using the nodal point of the eye as a new reference for ray tracing, and the concept of RCS for the evaluation of the peripheral refraction induced by an ophthalmic lens.

Following, a list of the main conclusions derived from this thesis is presented:

- A thorough review of the bibliography related to peripheral refraction, and its potential relationship with progression of myopia, has been realized. It is pointed out how the peripheral defocus has been proposed as a cause of progression of myopia. A specific focus on the latest bibliography which establishes the relationship of the IPR induced by an ophthalmic lens and such a hyperopic defocus has been presented, and used to justify the interest of the present work.

- In a basic review of ophthalmic lens performance, we have taken into account the fact that an ophthalmic lens is a simple optical system dominated basically by refraction effects, whose

design contemplates little degrees of freedom. The scheme for ray tracing in ophthalmic lens design for foveal vision conditions has been presented due to the parallelism with the approach taken along this Thesis.

- A detailed software tool for ray tracing according to the principles of ophthalmic lens design was programmed along the development of this work, starting from zero.

- With the purpose of implementing ray tracing procedures within such tool, a detailed theoretical model for ray tracing in ophthalmic lenses has been developed, enabling conventional ophthalmic lens design for foveal vision.

- The equations and calculation method for transfer and refraction operations, characterized by a finite ray backwards from image to object space of the lens have been presented in detail and implemented within the tool, following the concept of finite ray tracing (FRT).

- We have discussed and shown how 3D power map measurements in an ophthalmic lens going beyond the conventional Coddington equations can be implemented using the general concept of generalized ray tracing (GRT). This is based on the analysis of the geometrical changes undergone by a wavefront in the proximity of a ray traced exactly using FRT. This approach has been shown to go beyond conventional Coddington's equations, improving the accuracy (exact tracing) and performance (more efficient, faster computation than intensive ray tracing), while enabling a full 3D map of the power map of the lens.

- Between the different procedures discussed in the literature to trace rays and beams of light through optical systems we have chosen the GRT approach proposed by Stavroudis, where a local wavefront is associated to a particular ray and travels perpendicular to it. This associated wavefront changes its geometry when is propagated or refracted by a surface, and its changes are quantified using what happens to the principal directions and principal curvatures of the wavefront after transfer and refraction. GRT equations provide the refracted wavefront curvatures and the torsion of the refracted wavefront, starting from the equivalent values in the incident wavefront.

- Both the wavefront and the refractive surfaces of the lens need to be locally described in order to proceed with the GRT procedure. This local description is determined by the normal and the principal curvatures and its directions of these surfaces at the point of interest. We have seen how starting from a parametric description of a surface, the normal and the principal

curvatures and directions on each of its points can be obtained using Gauss fundamental forms. These fundamental forms allow build a matrix (Eq. 4.8) which describes the principal curvatures of the wavefront at a given point of the surface as its eigenvalues and the associated principal directions as its eigenvectors.

- We have presented in detail a ray tracing description for axially symmetric centered surfaces and for toric surfaces, obtaining in each case the surface normal and the values of the first and second fundamental form of Gauss. Using this information we have developed in detail the general equations for the propagation of the principal ray (based on FRT) and its associated local wavefront (calculated as GRT) for the general case of an ophthalmic lens with any geometry for its surfaces.

- The detailed procedure for a particular case of an astigmatic toric lens has been presented as an example, to the knowledge of the authors for the first time in the literature.

- The results obtained for FRT and GRT in the implemented code have been validated in detail using two different software applications, Beam4 and Primer. Beam 4 validated the accuracy of FRT simulations ray by ray, and Primer validated the implementation of GRT by reducing our code to the situation of the classical Coddington equations, showing consistent results (96).

- Using the general implementation of the software, a study of some results for spherical, aspherical and astigmatic lenses has been presented. We have analyzed these lenses for different directions of gaze and have presented its results for conventional foveal lens design graphically, both as discrete points described by tangential and sagittal powers, and as refracted surfaces described using associated power vectors. The methodology has been shown to enable a fast, easy implementation of the code in programming environments in order to produce 3D power maps of the optical properties of interest. The solid implementation based on FRT and GRT in the shape of software tool which allows an accurate analysis of ophthalmic lens performance is the first major step towards the main goal of this thesis.

- Once the software tool was reliably constructed, the second major and original step was to introduce two major modifications to the conventional ophthalmic lens design procedure, to enable the calculation of the IPR induced by an ophthalmic lens. The new scheme proposed is an original contribution, where the center of rotation of the eye is replaced by the nodal point of the eye and the remote sphere by a surface which is the conjugate of the retina through the

optics of the eye, which we have called the retinal conjugate surface (RCS). After detailing the hypothesis and the rationale behind the proposal, this scheme has been used to find the positions of the tangential and sagittal foci of a pencil of light that arrives to a particular eccentric point of the retina using the developed software tool adapted to the new configuration: in FRT each retinal eccentricity was characterized by a finite ray in 3D space, traced backwards from image to object space of the lens, passing through the nodal point of the eye and reaching the posterior surface of the lens being refracted by the lens to reach the object space. Then, GRT is applied from object to image space following the direction of the finite ray, enabling the calculation of the peripheral refracted surfaces induced by the ophthalmic lens on its own.

- Another original contribution is the purpose of two different models to take into account the refractive state of the eye, reflected in our model by the abovementioned RCS. Two different approaches have been proposed. The construction of a theoretical model of RCS based on the general assumptions done in the literature to describe it as an axially symmetrical surface, or the use of surface fitting techniques in order to build an experimental RCS out of values of peripheral refraction measured experimentally were proposed and demonstrated. The experimental approach includes, in addition, the potential for personalization of lenses to the refractive state of the eye by taking into the design the very relevant intersubject variability described in the literature, due to the contribution to peripheral refraction of aspects of the geometry of the eye and of its optical properties. However, the approach requires the development of techniques for accurately and repetitively measuring the peripheral refractive state of the eye.

- The combination of the peripheral refracted surfaces by the lens, and the dioptric power of the RCS in all directions, expressed in the form of power vectors M, J_0 and J_{45}, has been shown to enable the calculation of IPR at a given retinal eccentricity (97). Power vectors present advantages as the combination of refractive errors is involved. Final IPR values were obtained by the sum of peripheral refracted surfaces and dioptric powers of the RCS, and IPR was finally expressed as sphero-cylindrical refractions for a more understanding in a clinical environment.

- Using the experimental RCS model presented, an analysis of the different IPR values induced by different lens geometries has been presented in detail, including the use of spherical and aspherical surfaces. Spherical lenses reduce significantly the induced hyperopia when the base

curve is increased, while aspherical surfaces improve their performance depending on the aspheric coefficient *p*. A precise quantification of the effects on IPR induced by these changes in geometry has been described in plots describing sphere, cylinder and axis. This also demonstrated the potential for the control of peripheral refraction using the geometry of ophthalmic lenses.

- Finally, we have shown an example for the evaluation of IPR when under and over-correction are used in foveal compensation for an experimental RCS for myopic and emmetropic eye. We have exposed these cases to obtain the theoretical expected values for IPR to later compare with values of measured IPR, so we can evaluate the accommodative effects involved, which could allow a better understanding of the progression of myopia.

In conclusion, we now dispose of a methodology for the calculation of the IPR by an ophthalmic lens, which is quick, reliable and accurate. It contains a ray tracing procedure based on FRT and GRT through the ophthalmic lens having the nodal point of the eye as reference and a modeled RCS which allow us to contemplate personalized patters of peripheral refraction. This methodology and its implementation software present great potential. Furthermore, the ability to model and use a RCS opens the possibility of personalized designs for ophthalmic lenses to prevent the progression of myopia, combining criteria from foveal vision and peripheral vision using the proper weighting among them, and the novel design and manufacturing opportunities presented by free-form optics and 3D printing.

7. References.

1. Saw SM(1), Chua WH, Gazzard G, Koh D, Tan DT, Stone RA. Eye growth changes in myopic children in Singapore. *Br J Ophthalmol* 2005 Nov; 89(11):1489-94.

2. Lin H-J, Wan L, Tsai F-J, Tsai Y-Y, Chen L-A, Tsai AL, et al. Overnight orthokeratology is comparable with atropine in controlling myopia. *BMC Ophthalmology;* 2014;14(1):40.

3. Goss DA. Overcorrection as a Means of Slowing Myopic Progression. *Am J Optom Physiol Opt.* 1984;61(2):85–93.

4. Vasudevan B, Esposito C, Peterson C, Coronado C, Ciuffreda KJ. Under-correction of human myopia - Is it myopigenic?: A retrospective analysis of clinical refraction data. *J Optom*. Spanish Council of Optometry; 2014;7(3):147–52.

5. Chung K, Mohidin N, O'Leary DJ. Undercorrection of myopia enhances rather than inhibits myopia progression. *Vision Res*. 2002;42(22):2555–9.

6. Adler D, Millodot M. The possible effect of undercorrection on myopic progression in children. *Clin Exp Optom*. 2006;89(5):315–21.

7. Mutti DO, Sinnott LT, Mitchell GL, Jones-Jordan LA, Moeschberger ML, Cotter SA, et al. Relative Peripheral Refractive Error and the Risk of Onset and Progression of Myopia in Children. *Invest Ophthalmol Vis Sci.* 2011;52(1):199–205.

8. Berntsen D a, Barr CD, Mutti DO, Zadnik K. Peripheral defocus and myopia progression in myopic children randomly assigned to wear single vision and progressive addition lenses. *Invest Ophthalmol Vis Sci*. 2013;54(8):5761–70.

9. Mutti DO, Sholtz RI, Friedman NE, Zadnik K. Peripheral refraction and ocular shape in children. *Invest Ophthalmol Vis Sci*. 2000;41(5):1022–30.

10. Wallman J, Winawer J. Homeostasis of eye growth and the question of myopia. *Neuron*. 2004;43(4):447–68.

11. Rempt F, Hoogerheide J HW. Peripheral retinoscopy and the skiagram. *Ophthalmologica.* 1971;162(1):1–20.

12. Tabernero J, Vazquez D, Seidemann A, Uttenweiler D, Schaeffel F. Effects of myopic spectacle correction and radial refractive gradient spectacles on peripheral refraction. *Vision Res* 2009;49(17):2176–86.

13. Lin Z, Martinez A, Chen X, Li L, Sankaridurg P, Holden B, et al. Peripheral Defocus with Single-Vision Spectacle Lenses in Myopic Children. *Optom Vis Sci*.2010; 87(1):4–9.

14. Faria-Ribeiro M, Queirós A, Lopes-Ferreira D, Jorge J, González-Méijome JM. Peripheral refraction and retinal contour in stable and progressive myopia. *Optom Vis Sci*.2013;90(1):9–15.

15. Jalie M, Opticians A of D. The Principles of ophthalmic lenses. London: The Association of Dispensing Opticians; 1984.

16. Fannin T, Grosvenor T. Clinical Optics. 1996.

17. Jalie M. Ophthalmic Lenses and Dispensing. 2003.

18. Salvadó J, Fransoy B. Tecnología óptica. Lentes oftálmicas, diseño y adaptación. 1996.

19. Alonso J, Alda J. Ophthalmic Optics. *Encyclopedia of Optical Engineering;* 2007. p. 1563–76

20. Atchison DA. Spectacle lens design: a review. *Appl Opt*; 1992;31(19):3579–85.

21. Atchison D. Performance of aspheric spectacle lenses. *Clin Exp Optom*. 75(6).

22. Atchison D. Spectacle Lens Design-Development and Present State. *Austrial J Optom*. 1984;67(3):97–107.

23. Kingslake R. Who discovered Coddington's equations? *Opt Photonics News*. :20–3.

24. Welford WT. Aberrations of Optical Systems. 1986.

25. Thibos LN, Wheeler W, Horner D. Power vectors: An application of Fourier analysis to the description and statistical analysis of refractive error. *Optom Vis Sci*. 1997;74(6):367–75.

26. Geary JM. Introduction to lens design in Zemax. Willmann-Bell; 2002.

27. Nicholson M. Understanding paraxial ray tracing. Zemax's users knowledge base; 2005.

28. Gullstrand A. Die reelle optische abbildung. K Sven Vent Akad Handl. 1906;XLI:1–139.

29. Sturm JC. Mémoire sur l'optique. *J Math Pures Appl*. 1838;3:357.

30. Keating MP. Oblique central refraction in spherocylindrical lenses tilted around an off-axis meridian. *Optom Vis Sci*. 1993;70(10):785–91.

31. Kneisly AJ. Local Curvature of Wavefronts in an Optical System. *J Opt Soc Am*; 1964;54(2):229–34.

32. Burkhard DG, Shealy DL. Simplified formula for the illuminance of an optical system. *Appl Opt.* 1981;20:897–909.

33. Stavroudis ON. Simpler derivation of the formulas for generalized ray tracing. *J Opt Soc Am*. 1976 ;66(12):1330–3.

34. Stavroudis ON. Chaps. IIX and X. The Optics of Rays, Wavefronts and Caustics. New York: Academic; 1972.

35. Landgrave JEA, Moya-Cessa J. Generalized Coddington equations in ophthalmic lens design. *J Opt Soc Am*. 1996;13(8):1637–44.

36. Comastri SA, Simon JM. Alternative uses of Coddington's equations in optical design. *J Mod Opt.* 2001;48(3):379–404.

37. Campbell CE. Generalized Coddington equations found via an operator method. J Opt Soc Am *A-Optics Image Sci Vis*. 2006;23(7):1691–8.

38. Esser G, Becken W, Müller W, Baumbach P, Arasa J, Uttenweiler D. Derivation of the refraction equations for higher-order aberrations of local wavefronts at oblique incidence. *Opt Soc Am*. 2010; 27(2).

39. Fedtke C, Ehrmann K, Holden BA. A review of peripheral refraction techniques. *Optom Vis Sci*. 2009;86(5):429–46.

40. Smith III E, Hung L, Huang J, Blasdel T, Humbird T, Bockhorst K. Effects of optical defocus on refractive development in monkeys: evidence for local, regionally selective mechanisms. *Invest Ophthalmol Vis Sc*i. 2010; 51(8): 3864–3873.

41. Guyton DL, Greene PR, Scholz RT. Dark-Rearing Interference with Emmetropization in the Rhesus-Monkey. *Invest Ophthalmol Vis Sci*. 1989;30(4):761–4.

42. Smith EL, Harwerth RS, Crawford MLJ, Vonnoorden GK. Observations on the Effects of Form Deprivation on the Refractive Status of the Monkey. *Invest Ophthalmol Vis Sci.* 1987;28(8):1236–45.

43. Yamaguchi T, Ohnuma K, Konomi K, Satake Y, Shimazaki J, Negishi K. Peripheral optical quality and myopia progression in children. *Graefes Arch Clin Exp Ophthalmol* 2013;251(10):2451–61.

44. Mathur A, Atchison DA, Charman WN. Myopia and peripheral ocular aberrations. *J Vis*. 2009;9(10):15.

45. Stone RA, Flitcroft DI. Ocular shape and myopia. Ann Acad Med Singapore. 2004;33(1):7–15.

46. Smith III EL, Ramamirtham R, Qiao-Grider Y, Hung L-F, Huang J, Kee C-S, et al. Effects of foveal ablation on emmetropization and form-deprivation myopia. *Invest Ophthalmol Vis Sc*i. 2007;48(9):3914–22.

47. Smith, III EL, Hung L, Huang J. Effects of Local Myopic Defocus on refractive development in monkeys *Optom Vis Sci*. 2013;90(11):1176–86.

48. Hoogerhe.J, Rempt F, Hoogenbo.Wp. Acquired Myopia in Young Pilots. *Ophthalmologica*. 1971;163(4):209 – &.

49. Mathur, A; Atchison, D.† AM and DA. Peripheral Refraction Patterns Out to Large Field Angles. *Optom Vis Sci.* 2013;90(2):140–7.

50. Mutti DO, Sinnott LT, Mitchell GL, Jones-Jordan LA, Moeschberger ML, Cotter SA, et al. Relative Peripheral Refractive Error and the Risk of Onset and Progression of Myopia in Children. *Invest Ophthalmol Vis Sci.* 2011;52(1):199–205.

51. Seidemann A, Schaeffel F, Guirao A, Lopez-Gil N, Artal P. Peripheral refractive errors in myopic, emmetropic, and hyperopic young subjects. *J Opt Soc Am A-Optics Image Sci Vis*. 2002;19(12):2363–73.

52. Smith G. Design and performance of aspheric ophthalmic lenses. *Ophthalmic Optics* 1986. p. 34–41.

53. Schmid GF. Variability of retinal steepness at the posterior pole in children 7-15 years of age. *Curr Eye Res*. 2003 Jul;27(1):61–8.

54. Sng CCA, Lin X, Gazzard G, Chang B, Dirani M, Lim L, et al. Change in Peripheral Refraction over Time in Singapore Chinese Children. *Investig Ophthalmol Vis Sci* 2011;52(11):7880–7.

55. Radhakrishnan H, Allen P, Calver R, Theagarayan B, Price H,Rae S, Sailoganathan A OD. Peripheral Refractive Changes Associated with Myopia Progression. *Vis Psychophys Physiol Opt*. 2013;54(2):1573–81.

56. Thibos LN, Bradley A, Liu T, López-Gil N. Spherical aberration and the sign of defocus. *Optom Vis Sci*.2013;90(11):1284–91.

57. Wang, B., Ciufrda, K.J, Irish T. Blur Discrimination of the Human Eye in the near retinal periphery. *Optom Vis Sci*. 2005;82(1):52–8.

58. Wang B, Ciuffreda KJ. Depth-of-focus of the human eye: Theory and clinical implications. *Survey of Ophthalmology*. 2006. p. 75–85.

59. Hartwig A, Charman WN, Radhakrishnan H. Accommodative response to peripheral stimuli in myopes and emmetropes. *Ophthalmic Physiol Opt*. 2011 Jan;31(1):91–9.

60. Gu YC, Legge GE. Accommodation to stimuli in peripheral vision. *J Opt Soc Am A*. 1987;4(8):1681–7.

61. Cooper J, Schulman E, Jamal N. Current status on the development and treatment of myopia. *Optometry*. 2012;83(5):179–99.

62. Kang, P FY, , Oh K, Trac K, Zhang F SH. Effect of Single Vision Soft Contact Lenses on Peripheral Refraction. *Optom Vis Sci*. 2012;89(7):1014–21.

63. Smith III EL. Prentice Award Lecture 2010: A Case for Peripheral Optical Treatment Strategies for Myopia. *Optom Vis Sci*. 2011;88(9):1029–44.

64. Tabernero J, Schaeffel F. More Irregular Eye Shape in Low Myopia Than in Emmetropia. *Invest Ophthalmol Vis Sci.* 2009;50(9).

65. Fedtke C, Ehrmann K, Falk D, Bakaraju RC, Holden B a. The BHVI-EyeMapper: Peripheral Refraction and Aberration Profiles. *Optom Vis Sc*i. 2014 7;91(10):1199–207.

66. Atchison DA, Pritchard N, Schmid KL. Peripheral refraction along the horizontal and vertical visual fields in myopia. *Vision Res.* 2006;46(8-9):1450–8.

67. Lee T-T, Cho P. Relative peripheral refraction in children: twelve-month changes in eyes with different ametropias. *Ophthalmic Physiol Opt*. 2013 May;33(3):283–93.

68. Atchison DA, Pritchard N, Schmid KL, Scott DH, Jones CE, Pope JM. Shape of the retinal surface in emmetropia and myopia. *Invest Ophthalmol Vis Sci*. 2005;46(8):2698–707.

69. Mutti DO, Hayes JR, Mitchell GL, Jones LA, Moeschberger ML, Cotter SA, et al. Refractive error, axial length, and relative peripheral refractive error before and after the onset of myopia. *Invest Ophthalmol Vis Sci*. 2007 Jun;48(6):2510–9.

70. Chen X, Sankaridurg P, Donovan L, Lin Z, Li L, Martinez A, et al. Characteristics of peripheral refractive errors of myopic and non-myopic Chinese eyes. *Vision Res*. 2010;50(1):31–5.

71. Tabernero J, Ohlendorf A, Fischer MD, Bruckmann AR, Schiefer U, Schaeffel F. Peripheral Refraction Profiles in Subjects with Low Foveal Refractive Errors. *Optom Vis Sci.* 2011;88(3):E388–94.

72. Ehsaei A, Mallen EAH, Chisholm CM, Pacey IE. Cross-sectional Sample of Peripheral Refraction in Four Meridians in Myopes and Emmetropes. *Invest Ophthalmol Vis Sci.* 2011;52(10):7574–85.

73. Atchison DA, Jones CE, Schmid KL, Pritchard N, Pope JM, Strugnell WE, et al. Eye shape in emmetropia and myopia. *Invest Ophthalmol Vis Sci*. 2004;45(10):3380–6.

74. Verkicharla PK, Mathur A, Mallen EAH, Pope JM, Atchison DA. Eye shape and retinal shape, and their relation to peripheral refraction. *Ophthalmic Physiol Opt*. 2012;32(3):184–99.

75. Atchison, D.A, Mathur, A, Varnas SR. Visual Performance with Lenses Correcting. *Optom* 2013;90(11):1304–11.

76. Smith G, Atchison DA, Avudainayagam C, Avudainayagam K. Designing lenses to correct peripheral refractive errors of the eye. *J Opt Soc Am A Opt Image Sci Vis*. 2002;19(1):10–8.

77. Atchison D, Smith G. Optics of the Human Eye. Butterworth-Heinemann; 2000.

78. Navarro R, Santamaria J, Bescos J. Accommodation-dependent model of the human eye with aspherics. *Journal of the Optical Society of America.A, Optics and image science*1985;2(8) :1273-81.

79. Kang P, Swarbrick H. Peripheral Refraction in Myopic Children Wearing Orthokeratology and Gas-Permeable Lenses. *Optom Vis Sci.* 2011;88(4):476–82.

80. Queiros A, Manuel Gonzalez-Meijome J, Jorge J, Villa-Collar C, Gutierrez AR. Peripheral Refraction in Myopic Patients After Orthokeratology. *Optom Vis Sci*. 2010;87(5):323–9.

81. Ma LX, Atchison DA, Charman WN. Off-axis refraction and aberrations following conventional laser in situ keratomileusis. *J Cataract Refract Surg*. 2005;31(3):489–98.

82. Kwok E, Patel B, Backhouse S, Phillips JR. Peripheral refraction in high myopia with spherical soft contact lenses. *Optom Vis Sci*. 2012;89(3):263–70.

83. Shen J, Clark CA, Soni PS, Thibos LN. Peripheral Refraction With and Without Contact Lens Correction. *Optom Vis Sci*. 2010;87(9):642–55.

84. Shen J, Thibos LN. Peripheral Aberrations and Image Quality for Contact Lens Correction. *Optom Vis Sci.* 2011;88(10):1196–205.

85. Ho A, Smith L, Sankaridurg P, Holden BA. Method and apparatus for controlling peripheral image position for reducing progression of myopia. Google Patents; 2007.

86. Sankaridurg P, Donovan L, Varnus S, Ho A, Chen X, Martinez A, et al. Spectacle Lenses Designed to Reduce Progression of Myopia: 12-Month Results. *Optom Vis Sci*. 2010;87(10):802.

87. Smitth EL, Grreman N, Greeman P, Ho A, Holden BA. Methods and apparatuses fo altering curvature of field and positions of peripheral off-aaxis focal positions. 2006.

88. Bakaraju RC, Ehrmann K, Ho A, Papas EB. Pantoscopic tilt in spectacle-corrected myopia and its effect on peripheral refraction. *Ophthalmic Physiol Opt*. 2008;28(6):538–49.

89. Atchison DA. Optical models for human myopic eyes. *Vision Res* 2006;46(14):2236–50.

90. Gwiazda J, Hyman L, Hussein M, Everett D, Norton TT, Kurtz D, et al. A randomized clinical trial of progressive addition lenses versus single vision lenses on the progression of myopia in children. *Investigative ophthalmology & visual science*. 2003;44; 1492-1500.

91. Atchison DA. Third-Order Theory of Spectacle Lenses Applied to Correction of Peripheral Refractive Errors. *Optom Vis Sci*. 2011;88(2):E227–33.

92. Smith EL. Optical treatment strategies to slow myopia progression: effects of the visual extent of the optical treatment zone. *Exp Eye Res*; 2013;114:77–88.

93. Stavroudis ON. The Optics of Rays, Wavefronts, and Caustics. UK: Academic Press; 1972.

94. P.do Carmo M. Geometría diferencial de curvas y superficies. Alianza Universidad Textos; 1990.

95. Stavroudis ON, Fronczek RC. Caustic surfaces and the structure of the geometrical image. *J Opt Soc Am*; 1976 ;66(8):795–800.

96. Rojo P, Royo S, Ramírez J, Madariaga I. Numerical implementation of generalized Coddington equations for ophthalmic lens design. *J Mod O*pt. 2014;30;1–11.

97. Rojo P, Royo S, Caum J, Ramírez J, Madariaga I. Generalized ray tracing method for the calculation of the peripheral refraction induced by an ophthalmic lens. *Opt Eng*. 2015;54:025106.

98. Charman WN. Optics of the eye. Handbook of optics 1. Second Edi. McGraw-Hill;1995.

99. Bores L. Refractive eye surgery. Blackwell Science; 2001.

100. Harris WF. Nodes and nodal points and lines in eyes and other optical systems. Ophthalmic Physiol Opt 2010;30(1):24–42.

101. Wang B, Ciuffreda KJ. Depth-of-focus of the human eye in the near retinal periphery. *Vision Res*. 2004;44(11):1115–25.